Sorption / Desorption Reversibility of Polycyclic Aromatic Hydrocarbons (PAHs) in Soils and Carbonaceous Materials

Dissertation

zur Erlangung des Grades eines Doktors der Naturwissenschaften

der Geowissenschaftlichen Fakultät
der Eberhard-Karls-Universität Tübingen

vorgelegt von
Guohui Wang
aus Baoding

2008

Tag der mündlichen Prüfung:	28.07.2006
Dekan:	Prof. Klaus G. Nickel, Ph.D.
1. Berichterstatter:	Prof. Dr. Peter Grathwohl
2. Berichterstatter:	Prof. Dr. Christoph Schüth

Herausgeber: Institut für Geowissenschaften der Universität Tübingen
Sigwartstraße 10, D-72076 Tübingen

Schriftleitung der Reihe C: Zentrum für Angewandte Geowissenschaften (ZAG)
Lehrstuhl für Angewandte Geologie

Prof. Dr. Thomas Aigner
Prof. Dr. Erwin Appel
Prof. Dr. Peter Grathwohl
Prof. Dr. Stefan Haderlein
Prof. Dr.-Ing. Olaf Kolditz
Prof. Dr. Georg Teutsch

Redaktion: Dipl.-Geol. Björn Sack-Kühner

ISSN 0935-4948 (Print)
ISSN 1610-4706 (Internet)

ACKNOWLEDGEMENTS

I would like to thank the Deutsche Forschungsgemeinschaft (DFG) and "AquaTerra", a European Union FP6 integrated project (Project no. 505428 (GOCE), for providing financial support for this work.

I would like to first thank my supervisor, Prof. Dr. Peter Grathwohl. It was a great pleasure to work under his supervision, not only because of his outstanding academic expertise, but also his caring for students. I would also like to give my sincere thanks to Dr. Sybille Kleineidam, Prof. Dr. Christoph Schüth, and Prof. Dr. Charlie Werth for their help and advice.

Thanks to those who have aided me in the lab including: Bernice Nish, for getting started in HPLC and doing certain measurements; Renate Seelig and Thomas Wendel, for the GC/MS data; Renate Riehle, for the DOC equipment operation introduction, and Annegret Walz, for the N_2-BET measurement.

I would like to thank my colleagues Johannes Barth, Christina Eberhard, Till Gocht, Rainer Henzler, Jie Jiang, David Kuntz, Rudolf Liedl, Bertrand Ligouis, Sanheng Liu, Lihua Liu, Iris Madlener, Uli Maier, Andrea Mattos, Åsa Olsson, Matthias Piepenbrink, Kerstin Ruopp, and Dietmar Steidle for their help in a variety of matters.

I save the last words of thanks for my wife and my son. Their love and support greatly facilitated this journey through science.

ABSTRACT

Understanding sorption/desorption is an important prerequisite for the prediction of fate and transport of pollutants in the environment. During the last two decades, numerous studies have reported hysteresis phenomenon for the interaction of hydrophobic organic contaminants (HOCs) with natural organic matter (NOM). It manifests as nonsingular sorption/desorption isotherms or different rates for sorption and desorption, where during desorption a higher affinity of a compound on a given sorbent and a longer time scale for release than for sorption is observed. Other studies showed that some of the reported sorption/desorption hysteresis phenomena are due to experimental artifacts, mainly resulting from non-attainment of sorption equilibrium before desorption experiments, which result in "pseudo-hysteresis". Except for the hypothesis of sorbent reconfiguration, clear experimental evidence for the physical or chemical mechanisms proposed to lead to hysteresis is still lacking. In this study, sorption/desorption equilibrium and kinetics of phenanthrene sorption/desorption from two soils and three carbonaceous samples were investigated using both batch and column techniques. The main objective of this work was to monitor hysteresis phenomenon by carefully recovering the solute mass in the system and to compare sorption/desorption equilibria and kinetics thermodynamically. Nonsingular isotherms and higher desorption enthalpies as well as increased activation energies with proceeding desorption are expected if significant hysteresis exists.

Sorption-desorption cycles were carried out to compare equilibrium isotherms and associated sorption/desorption enthalpies (ΔH, isosteric heats). Instead of the traditional decant-and-refill batch method, the experiments were conducted using a newly designed batch protocol, which enables the determination of sorption/desorption isotherms at different temperatures using a closed batch system. This method additionally allows the determination of the sorption/desorption enthalpies which gives insight into the sorbent-sorbate interactions. In order to attain sorption/desorption equilibrium, all the samples were pulverized to shorten the laboratory experimental time. The sorbate losses were carefully monitored and considered in the isotherm calculation. Additionally, release of native phenanthrene was also investigated at different temperatures and compared with the freshly spiked samples to investigate the aging effect. The batch results show that for all individual temperature steps sorption and desorption isotherms coincide. Furthermore, the solubility-normalized sorption/desorption isotherms at different temperatures collapse to unique overall isotherms. Leaching of native phenanthrene occurred at

much lower concentrations but was well predicted by extrapolation of the spiked equilibrium sorption isotherms. The absolute values of sorption/desorption isosteric heats (ΔH) determined are in a range of 19 - 35 kJ mol^{-1}, which is higher than the heat of aqueous solution of subcooled phenanthrene but much less than the heat of condensation of solid phenanthrene from water. No significant difference of the enthalpies between sorption and desorption was observed. Furthermore, the desorption enthalpy of the native phenanthrene was not significantly higher than expected from the sorption experiments with spiked samples. Sorption and desorption kinetics were monitored in on-line column experiments with stepwise increases of temperature. An intraparticle diffusion model was used to simulate the desorption profile in order to get the apparent diffusion coefficients of phenanthrene from the carbonaceous materials. Desorption activation energies were calculated by Arrhenius relationship based on the high-resolution measurement of concentration increases at each temperature step. The activation energies determined range from 58 – 71 kJ mol^{-1}. No siginificant trend of increasing desorption activation energies along with the increased degree of desorption was observed although desorption was almost completed, i.e., only 0.2% (lignite) and 6% (high-volatile bituminous coal) of the initially sorbed mass were present after the last temperature step. Both batch and column results imply that no significant hysteresis occurred for the sorption/desorption of phenanthrene with the samples investigated in this study.

Reversibilität der Sorption/Desorption von Polyzyklischen Aromatischen Kohlenwassserstoffen (PAK) in Böden und kohligen Materialien

Kurzfassung: Sorptions- und Desorptionsprozesse spielen eine bedeutende Rolle bei der Beurteilung und Vorhersage von Schadstofftransport und -abbau in der Umwelt. In den letzten beiden Jahrzehnten berichteten etliche Untersuchungen über Hysterese-Phänomene bei der Interaktion von hydrophoben organischen Schadstoffen (HOCs) mit natürlichem organischem Material (NOM). Dies zeigt sich nicht-singulären Sorptions/Desorptions-Isothermen, wobei bei der Desorption eine höhere Affinität eines Stoffes auf einem gegebene Sorbenten und eine längere Zeitskala für Freisetzung beobachtet wird als bei der Sorption. Weiterführende Untersuchungen zeigten jedoch, dass einige der beobachteten Sorptions/Desorptions-Hysterese-Phänomene auf experimentelle Artefakte zurückzuführen sind, v.a. wegen nicht erreichtem Sorptionsgleichgewicht vor Begin von Desorptionsexperimenten. Dies führt zu sog. „Pseudo-Hysterese“. Abgesehen von der Rekonfiguration der Sorbenten bei der Sorption sind bisher keine Hypothesen bekannt, die durch experimentelle Befunde physikalische oder chemische Prozesse als Ursache dafür klar belegen. In der vorliegenden Arbeit wurde die Sorption/Desorption von Phenanthren an zwei Bodenproben und an zwei Kohleproben sowohl im Gleichgewicht als auch bzgl. der Desorptionskinetik untersucht (Batch- und Säulenversuche). Ziel dieser Arbeiten war es, Hysterese-Phänomene zu identifizieren und die zugehörigen Parameter zu quantifizieren indem Sorptions- und Desorptionsisothermen sowie Desorptionsraten in hoher Präzision bei unterschiedlichen Temperaturen gemessen wurden. Vorraussetzung war es, sorgfältige Massenbilanzen aufzustellen und Artefakte zu vermeiden. Nicht-singuläre Isothermen, erhöhte Desorptions–Enthalpien sowie erhöhte Aktivierungsenergien bei fortschreitender Desorption wären Indikatoren für signifikante Hysterese Effekte.

Sorptions/Desorptions-Zyklen wurden durchgeführt, um Gleichgewichtssorptions-isothermen und die zugehörigen Sorptions/Desorptionsenthalpien (ΔH) zu vergleichen. Anstatt der traditionellen "decant-and-refill" Batchmethode wurde für die Experimente jedoch ein neu entwickeltes Verfahren verwendet. Dieses erlaubt die Messung von Sorptions-/Desorptionsisothermen bei verschiedenen Temperaturen in einem geschlossenen Batch-System. Zusätzlich ist eine Bestimmung der Sorptions/Desorptionsenthalpien möglich, welche Einblicke in die Sorbent-Sorbat Wechselwirkung erlaubt. Um die Zeit zur Gleichgewichtseinstellung (Sorption) zu

verringern, wurden alle Proben pulverisiert. Sorbat-Verluste wurden sorgfältig verfolgt und bei der Berechnung der Isothermen berücksichtigt. Des Weiteren wurde die Freisetzung von "natürlichem" Phenanthren bei verschiedenen Temperaturen untersucht und mit frisch gespikten Proben verglichen, um den Alterungseffekt zu quantifizieren. Die Batchversuche zeigen, dass für jeden Temperaturschritt die Sorptions- und Desorptionsisothermen übereinstimmen. Außerdem kollabieren die auf Löslichkeit normierten Sorptions/Desorptionsisothermen bei verschiedenen Temperaturen zu einer Einheitsisotherme. Die Elution des natürlichen Phenanthrens fand bei sehr viel niederigeren Konzentrationen statt, entsprach aber dem, was man aufgrund der Extrapolation der gespikten Gleichgewichtssorptionsisothermen erwarten konnte. Die Absolutwerte der bestimmten Sorptions/Desorptionsenthalpien (ΔH) liegen im Bereich von 19 kJ mol^{-1} bis 35 kJ mol^{-1} und sind damit höher als der Lösungsenthalpie von unterkühltem Phenanthren in Wasser. Kein signifikanter Unterschied zwischen den Enthalpien bei Sorption und Desorption konnte festgestellt werden. Auch die Desorptionsenthalpie von natürlichem Phenanthrene war nicht signifikant höher die aus den Sorptionsexperimenten mit gespikten Proben erwartete. Die Sorptions- und Desorptionskinetik wurde in on-line Säulenversuchen bei schrittweiser Erhöhung der Temperatur untersucht. Ein Intrapartikel-Diffusionsmodell wurde zur Simulation der Desorptionsprofile angewandt, um die scheinbaren Diffusionskeffizienten von Phenanthren in kohligem Material zu erhalten. Die Aktivierungsenergien der Desorption wurden berechnet über die Arrhenius-Gleichung basierend auf hochaufgelösten Messungen der Konzentrationsverläufe bei jedem Temperaturschritt. Die so bestimmten Aktivierungsenergien reichen von 58 kJ mol^{-1} bis 71 kJ mol^{-1}. Mit erhöhtem Desorptionsgrad konnte kein signifikanter Trend zu einer erhöhten Aktivierungsenergie festgestellt werden, obwohl am Ende der Experimente die Desorption fast vollständig war (lediglich 0,2% (lignite) und 6% (high-volatile bituminous coal) der ursprünglich sorbierten Masse waren nach dem letzten Temperaturschritt noch vorhanden). Sowohl die Ergebnisse der Batch- als auch der Säulenversuche zeigen, dass keine signifikante Hysterese für Sorption/Desorption von Phenanthren zumindest in den in dieser Arbeit untersuchten Proben auftritt.

TABLE OF CONTENTS

Nomenclature

The abbreviations shown in brackets represent the dimensionality of the variable being used: M = mass; L = length; L^3 = volume; t = time

A	Arrhenius preexponential factor	[-]
b	exponent in the polanyi-Dubinin-Manes model	[-]
C	concentration	[M L^{-3}]
$C_{ref,initial}$	initial concentration in batch reference vial	[M L^{-3}]
C_s	concentration sorbed onto solids	[M M^{-1}]
C_s^p	sorbate concentration due to partitioning in solid	[M M^{-1}]
C_s^{ad}	sorbate concentration due to adsorption in solid	[M M^{-1}]
C_w	solute concentration in water	[M L^{-3}]
C_w^*	apparent aqueous concentration	[M L^{-3}]
D_a	apparent diffusion coefficient	[L^2 t^{-1}]
D_{aq}	diffusion coefficient in aqueous phase	[L^2 t^{-1}]
D_k	Damkohler number	[-]
D_L	hydrodynamic dispersion coefficient	[L^2 t^{-1}]
E	characteristic free energy of adsorption of a compound	[kJ mol^{-1}]
E_a	desorption activation energy	[kJ mol^{-1}]
f_{oc}	fraction of organic carbon	[-]
f_{doc}	concentration of dissolved organic carbon	[M L^{-3}]
f_{ocp}	fraction of organic carbon available for partitioning	[-]
f_r	fraction of contaminant presenting in rapid kinetics	[-]
f_s	fraction of contaminant presenting in slow kinetics	[-]
ΔH	isosteric heat (enthalpy)	[kJ mol^{-1}]
$\Delta H_{a,d}$	sorption/desorption enthalpy	[kJ mol^{-1}]
ΔH_{fus}	heat of fusion	[kJ mol^{-1}]
HI	hysteresis index	[-]
k, k_r, k_s	first-order kinetic rate constants	[L^2 t^{-1}]
K_d	distribution coefficient	[L^3 M^{-1}]
K_{doc}	dissolved organic matter based distribution coefficient	[L^3 M^{-1}]
K_{Fr}	Freundlich sorption coefficient	[L^3 M^{-1}]
K_{Fr}^*	solubility-normalized freundlich sorption coefficient	[M M^{-1}]
K_L	Langmuir sorption coefficient	[L^3 M^{-1}]
K_{oc}	organic carbon based distribution coefficient	[L^3 M^{-1}]
K_{ow}	octanol/water partition coefficient	[-]
L	length of the column	[L]
M	mass of solute which has diffused into/out of solid particle	[M]
m_d	dry mass of solid	[M]
M_{eq}	mass of solute in a particle under equilibrium conditions	[M]
m_i	native loaded mass in solid	[M M^{-1}]
m_{loss}	mass loss in the batch system	[M]
m_s	sorbed mass in solid	[M]

m_w / X_w	dissolved sorbate mass in water	[M]
q_{max}	maximum sorbate concentration in a solid	[M M^{-1}]
q_s	concentration in column solid in unit of mol/L pore water	
r	radial distance	[L]
R	universal gas constant	[kJ $mol^{-1}K^{-1}$]
R_d	retardation faction	[-]
S	water solubility	[M L^{-3}]
S_{solid}	aqueous solubility of solid compounds	[M L^{-3}]
S_{sub}	subcooled liquid solubility	[M L^{-3}]
t	time	[t]
T, T'	temperature	[K, °C]
T_m	solid melting point	[K, °C]
v	groundwater flow velocity	[L t^{-1}]
V_0	maximum volume of sorbed sorbate per unit mass of sorbent	[L^3 M^{-1}]
V_{ref}	water volume in batch reference vials	[L^3]
V_w	volume of water in batch vial	[L^3]
x	distance	[L]
X_{input}	initial contaminant mass spiked in solution	[M]
X_{tot}	total sorbate mass in the batch system	[M]
$1/n$	Freundlich exponent	[-]

Greek symbols

ß	ratio of solute mass dissolved to mass in the solid phase in a batch system	[-]
ε	intraparticle porosity	[-]
ρ	bulk density of solid	[M L^{-3}]
ρ_0	chemical compound density	[M L^{-3}]
φ, η	the gamma distribution parameters	[-]

Chapter 1

INTRODUCTION

1.1 Motivation

Sorption/desorption hysteresis refers to the apparent asymmetry of sorption/desorption equilibrium and/or kinetics. It manifests as a nonsingular isotherms or different rates for sorption and desorption, where during desorption a higher affinity of a chemical compound on a given sorbent and a longer time scale for compound release than during sorption are observed. Numerous studies have reported the phenomenon of hysteresis or non-sigularity of sorption/desorption isotherms for the interaction of hydrophobic organic contaminants (HOCs) with natural organic matter (NOM) sorbents (*17, 30, 23, 28*). However, for non-polar compounds, there are also many reports of non-hysteretic sorption/desorption behavior (*33, 36, 11, 19, 20*). Other studies showed that some of the reported sorption/desorption hysteresis phenomena are due to experimental artifacts. Nonsingular sorption/desorption isotherms can be due to pseudo-hysteresis (*1-3, 5, 6, 14, 15, 20, 24, 27*). Schwarzenbach and Westall (*36*) conducted a variety of laboratory batch and column experiments to elucidate the sorption behavior of halogenated alkenes and benzenes in a river water-groundwater infiltration system and found that, for concentrations typically encountered in natural water, the sorption of these compounds by aquifer materials was reversible. Huang et al. (*17*) used three different batch experimental protocols to study sorption/desorption of phenanthrene on five EPA reference soils and sediments, and found different experimental setups introduced different types of artifacts and different degrees of apparent hysteresis.

There are several causes leading to observed hysteresis phenomenon. The different manifestations and processes of hysteresis are summarized in Figure 1.1.

Kinetic hysteresis could be due to different sorption and desorption rates arising from steric hinderance effects (*9, 12, 18*), sorbate entrapment in micropores (*29, 32*) or heterogeneous NOM properties. Non-linear sorption isotherms also lead to kinetic hysteresis, i.e. self-sharpening concentration front during sorption and extended tailing during desorption. There are several examples reporting kinetic hysteresis, in which sorption appears to be faster than desorption (*10, 15, 25*). Lin et al. (*21*) studied vapor

uptake of TCE and Benzene by soil grains using a diffusion model and suggested that the sorption/desorption diffusion asymmetry can be explained by the isotherm nonlinearity when the Freundlich exponent is smaller than 0.75.

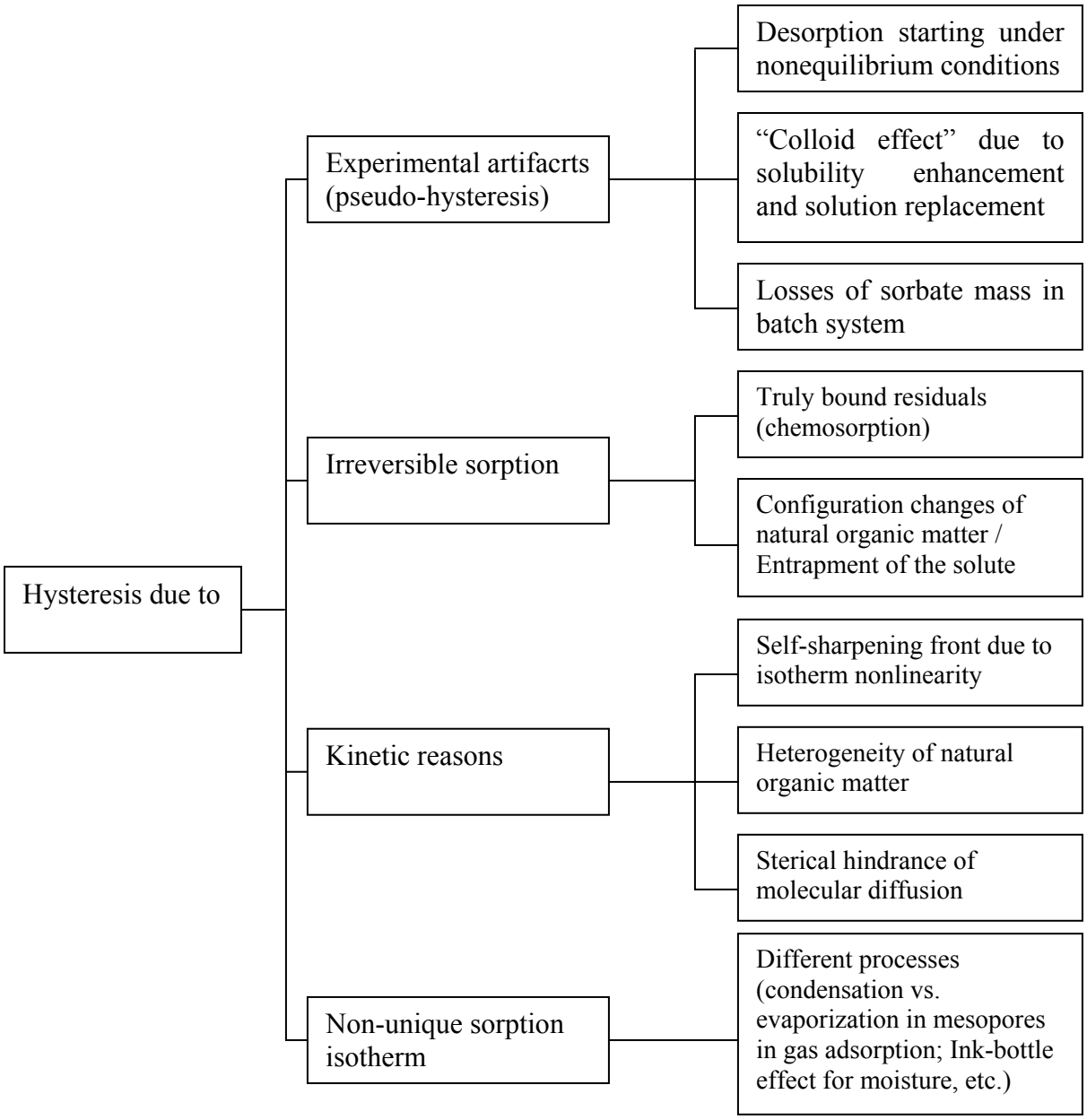

FIGURE. 1.1 Processes and manifestations of hysteresis.

Irreversibility even under elevated pressure and temperature conditions can be seen as evidence for chemicaly bound residues. Desorption hysteresis for pesticides sorbed in soil has frequently been reported (e.g., *8, 13, 35*), and is generally attributed to irreversible pesticide binding with humic substances. This kind of sorbate-sorbent interactions will not likely occur between HOCs and NOM due to the non-ionized property of HOCs. Non-unique sorption-desorption isotherms occur in the gas adsorption on mesopores (e.g. BET) due to different condensation and evaporation processes under higher relative pressures, which, however, are not representative for ambient aqueous systems.

"Pseudo-hysteresis" due to experimental artifacts in the traditional batch sorption/desorption method can be classified mainly into three categories: (1) desorption starting under nonequilibrium conditions (nonattainment of equilibrium due to rate-limited diffusion can lead to an underestimation of equilibrium sorbed concentration in the sorption direction and an overestimation in desorption direction (*26*)); (2) sorbate losses from the batch system (these include biotic or abiotic degradation of the sorbate and losses of sorbate to batch vial components, especially polymer liners and seals (e.g. PTFE-lined rubber septa) and volatilization. If these losses are not considered, it could lead to incomplete mass balances used to construct the sorption isotherm, resulting in hysteresis due to overestimating the sorbed concentrations); (3) the "colloid effect" in the conventional batch vial decant-and-refill method (association of solute with dissolved or suspended matter in the batch system results in apparent solubility enhancement, thus less sorption, dilution of the aqueous phase in the batch by solution replacement to initiate desorption then clearly results in artificial hysteresis).

In addition to experimental artifacts, for hydrophobic organic compounds sorption on natural organic matter, several hypotheses were developed to explain hysteresis. The most plausible explanation is irreversible deformation of the sorbent by the sorbate uptake. The structural deformation of sorbent could cause different microscopic pathways for sorptive uptake and release process, which result in hysteresis.

Bailey et al. (*4*) first postulated "low pressure" sorption hysteresis of non-polar organic vapors on active carbon. This term was employed to distinguish this phenomenon from irreversible sorption at higher pressures associated with capillary condensation in mesopores (irreversible sorption/desorption branch in BET method). Low pressure hysteresis assumes to result from the intercalation of molecules of sorbate in narrow pore spaces leading to irreversible changes in the pore structure.

Weber et al. (*31*) and Braida et al. (*7*) explained the cause of hysteresis using a concept of "matrix trapping". This concept postulates that sorbent swells due to sorbate uptake. Upon abruptly decreasing the solute concentration during desorption, the matrix collapses and certain sorbate molecules are entrapped in the sorbent.

Lu and Pignatello (*22*) introduced the "pore deformation" hypothesis from an analogy between natural organic matter (NOM) and polymers, assuming that the total organic matter is comprised of two different organic phase domains, i.e., the soft (rubbery) amorphous part and the hard glassy part. The rubbery state is characterized by relatively flexible macromolecules. Cavities in the soil organic matter (SOM) matrix will be created to volumetrically accommodate the incoming sorbate molecules. This process of cavity creation is reversible in rubbery/soft NOM domains due to the structural flexibility, therefore a reversible sorption process in this domain can be expected. In contrast, the glassy/hard domain in NOM contains poorly interconnected pores (isolated holes). The pore deformation hypothese postulates that the un-relaxed free pore volume increases due to the dilating of existing pores and creation of new holes during the uptake of sorbate, but does not relax synchronously during desorption due to the structural rigidity of this domain. Therefore, the increased internal volume during sorption is partially conserved during desorption and the affinity for sorbate molecules is stronger in desorption branch, which manifests in hysteresis phenomenon. Lu and Pignetallo (*22*) demonstrate a "conditioning effect" phenomenon to support the pore deformation mechanism, where enhanced sorption capacity was observed in the second sorption cycle following a prior sorption-desorption cycle involving dichloromethane.

Clear experimental evidence for the physical or chemical mechanism proposed to lead to hysteresis is still lacking. Reasons for desorption hysteresis can be manifold. More than a single mechanism may be responsible for the many observed desorption hysteresis phenomena. The most common experimental artifacts result from nonattainment of sorption/desorption equilibrium since the true equilibrium can require very long times. Literature reported sorption/desorption experiments varied form hours to weeks and further up to more than a thousand days. In addition, two other sources of artifacts due to sorbate mass loss are difficult to be ruled out using the traditional decant-and-refill batch method. To differentiate "pseudo-hysteresis" resulting from experimental artifacts from true hysteresis due to kinetic reasons or sorbent reconfiguration of the natural organic matter, a prerequisite for such experiments is to improve the experimental set up in order to minimize or eliminate the artifacts. If under these conditions differences in the sorption and desorption isotherms are observed, kinetic reasons or irreversible sorption as summarized in Figure 1.1 are likely.

1.2 Research Objectives

The main objective of this work was to quantify sorption/desorption hysteresis through (a) comparison of sorption/desorption equilibrium isotherms and enthalpies (ΔH), and (b) determination of the thermodynamic parameters in sorption/desorption kinetics. In addition, a numerical model code based on pore retarded intraparticle diffusion was used to simulate the sorption/desorption kinetics in carbonaceous materials. More specific objectives are introduced in the following:

Sorption/desorption cycles using a newly designed experimental protocol. Corresponding to the above-mentioned experimental artifacts, a new sorption/desorption batch experimental protocol was developed, where the sorption/desorption cycle is driven by temperature changes, rather than the usual decant-and-refill procedures to avoid the potential "colloid effect". Sorption is started at high temperatures (low sorption), stepwise equilibrated at lower and lower temperatures (increasing sorption) until the lowest temperature is reached. After that the process is reversed, which leads to

desorption of the sorbate with increasing temperature. The corresponding sorption/desorption isotherms at each temperature are calculated and the isotherms' singularity at each temperature step can be compared. The system losses for each temperature step have to be carefully monitored by measuring the sorbate mass attached on the batch components, especially the seals of vial caps. In order to establish sorption/desorption equilibrium in a relative short time period, all sorbents are pulverized to very fine particles using a zirconium oxide planet ball mill (Laborette, Fritsch).

Comparison of the sorption/desorption enthalpy. The newly developed batch protocol additionally allows the determination of the isosteric heats (ΔH) of sorption and desorption. Based on the thermodynamics, at equilibrium the contaminant distribution between solid and aqueous phases ultimately is governed by the sorption/desorption enthalpies and entropies. The absolute enthalpy values of sorption/desorption give improved insight on the molecular interactions between sorbate and sorbent. If true hysteresis exists, different enthalpies for sorption and desorption are expected.

Leaching of native compound. All the selected sorbents in this study include historically aged trace-level PAHs. Comparisons between the leaching of native PAHs with sorption isotherms and desorption using spiked samples would clearly show hysteresis if it exists.

Sorption/desorption kinetics. On-line column sorptive uptake and subsequent desorption is monitored. In addition, desorption experiments are executed with stepwise temperature increases in order to determine the activation energy of desorption, which should increase if hysteresis occurs. Exhausting solvent extraction is carried out after the column experiments to recover the residual mass in the column, which could imply the persistence of the target compound.

1.3 Study Significance

Contamination of soils and sediments by organic compounds are frequently encountered in the environment and this may cause severe contamination of aquifers and thus drinking water. Sorption/desorption information is an important prerequisite for the prediction of the fate and transport of pollutants in the environment. Most transport models, for example, are based on the sorption reversibility. This assumption is questioned by the observations of sorption/desorption hysteresis phenomena. However, many reported hysteresis phenomena could result from laboratory artifacts. Therefore, it is very important to avoid "pseudo hysteresis" by improving the experimental technique and to clarify sorption hysteresis mechanisms. The outcome of this study will allow the evaluation of remediation technologies and strategies, and help to set endpoints for concentrations in soils and sediments at contaminated sites.

1.4 References

1. Allen-King, R.M.; Grathwohl, P.; Ball, W.P. New modeling paradigms for the sorption of hydrophobic organic chemicals to heterogeneous carbonaceous matter in soils, sediments, and rocks. *Advances in water resources*, 2002, 25, 985-1016

2. Altfelder, S.; Streck, T.; Richter J. Nonsingular sorption of organic compounds in soil: the role of slow kinetics. *J. Environ. Qual.* 2000, 29, 917-25

3. Altfelder, S.; Streck, T.; Maraqa, M.A. Nonequilibrium sorption of dimethylphtalate - Compatibility of batch and column techniques. *Soil Sci. Soc. Am. J.* 2001, 65, 102-110

4. Bailey, A., Cadenhead, D.A., Davies, D.D., Everett, D.H., Miles, A.J. Low pressure hysteresis in the adsorption of organic vapours by porous carbon. *Trans. Farad. Soc.* 1971, 67, 231-243.

5. Ball, W.P.; Roberts, P.V. In *Organic substances in sediments and water*; Baker, R.A. Ed.; Lewis Publishers, Inc.: Chelsea, MI, Vol. 2, Chapter 13. 1991

6. Ball, W.P.; Roberts, P.V. Long-term sorption of halogenated organic chemicals – part 2. Intraparticle diffusion. *Environ. Sci. Technol.* 1991b, 25, 1237-1249

7. Braida, W.; Pignatello, J.J.; Lu, Y.; Ravikovitch, P.I., Neimark, A.V.; Xing, B. Sorption hysteresis of benzene in charcoal particles. *Environ. Sci. Technol.* 2003, 37, 409-417.

8. Celis, R.; Cornejo, J.; Hermosin, M.C.; Koskinen, W.C. Sorption-desorption of atrazine and simazine by model soil colloidal components. *Soil Sci. Soc. Am J.* 1997, 61

9. Chen, W.; Kan, A.T.; Tomson, M.B. Irreversible adsorption of chlorinated benzenes to natural sediments: implications for sediment quality criteria. *Environ. Sci. Technol.* 2000, 34, 385-392.

10. Farrell, J., Reinhard, M. Desorption of halogenated organics from model solids, sediments, and soil under saturated conditions. 2. Kinetics. *Environ. Sci. & Technol,* 1994b, 28, 63-72

11. Friesel, P., Milde, G., Steiner, B. Interactions of halogenated hydrocarbons with soils. Fresenius, Z. *Anal. Chem*. 1984, 319, 160-164

12. Fu, G.; Kan, A.T.; Tomson, M.B. Adsorption and desorption hysteresis of PAHs in surface sediments. *Environ. Toxicol. Chem.* 1994, 13, 1559-1567

13. Gan, J.; Weimer, M.R.; Koskinen, W.C.; Buhler, D.D.; Wyse, D.L.; Becker, R.L. Sorption and desorption of imazethapyr and 5-hydroxyimazethapyr in Minnesota soils. *Weed Sci*. 1994, 42, 92-97.

14. Grathwohl, P.; Reinhard M. Desorption of trichloroethylene in aquifer material: rate limitation at the grain scale. *Environ. Sci. Technol.* 1993, 27, 2360-2366

15. Harmon, T.C.; Roberts, P.V. Comparison of intraparticle sorption and desorption rates for a halogenated alkene in a sandy aquifer material. *Environ. Sci. Technol.* 1994, 28, 1650-1660

16. Huang, W.; Weber, W.J., Jr. A Distributed Reactivity Model for Sorption by Soils and Sediments. 10. Relationships between Desorption, Hysteresis, and the Chemical Characteristics of Organic Domains. *Environ. Sci. Technol.* 1997, 31, 2562-2569

17. Huang, W.; Yu, H.; Weber, W.J., Jr. Hysteresis in the sorption and desorption of hydrophobic organic contaminants by soils and sediments. 1. A comparative analysis of experimental protocols. *J. Contam.Hydrol.* 1998, 31, 129-148

18. Hunter, M.A.; Kan, A.T.; Tomson, M.B. Development of a surrogate sediment to study the mechanisms responsible for adsorption/desorption hysteresis. *Environ. Sci. Technol*. 1996, 30, 2278-2285.

19. Karickhoff, S.W., Brown, D.S., Scott, T.A. Sorption of hydrophobic pollutants on natural sediments. *Water Res.* 1979, 13, 241

20. Kleineidam, S.; Rügner, H.; Grathwohl, P. Desorption kinetics of phenanthrene in aquifer material lacks hysteresis. *Environ. Sci. Technol*. 2004, 38, 4169-4175.

21. Lin, T.; Little, J.C.; Nazaroff, W.W. Transport and sorption of volatile organic compounds and water vapor within dry soil grains. *Environ. Sci. Technol.* 1994, 28, 322-330.

22. Lu, Y.; Pignatello, J.J. Demonstration of the "Conditioning effect" in soil organic matter in support of a pore deformation mechanism for sorption hysteresis. *Environ. Sci. Technol.* 2002, 36, 4553-4561.

23. Lu, Y.; Pignatello, J.J. History-dependent sorption in humic acids and a lignite in the context of a polymer model for natural organic matter. *Environ. Sci. Technol.* 2004, 38, 5853-5862.

24. Miller, C.T.; Pedit, J.A. Use of a reactive surface-diffusion model to describe apparent sorption-desorption hysteresis and abiotic degradation of lindane in a subsurface material. *Environ. Sci. Technol* 1992, 26, 1417-1427

25. Pignatello, J.J.; Ferrandino, F.J.; Huang, L.Q. Elution of aged and freshly added herbicides from a soil. *Environ. Sci. Technol.* 1993, 27, 1663-1671.

26. Pignatello, J.J. The measurement and interpretation of sorption and desorption rates for organic compounds in soil media. *Advances in Agronomy*, 2000, 69, 1-73.

27. Sabbah I.; Ball W.P.; Young D.F.; Bouwer E.J. Misinterpretations in the Modeling of contaminant desorption from environmental solids when equilibrium conditions are not fully understood. *Environ. Eng. Sci.* 2005, 22, 350-366

28. Sander, M., Lu, Y., Pignatello, J.J. A thermodynamically based method to quantify true sorption hysteresis. *J. Environ. Qual.* 2005, 34, 1063-1072.

29. Steinberg, S.M.; Pignatello, J.J.; Sawhney, B.L. Persistence of 1,2-Dibromoetnane in soil: Entrapment in intraparticle micropores. *Environ. Eng. Sci.* 1987, 21, 1201-1208.

30. Weber, W.J., Jr.; Huang, W.; Yu, H. Hystersis in the sorption and desorption of hydrophobic organic contaminants by soils and sediments. 2. Effects of soil organic matter heterogeneity. *J. Contam. Hydrol.* 1998, 31, 149-165

31. Weber, J.W., Jr.; Kim, S.; Johnson, M.D. Distributed reactivity model for sorption by soils and sediments. 15. High-concentration co-cotaminant effects on phenanthrene sorption and desorption. *Environ. Sci. Technol.* 2002, 36, 3625-3634.

32. Werth, C.J.; Reinhard, M. Effect of temperature on trichloroethylene desorption from silica gel and natural sediments. 2. Kinetics. *Environ. Sci. Technol*. 1997, 31, 697-703.

33. Wu, S., Gschwend, P.M. Sorption kinetics of hydrophobic organic compounds to natural sediments and soils. *Environ. Sci. & Technol.* 1986, 20, 717

34. Xia, G., Pignatello, J.J. Detailed sorption isotherms of olar and apolar compounds in a high-organic soil. *Environ. Sci. & Technol.* 2001, 35, 84-94

35. Xue, S.K; Selim, H.M. Modeling adsorption-desorption kinetics of alachlor in a typic fragiudaf. *J. Environ. Qual*. 1995, 24, 896-903

36. Schwarzenbach, R.P., Westall, J. Transport of nonpolar organic compounds from surface water to groundwater. Laboratory sorption studies. *Environ. Sci. & Technol.*1981, 15, 1360

Chapter 2

THEORY OF SORPTION/DESORPTION OF HYDROPHOBIC ORGANIC COMPOUND (HOCs) IN NATURAL ORGANIC MATTER (NOM) AND EXPERIMENTAL METHODOLOGY

2.1 Sorption of Hydrophobic Organic Compounds (HOCs) on Natural Organic Matter (NOM)

Sorption is fundamental to the fate and transport of organic chemicals in the subsurface environment. The distribution of contaminant between solid and aqueous phases is a central aspect of contaminant risk assessment and remediation. Sorption/desorption processes control the physical and biological availability of contaminants in soil/sediment and groundwater system. Defined broadly, the term sorption/desorption refers to bulk mass-transfer phenomena in which molecules leave the fluid phase (vapor or liquid) and become associated with an immobile phase and vice versa (*35*). Sorption describes the association of dissolved contaminant molecules with a solid phase, and may be broadly divided into two sorption categories based on different sorption phenomena: absorption and adsorption. Adsorption describes a process in which the solute accumulation is generally restricted to a surface or interface, e.g. solid/liquid. In contrast, absorption describes a process in which the solute penetrates the sorbent – similar to solution in solvent (*19*). Due to the heterogeneity of the soil/sediment components, both processes may take place simultaneously and can not be separated from each other experimentally.

Natural minerals and organic matter are two solid phase components in natural soil and sediments. For hydrophobic organic compounds, it is well established that sorption of HOCs out of aqueous solution or at high relative humidity is dominated by the organic matter (OM) fraction in soils and sediments. Therefore organic matter in the subsurface is the most important parameter governing the sorption and desorption processes of HOCs. For each contaminant, sorption/desorption behavior will strongly depend on the properties of local geosorbents. Different sorbents show different sorption capacities, linearities and finally sorption mechanisms. Recently, Allen-King et al. (*2*) reviewed geosorbents heterogeneity in detail and divided geosorbents in several classes according to their geological history and origin.

2.1.1 Natural Organic Matter

Soil organic matter (SOM). The term soil organic matter generally refers to the total organic carbon-containing substances in soil. More specifically, the term SOM refers to the nonliving organic components, which are largely composed of products resulting from microbial and chemical transformations of organic debris. SOM is usually bound to mineral particles as an organic film or discrete organic particle. As a coating, SOM is regarded to enhance the surface affinity for HOCs by making the surface more hydrophobic. Random network polymers provide a three-dimensional hydrophobic environment for HOCs like a solvent. In addition to the unaltered or partially altered biomass (undecomposed plants parts or plant roots, which account for a small fraction of the total SOM and show low sorption capacity), SOM generally refers to the humus- the dark-colored constituents of the solid organic matter. It is comprised of biomolecules and humic substances. The biomolecules mainly include aliphatic organic acids and carbohydrates, such as cellulose, lignin, etc.. The humic substances comprise a heterogeneous mixture of chemically unidentifiable macromolecules. The most investigated humic substances are humic acids ($\approx C_{187}H_{186}O_{89}N_9S$) and fulvic acids ($\approx C_{135}H_{182}O_{95}N_5S_2$) (*42*). Humic substances comprise the majority of organic matter in surface soil and have similar properties despite their starting materials, whereas the amount and type of humic substance in the subsurface (sediment) depends strongly on the environment of deposition or formation.

Carbonaceous materials. Soils and sediments may contain other forms of carbon usually not classified as normal SOM. These mainly include geologically aged materials such as coals and kerogen. Such carbonaceous materials are widely distributed in the environment due to erosion and sedimentation process as well as anthropogenic impact. Because of their physical structure and hydrophobicity, such materials are expected to have high affinities for HOCs. Isotherms are usually highly non-linear and adsorption is the dominant sorption process. In general, these materials are characterized by condensed, rigid and aromatic structures, with high carbon contents and relatively few polar functional groups (*14, 17, 18, 20, 24, 39, 56*). For investigation of contaminant

transport and fate in soil and sediment, these carbonaceous materials are playing very important roles and have became a hot research topic in the last ten years.

Kerogen can originate from algae of marine or lacustrine environments, residues of higher terrestrial plants or from herbaceous terrestrial materials. These thermally altered substances are, per definition, finely dispersed as discrete particles in sediments and sediment rocks. Such disseminated organic matter is insoluble in nonoxidizing acids, base, and organic solvents. Coals are considered sedimentary rocks made up almost completely of organic matter. They consist of a macromolecular three-dimensional network of condensed aromatics (polymers) and separate molecular compounds (not polymer). According to several coalification stages (increased temperature and pressure during sediment burial), different forms of coal with increased carbon content and aromaticity have been characterized. Following the coalification ranks, lignite, sub-bituminous coal, high-volatile bituminous coal, and anthracite can be distinguished. It should be noted that coals by definition are heterogeneous, consisting of a variety of different macerals (*2*). Due to their high surface area and microporosity as well as high OC contents, sorption of HOCs on coals is very strong and nonlinear, especially if higher rank coals are involved. The term black carbon (BC) is generally used to indicate charcoal and soots, which are produced by the incomplete combustion of biomass and fossil fuels. This class of high-temperature altered organic matter also includes activated carbon and coke. BC occurs widely in soils and sediments and is highly persistent in the environment.

Recently, more and more evidence appears showing that sorption on kerogens, coals and black carbon is strongly nonlinear. Since these inert, condensed and aromatic materials are widely distributed in the environment, they are of great significance for sorption of organic compounds in the environment.

2.1.2 Sorption Mechanisms and Equilibrium Sorption Models

Equilibrium sorption/desorption of compounds by soils and sediments from aqueous solution is usually measured by sorption experiments at constant temperature that yield

sorption isotherms**,** i.e. by plotting the equilibrium concentration of a compound in the sorbent as a function of its equilibrium concentration in solution at a given temperature. In general, sorption can be quantified by a distribution coefficient.

Linear isotherms. In the simplest case, the equilibrium concentration of a compound in solid phase C_s [mg L^{-1}] is directly proportional to its equilibrium concentration in the aqueous phase, C_w [mg L^{-1}]:

$$C_s = K_d C_w \tag{2.1}$$

where the parameter K_d [L/kg] is the distribution coefficient (also named partition coefficient, if independent of aqueous concentrations). Thus, a linear sorption isotherm can be plotted. Absorptive partitioning of compounds into soil and sediment organic matter is a classic concept first reported by Chiou et al. (*9*). Mechanistically, the absorption process was regarded as simple dissolution in the organic matrix, analogous to dissolution of HOCs in organic solvents or rubbery polymers (*24, 25, 29, 34, 53*). This is believed to be true for compounds of low polarity in amorphous sorbents (e.g. partly degraded and reconstituted biopolymers, lipids, and humic/fulvic substances) and when concentrations of compounds are sufficiently high to effectively saturate the usually spare opportunities for surface adsorption (*2, 11, 12*). In transport modeling, linear sorption isotherms for HOCs with natural sorbents are widely adopted for the sake of simplicity.

For hydrophobic organic compounds, sorption in natural soils and sediments is highly correlated with the amount of organic matter in it. The distribution coefficient, K_d, is estimated based on the fraction of organic carbon in soils/sediments (f_{oc}) and contaminant chemical properties:

$$K_d = f_{oc} K_{oc} \tag{2.2}$$

where K_{oc} is the water-organic carbon partition coefficient, which can be estimated based on the octanol-water partition coefficient (K_{ow}) or based on the aqueous solubility using a series of empirical relationships (*27, 40, 41*). The relation of K_{oc} to K_{ow} is also affected by the type of organic matter involved. For example, Grathwohl (*18*) correlated the K_{oc} with different geosorbents where the atomic ratio of hydrogen to oxygen (H/O) was used to distinguish different types of organic matter.

Nonlinear adsorption isotherm. In contrast to the well-established linear partitioning model, non-linear sorption isotherms and extremely high sorption capacities are often observed. This indicates that there are a number of important environmental scenarios where the simple linear isotherm is inadequate. For non-linear sorption K_d changes with contaminant aqueous concentrations and several sorption models have been developed for describing the non-linear isotherms.

The empirical Freundlich model is most commonly used to describe non-linear sorption isotherms:

$$C_s = K_{Fr} C_w^{1/n} \tag{2.3}$$

Here K_{Fr} is the Freundlich coefficient and the empirical exponent $1/n$ represents the slope in a Log C_s versus Log C_w plot. The smaller $1/n$, the less linear the sorption process with respect to concentration; for carbonaceous materials it can be as low as 0.5.

The Langmuir isotherm was originally developed for monolayer adsorption of gases onto homogeneous dry surfaces, but it can also be used to describe adsorption of solutes in soil and sediments.

$$C_s = \frac{K_L q_{\max} C_w}{1 + K_L C_w} \tag{2.4}$$

where K_L is the Langmuir sorption coefficient and q_{max} is a maximum sorbate concentration.

For a sorption domain comprised of micropores, the pore-filling process is likely the dominant sorption mechanism, where the adsorption can be well described by the Polanyi potential theory. Adsorption in micro- and mesoporous solids is considered as a pore-volume-filling process, where the guest molecules undergo an adsorption-like interaction with the pore walls. This theory was developed for the gas phase and has been successfully introduced to aqueous system by Manes and co-workers (*31*). This so-called Polanyi-Dubinin-Manes model approach (eq. 2.5) provides both mechanistic and modeling advantages in describing an adsorption component.

$$C_s = V_0 \rho_0 \exp\left[-\left[\frac{RT(-\ln \frac{C_w}{S})}{E} \right]^b \right] \quad (2.5)$$

where C_s, V_0, ρ_0 denote the adsorbed concentration [mg/kg], the maximum volume of sorbed chemical per unit mass of sorbent [cm^3/kg] and the compounds density [g/cm^3] respectively. R and T are the ideal gas constant [kJ mol^{-1} K^{-1}] and the temperature [K]. C_w/S is the equilibrium aqueous phase concentration normalized to the compound's solubility S [mg L^{-1}]. E [kJ mol^{-1}] is the characteristic free energy of adsorption of a compound (often compared to that of a reference compound in a specific adsorbent). The exponent b is often set to an integer. Note that if b is fixed, V_0 and E are the only fitting factors in this equation.

Combined sorption mechanism concepts in natural soils and sediments. Subsurface sorption processes are intrinsically heterogeneous. It is well established that the total HOC can be considered as a superposition of a partitioning and an adsorption process, which explains nonlinear and high sorption capacity phenomena. The developed adsorption-partitioning combination approach can be derived from two basic concepts. One concept favors the analogy between OM and polymers (*30, 32, 34, 54*). In the OM-polymer analogy, the sorption isotherms are described by a "dual-model" where the total organic matter is comprised by two different organic phase domains, i.e., the soft (rubbery) amophoeus OM part and the hard (glassy) OM parts. The former OM matrix can be penetrated by the sorbates and partitioning is the sorption process. In contrast, the hard (glassy) part of the OM, has pores of subnanometer dimension in which the guest molecules undergo an adsorption-like interaction with the pore walls, giving rise to non-linearity and competitive sorption. Xing et al. (*54*) combine these two sorption mechanisms using a linear partitioning model plus the Langmuir surface adsorption:

$$C_s = C_s^p + C_s^{ad} = K_d C_w + \sum_{i=1}^{n} \frac{K_{L,i} q_{\max,i} C_w}{1 + K_{L,i} C_w} \quad (2.6)$$

where $K_{L,i}$ and $q_{max,i}$ are the Langmuir affinity and capacity constants for the ith unique site in the hole-filling or Langmuir domain. Weber et al. (*51*) postulated a similar

equation named "distributed reactivity model" where the Langmuir adsorption component is replaced by a weighted Freundlich model expression.

Another sorption mechanism combination concept emphasizes the heterogeneity of the OM and the presence of high-surface-area carbonaceous materials with high sorption capacities (*11*), where the adsorption component is described by the Polanyi-Dubinin-Manes model (*29, 53*). The equation for this combined model is:

$$C_s = V_0 \rho_0 \exp\left[-\left[\frac{RT(-\ln \frac{C_w}{S})}{E} \right]^b \right] + f_{ocp} K_{oc} C_w \qquad (2.7)$$

where f_{ocp} is the organic carbon fraction available for partitioning.

2.1.3 Kinetic Sorption Models

Sorption/desorption profiles. Being able to predict how quickly sorption/desorption approaches equilibrium is quite important both for practical activities in the field of contaminant risk assessment and design of remediation strategies. Much work has been done measuring sorption/desorption rates of HOCs on soil, sediment and aquifer materials. A large time scale from hours (*52*) to several days (*28*), several months (*4*) and finally years (*38*) to reach sorption/desorption equilibrium have been reported. Transport of hydrophobic organic compounds in groundwater often occurs under nonequilibrium conditions due to slow sorption/desorption kinetics. Sorption/desorption kinetics shows usually a fast initial uptake/release followed by a long-term tailing, typical for a transient diffusion process.

It is well established that sorption of a chemical molecule from the bulk aqueous solution onto a sorption site in the sorbent undergoes subsequently three steps: transport from the bulk fluid to the vicinity of the external surface of the particle; transport through the stagnant water layer, and finally transport through the pore structure or interstices of the particle, before the sorption site is reached. The physical adsorption process at the sorption site then proceeds at a fast rate in the order of 10^{-6} to 10^{-5} seconds (*1*). The time

scale for the sorbate passing through the stagnant water solution layer from the turbulent bulk solution is on the order of seconds (*40*). Therefore, slow sorption rates are likely to be limited by slow pore diffusion or intra-SOM matrix diffusion. Studies on diffusion through the organic matter matrix are limited; mostly it is assumed that organic matter is a polymer-like material within the sorbate can diffuse (*5-7*). The molecular diffusion in SOM is several orders of magnitude smaller than in water due to the highly viscous SOM or the more rigid and condensed glassy materials (*35*). That pore diffusion limits the rate at which the compound travels to the sorption site is well accepted as the mass transfer bottleneck in the sorption/desorption process (*4, 52*). In addition, Steinberg et al. (*44*) suggested entrapment of molecules in narrow pores in combination with slow pore diffusion. Several models are developed to describe sorption/desorption kinetics.

First-order mass transfer. This model simply assumes that sorption kinetics can be described by a first-order rate expression:

$$\frac{M}{M_{eq}} = \exp^{(-kt)} \tag{2.8}$$

where M and M_{eq} denote the sorbed mass at a certain time and at equilibrium, respectively. k is the first-order kinetic rate constant and t represents time.

Two-site / three-site desorption. The two-site model assumes that there are two classes of sorbing sites, two chemical reactions in series or a sorbent with an exterior part (easily accessible/fast) and an inner part (exchange slowly) (*13*).

$$\frac{M}{M_{eq}} = f_r \exp^{-k_r t} + f_s \exp^{-k_s t} \tag{2.9}$$

where f_r and f_s denote the fractions of contaminant present in the rapid and slow sorption/desorption compartment. Similar to the two-site desorption model, the three-site model additionally includes a very slow site class in order to fit data better (e.g. ref. *45*).

Continuum-site desorption. This model assumes the existence of a diverse distribution of desorption rate constants which is described by a probability density function (pdf). Culver et al. (*15*) used a gamma pdf to simulate a continuum of sorption/desorption rates

or diffusion domains. This gamma model assumes that desorption from heterogeneous sites occurs over a continuum of energies and rates.

$$f(k) = \frac{\varphi^{\eta} K^{\eta-1} \exp^{(-\varphi K)}}{\Gamma(\eta)} \tag{2.10}$$

where φ and η are the gamma distribution parameters for the probability *f* of a domain with desorption rate *k*.

Retarded intraparticle pore diffusion. This model describes the diffusion of molecules through the fixed intraparticle pore system inside the sorbent particles and aggregates. It assumes the aqueous-phase diffusion of the solute within pores inside particles mediated by retardation resulting from instantaneous sorption at sorption sites (e.g. pore walls) (see Figure 2.1) (*4, 52*). Assuming the matrix grains are spherically symmetric, the diffusion process can be described by Fick's 2nd Law in spherical coordinates:

$$\frac{\partial C}{\partial t} = D_a \left[\frac{\partial^2 C}{\partial r^2} + \frac{2}{r} \frac{\partial C}{\partial r} \right] \tag{2.11}$$

where D_a denotes the apparent diffusion coefficient and *r* is the radial distance from the center of a grain.

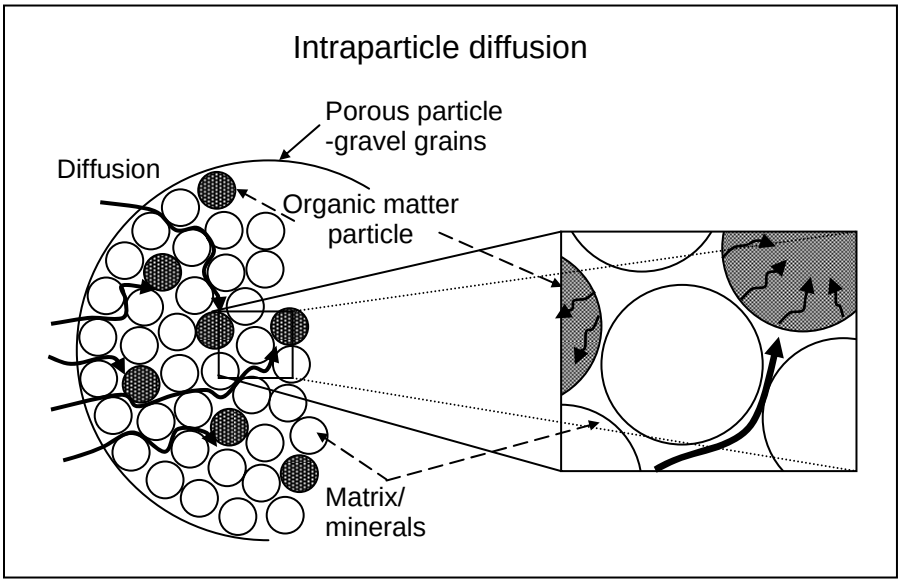

FIGURE. 2.1 Physical concepts of the intraparticel diffusion model (from Kleineidam et al. (*ref. 20* in chapter 1), Reproduced with permission)

This model is getting more and more accepted compared to other models because of the clear physical concept for the processes governing the sorption kinetics. It offers an opportunity to estimate the apparent diffusion coefficient (D_a) a priori on the basis of correlations with chemical and sorbent properties. It is possible to simulate the approximate time scale of the sorption and desorption only based on the chemical and sorbent properties. Therefore, this model can be used as a tool to quickly predict the mobility of an organic pollutant in the environment.

2.2 Thermodynamics of Sorption/Desorption

Similar to other physico-chemical reactions, sorption/desorption processes can be studied using different methods. One way is to measure the sorbate concentrations in both aqueous and solid phase at a series of times after the reaction is initiated. Another way is to monitor the sorption/desorption process at a series of different temperatures. It includes the temperature effects on both equilibrium and kinetic sorption/desorption. Sorption occurs when the free energy of the interaction between sorbent and sorbate is negative. The thermodynamic study gives improved insight on the molecular interactions between sorbate and sorbent, and provides a useful tool to assess the temperature dependency of sorption/desorption. For example, Johnson and Weber (*26*) carried out desorption experiments using heated and superheated water at different temperatures for rapid prediction of long-term desorption rates from soils and sediments based on the activation energies determined.

2.2.1 Temperature Dependence of Sorption/Desorption Equilibrium

Upon sorption from aqueous solution, an organic molecule exchanges one set of interactions with the solvent for another set of interactions with the sorbent. The driving forces in the sorption process fall into two categories: enthalpy-related forces and entropy-related forces. The former one affects the relative affinity of a compound to the sorbent compared to the solvent. These intermolecular forces include London-van-der-Waals forces, hydrogen bonds, ligand exchange, dipole-dipole interactions and chemisorption. The entropy-related forces include the change in randomness or disorder

of the sediment/water system (*21, 22*). The entropy in aqueous phase is increased resulting from the increasing disorder due to the disappearance of the highly structured water cage around the dissolved compounds, and the entropy in sorbent will also increase due to the entrance of sorbate. For hydrophobic molecules in aqueous systems, the so-called "hydrophobic bonding", a term describing the combination of the London dispersion forces between sorbate and sorbent and the repulsion forces in the solution, is the predominant driving force which leads to sorption (*21*). The magnitude of this physical sorption force can be determined from the isosteric heats of the sorption/desorption processes. The effect of temperature on sorption equilibrium is a direct indication of the sorption strength. For weaker bonds, less influence of temperature is expected due to the lower sorption enthalpy (*21*).

Based on thermodynamics, using the fugacity approach, the sorption/desorption equilibrium can be defined as the state at which the compound fugacities in the sorbent and aqueous phases are equal. Generally sorption/desorption processes are exothermic/endothermic, therefore sorption capacity decreases with increasing temperature. The sorption/desorption enthalpies can be calculated using the Clausius-Clapeyron equation (see chapter 5) or the Van't Hoff plot:

$$\Delta H_{a,d} = -R \frac{d \ln K_d}{d(1/T)} \tag{2.12}$$

where $\Delta H_{a,d}$ denotes the sorption/desorption enthalpy change [kJ mol^{-1}], R and T is the gas constant and temperature [K], respectively.

2.2.2 Temperature Dependence of Sorption/Desorption Kinetics

The dependency of sorption/desorption rates on temperature can be quantified by activation energies, which essentially describe how chemical rate constants vary with temperatures. The activation energy can be calculated with the Arrhenius equation:

$$k = Ae^{-E_a/RT} \tag{2.13}$$

where A is the Arrhenius preexponential factor, E_a is the activation energy [kJ mol^{-1}], and R is the gas constant. k denotes the chemical reaction rate. High values for E_a indicate that the rate of reaction is more sensitive to temperature.

2.3 Experimental Methodology

Batch and column experiments are the two popular techniques for sorption/desorption studies. The batch technique is used not only for equilibrium sorption studies but also for sorption kinetics. Column techniques are mainly used to study desorption kinetics. The column's effluent profile results from both hydrodynamic dispersion and sorption/desorption processes. Therefore it is a more realistic simulation of field scenarios.

2.3.1 Batch Techniques

In batch experiments on sorptive uptake the distribution coefficient K_d is determined based on mass balances. Usually the sorbent is first brought into contact with water, which is then spiked with the solute. The decrease of the aqueous concentration of the solute determines the amount of compound sorbed. A prerequisite is that the reduction of the aqueous concentration is due solely to sorption of the compound by the sorbent. If volatilization, degradation (biotic and abiotic), or sorption of the solute onto glass or seals occurs, a correction term in the mass balance equation is necessary. The decrease of the aqueous concentration due to sorption should be significantly higher than the analytical errors of the aqueous concentration measurements, which are typically between 5% and 15%. In batch experiments, some general issues need to be taken into account:

K_d estimation should be the first step in the experimental design in order to enable selection of a suitable solid-to-water ratio. For organic compounds, the K_d value can be estimated by $K_d = K_{oc} f_{oc}$, where the K_{oc} value can be estimated from K_{ow} or the aqueous solubility (S) (see Figure 4 in *ref. 2*). K_{ow} and S values are, for instance, listed in Verschueren (*50*) or Schwarzenbach et al. (*40*), while f_{oc} can be measured directly by combustion under oxygen and subsequent quantification of the CO_2. This so-called K_{oc} concept is only valid for linear sorption. Alternatively, according to Allen-King et al. (*2*) a solubility normalized sorption coefficient K_{Fr}^* can be used which for HOCs lies

between 60 to 160 μg/kg. With such an approach the non-linearity of the expected sorption isotherm can be taken into account.

Triplicate vials should be used for all experiments**.** Vial types range from flame-sealed glass ampoules, crimp top glass vials that are sealed with PTFE-lined butyl rubber septa (Alltech ®), to centrifugation tubes. For relatively quick sorption tests crimp top glass vials can be used, while for long-term experiments, flame-sealed glass ampoules are recommended.

Loss in the system, blanks. In any case, compound loss as a result of sorption to the septum or diffusive escape from the vial has to be quantified. Therefore, each concentration step should also include triplicate control vials with no sorbent but the same amount of solute as the test samples. Additionally, blank vials with the same amount of sorbent as in the test samples but no solute should be used to determine any background contamination by target compounds.

The headspace in the vial should be less than 5-10% of the total volume in order to minimize the mass partitioning to the gas phase. For non-volatile compounds, such as some pesticides, the size of the headspace is less relevant.

Minimizing potential biodegradation. The water and the sorbent used in the experiment should be pre-treated as follows: De-ionized Millipore® water can be de-oxygenated by purging with nitrogen gas in order to reduce potential aerobic biodegradation. Furthermore, sodium azide can be added to the water (200 mg L^{-1}) in order to inhibit bacterial growth. Alternative methods of limiting biodegradation are, for instance, poisoning by $HgCl_2$ or irradiation.

Degassing. Sorbent samples, which have significant intraparticle porosity, should first be submerged in a small amount of water in order to extrude trapped gases in a vacuum degasser. This allows water to replace air in the pore space. The degree of vacuum and evacuation time depends on the sorbent material and its grain size. The procedure can be

finished after the disappearance of bubbles from the liquid phase. The amount of water should be weighed before and after degassing to account for water loss under vacuum. After this step the reactor vials can be filled with water to the expected volume.

Selection of the equilibrium water phase concentration (C_w). In order to represent a wide range of environmental conditions, the equilibrium concentration in the water phase should cover about three orders of magnitude. For logarithmic plots, it is important to use constant interval distances between log C_w/S values along the abscissa axis. For example, a 6 point sorption isotherm with C_w/S values of 0.001, 0.003, 0.01, 0.03, 0.1 and 0.3.

Water/solid ratio. The optimum water/solid ratio can be calculated based on K_d and the desired equilibrium water phase concentration:

$$K_d = \frac{C_s}{C_w} = \frac{(X_{tot} - X_w)V_w}{X_w m_d} \quad \rightarrow \quad \frac{V_w}{m_d} = \frac{K_d X_w}{X_{tot} - X_w} = K_d \beta \tag{2.14}$$

where X_{tot} is the initial contaminant mass spiked to the water, X_w is the mass of contaminant in water. V_w denotes the volume of water and m_d is the dry mass of solid. β represents the ratio of solute mass dissolved to mass in the solid phase in a batch system.

Note, that this equation has to include a factor to correct for losses in the system if this is relevant (as determined by the controls). Since some of the solute adheres to the sorbent in the test vial, the mass loss in the blank due to secondary processes (e.g. diffusion and take up by the septum) may seem higher. It is therefore important to express these mass losses proportional to concentrations.

As a rule of thumb, one should aim to sorb at least half of the solutes spiked to the water (β = 1). In this case, the water to solid ratio (V_w/m_d) required to achieve 50% equilibrium sorption equals K_d. The smallest K_d that can be measured under these assumptions is about 0.5 (e.g. 50 mL of water and 100 g of dry solid).

Sorption competition from other solvents. If solvents such as methanol are required to establish stock solutions, their concentration should be kept below 0.5 % of the water

volume in order to avoid sorption competition or cosolvent effects. By following this limitation, a series of stock solutions of different concentrations can be prepared in order to facilitate the spiking of samples.

Mass balance. The solid phase concentration (C_s) is determined by the difference of the total mass injected into the reactor and the measured equilibrium concentration in the water phase. The following errors are possible: (1) Mass losses in the reactor system (e.g. volatilization into the vial headspace and further diffusion into the caps and/or diffusive losses from the vial); (2) biodegradation that could not be eliminated by de-oxygenation and poisoning; (3) measurement errors of the concentration in the water phase. For the latter, batch experiments usually have much higher water to solid ratios than those in column packings and the determination of K_d values involves significant errors if the difference of the initial concentration in the spiked water and after equilibration is below 50% (e.g. 30% error in $K_d = 0.5$ if an error in X_w of 15% is assumed and errors in X_{tot}, V_w and m_d are negligible). One possibility to minimize this is to adjust the water-to-solid ratio by increasing sorption of the solute in the reactor (decreasing β). This will lead to a smaller influence of the measurement error due to a more drastic decrease of the equilibrium aqueous concentration. In other words, sorption can be determined with high accuracy if more solute is sorbed. However, care should be taken that the concentration in the water does not approach the detection limit, which again involves increases in the analytical errors. For long experimental times (> 4 weeks) or under higher temperatures, the reactor caps and the sorbent should also be extracted by a strong solvent (e.g., toluene) after the experiment to ensure a good mass balance even for non-volatile compounds (see Figure 4.2 in chapter 4). For short equilibration periods such losses can be neglected from the mass balance calculation.

Shaking. All the reactor vials should be shaken in order to facilitate mass transfer of the solute between the solid particles and water. This is especially important initially when steep gradients exist. For PAH sorption experiments, shaking takes place continuously during the first 3 days. After that it continues sporadically by hand for several times per

day. The shaking frequency drops to once per day after one week and to one time per week for experimental times longer than one month.

DOC (dissolved organic carbon) effect. The solubility enhancement due to DOC usually increases the measured water phase concentration and thus leads to a smaller K_d. This necessitates DOC measurements for correction when sufficient DOC levels are present to disturb the experiment (e.g. more than 20 mg L^{-1} and compounds with log K_{ow} > 4).

Sampling and analysis. After equilibration, the vials are centrifuged in order to separate the sorbent from the solution. For some sorbents, such as activated carbon, filtration is preferable to obtain a clear liquid. Subsequently an aliquot of the supernatant water can be sampled. The solute is extracted from the water with a suitable solvent, e.g. cyclohexane. Recovery rates can be estimated based on K_{ow} and the solvent to water ratio. Internal standards (e.g. deuteriated compounds) can be used, if the recovery is significant less than 100%. Depending on the characteristics of the solute, the concentration is determined by, for instance, HPLC or GC. Direct injection of supernatant using a HPLC syringe without solvent phase transfer and addition of internal standard can also be adopted with HPLC (see chapter 4). Using this sampling method, a standard calibration has to be carried out with the same injection size of the standard solution. Sorption isotherms are then plotted on a log-log diagram with C_s on the ordinate and C_w/S on the abscissa, in which the slope of the linear regression denotes $1/n$. For each concentration range (i.e. C_w/S value) an individual unit normalized Freundlich coefficient, K_{Fr}^*, can be determined from the slope.

The equilibration time is crucial in batch sorption experiments and is usually determined by pre-tests. A rough definition for sufficient equilibration is when K_d is stable between two successive measurements that are at least a factor of three apart (e.g. 3 days, then 10 days). Note, that K_d may be a much more robust measure for checking equilibration than aqueous concentration changes alone.

The equilibration time depends on the diffusion rate of the solute, the type of compound and sorbent particle size. For batch experiments (baths of limited volume) sorptive uptake can be calculated:

$$\frac{M}{M_{eq}} = 6\left(\frac{1}{\beta}+1\right)\sqrt{\frac{D_a\, t}{\pi\, r^2}} \tag{2.15}$$

where M is the mass that has diffused into a particle after a certain time t; M_{eq} denotes contaminant mass that is in the grain under equilibrium; r is the particle radius or diffusion distance; D_a is the effective or transient diffusion coefficient which depends on the diffusion coefficient in water (D_{aq}), the intraparticle porosity (ε), the bulk density (ρ) and K_d. Solving eq. 2.15 leads to:

$$t = \frac{\rho\,\pi\, r^2\left(\frac{M}{M_{eq}}\right)^2}{36\left(\frac{m_d}{V_w}\right)^2 K_d\, D_{aq}\, \varepsilon^2} \tag{2.16}$$

For a certain compound it is clear that with m_d (sorbent mass) and V_w (solution volume) being fixed for an optimal ratio and the other values being constants, the grain radius "r" is the most important term determining the equilibration time of the sorption uptake. Unfortunately, despite the very slow sorption kinetics most investigators combined relatively short contact time (on the order of weeks, days, and even hours) and non-pulverized sorbents (e.g. sandy soils) in their sorption uptake experiments. Under such conditions, for some sorbent/solute system, months to years of contact time may be needed to establish equilibrium. Therefore, short-term equilibration periods will likely leads to artifacts, even if this short-term equilibrium period is often justified on the basis of additional experiments conducted at only marginally longer contact times and which show uptake that is not significantly greater. However, long-term experiments (months to years) are not likely to be achieved in the laboratory. One possibility to shorten the equilibrium time is to shorten the diffusion distance in the intraparticle pathways in the sorbent. For instance, based on eq. 2.16, the equilibration can be reached 10000 times faster if the grain radius of the sorbent is reduced by factor 100. Pulverized samples with particle sizes smaller than 63 μm are recommended. Table 2.1 shows the equilibration time needed for phenanthrene for different grain size lignite and HC particles under

certain aqueous concentrations in this study. It illustrated that the kinetic - oriented artifacts can be ruled out by using pulverized samples in a relative short contact time.

TABLE 2.1. Comparison of batch equilibration times (day) at 20°C of phenanthrene on lignite and HC by using different sample grain radius based on the intraparticle diffusion kinetic model

Samples		Lignite		HC	
Intraparticle porosity[a]		0.8%		1.4%	
The equilibrium aqueous concentrations in vials		1.6% S_{solid}	11% S_{solid}	5.4% S_{solid}	51.7% S_{solid}
K_d values at each bottle point vials [L kg^{-1}]		44126	32214	160286	52404
Equilibrium time under different grain size [day]	r = 0.005 mm (lignite) r = 0.019 mm (HC) (M/M_{eq} = 0.50)	0.4	0.5	0.6	1.9
	r = 0.5 mm (lignite/HC) (M/M_{eq} = 0.20)	571	782	71	216
	r = 0.5 mm (lignite/HC) (M/M_{eq} = 0.50)	3570	4890	441	1350
D_{aq} of phenanthrene in water at 20°C [cm^2/s][b]		$5.86e^{-6}$			

[a] intraparticle porosity was calculated based on the pore volume (BET measurement, see chapter 3) and the bulk density of the sorbent with a equation of ε = IP/(IP+m_d/ρ);
[b] D_{aq} was calculated using $D_{aq} = 13.26x10^{-5}/(\eta^{1.14} V^{0.589})$ (*23*)

2.3.2 Column Techniques

Column studies are widely used for contaminant transport investigations, especially in studying the leaching behaviors from contaminated soils and sediments. In this study, desorption kinetics for phenanthrene on carbonaceous materials was investigated using breakthrough fronts in water-saturated columns. When no decomposition of target compound occurs, the solute transport in a saturated column is described by the advection-dispersion equation:

$$\frac{\partial C}{\partial t} = -v\frac{\partial C}{\partial x} + D_L\frac{\partial^2 C}{\partial x^2} - \frac{\partial q_s}{\partial t} \qquad (2.17)$$

where v is pore water flow velocity [m s^{-1}] and x is the longitudinal distance [m]. D_L denotes hydrodynamic dispersion coefficient [m^2 s^{-1}], q_s is the concentration in solid (mol L^{-1} pore water). The sorption kinetic term $\partial q_s/\partial t$ represents the sorption rate.

The shape of the breakthrough profiles is influenced by isotherm shape, dispersion, diffusion, and other mass transfer resistances. High dispersion and slow diffusion-limited

sorption will lead to early breakthrough of a concentration front at the column outlet. Nonlinear isotherms may lead to tailing and strongly asymmetrical breakthrough profiles. In addition, if sorption/desorption nonequilibrium occurs depending on sorption kinetics and the flow velocity or the mean residency time of the solute in the column very slow sorption kinetics will lead to early breakthrough. The sorption/desorption nonequilibrium in column experiments can be assessed using *Damkohler number,* which compares the sorption time scale with the residence time of the water (*3*):

$$D_k = \frac{R_d k}{v / L} \tag{2.18}$$

where k denotes the mass transfer rate constant, R_d is the retardation factor and L is the length of the column. *Damkohler number*s exceeding 10 are necessary for the local equilibrium assumption to be valid. Practically, it is very difficult to attain local equilibrium in column experiments even with very low flow velocity if the mass transfer rate is small.

Several models are employed to account for sorption kinetics in one-dimensional transport of sorbing chemicals through soil. Van Genuchten and Wierenga (*46, 47*) and Van Genuchten et al. (*48*) proposed a two-region nonequilibrium model for solute transport through an aggregated porous medium with advection, dispersion, and mass transfer to the immobile fluid. The pore space is divided into mobile water and immobile water regions. Advection and dispersion occur only in the mobile region. The aqueous concentration gradient between mobile and immobile regions is assumed to be the driving force for the mass transfer between these two regions.

In the two-site sorption model, sorption is divided into two domains: instantaneous local equilibrium and mass transfer limited (corresponding to two different kinds of sorption sites). The kinetic part is described by either a first-order model or molecular diffusion. Several researchers reported solute transport simulations with the first-order model (*8, 43, 49*). Meanwhile, the intraparticle diffusion model is widely adopted. Rao et al. (*36, 37*) compared sorption kinetic models and suggest that better predictions are obtained if mass transfer rates to aggregates are described by diffusion (Fick's 2nd law). Crittenden et

al. (*16*) analyzed the relative effects of various solute spreading mechanisms in saturated one-dimension columns and developed a model which includes the transport and retardation mechanisms of advection, axial dispersion, film diffusion, and intraparticle diffusion to describe the migration of nondegadable organic chemicals through a column of saturated, aggregate soil.

2.4 References

1. Adamson, A.W. *Physical chemistry of surfaces*, Wiley, New York, 1982.

2. Allen-King, R.M.; Grathwohl, P.; Ball, W.P. New modeling paradigms for the sorption of hydrophobic organic chemicals to heterogeneous carbonaceous matter in soils, sediments, and rocks. *Advances in water resources*, 2002, 25, 985-1016

3. Bahr, J.M.; Rubin, J. Direct comparison of kinetic and local equilibrium formulations for solute transport affected by surface reactions. *Water Resources Research*. 1987, 23, 438-452.

4. Ball, W.P.; Roberts, P.V. Long-term sorption of halogenated organic chemicals – part 2. Intraparticle diffusion. *Environ. Sci. Technol.* 1991b, 25, 1237-1249

5. Brusseau, M.L.; Rao, P.S.C. The influence of sorbent-organic matter interactions on sorptive nonequilibrium. *Chemosphere*, 1989, 18, 1691-1706

6. Brusseau, M.L.; Rao, P.S.C. Influence of sorbate structure on nonequilibrium sorption of organic compounds. *Environ. Sci. Technol*. 1991, 25, 1501-1506.

7. Brusseau, M.L.; Jessup, R.E.; Rao, P.S.C. Nonequilibrium sorption of organic chemicals: Elucidation of rate-limiting processes. *Environ. Sci. Technol*. 1991, 25, 134-142.

8. Cameron, D.R.; Klute, A. Convective-dispersion solute transport with a combined equilibrium and kinetic adsorption model. *Water Resour. Res.* 1977, 13, 183-188.

9. Chiou, C.T.; Peters, L.J.; Freed, V.H. A physical concept of soil-water equilibria for nonionic organic compounds. *Science* 1979, 206, 831-832.

10. Chiou, C.T. Soil sorption of organic pollutants and pesticides. In: Mayers RA, editor. *Encyclopedia of environmental analysis and remediation*. New York. John Wiley &Sons. 1998

11. Chiou C.T.; Kile D.E. Deviations from sorption linearity on soils of polar and nonpolar organic compounds at low relative concentrations. *Environ. Sci. Technol*. 1998, 32, 338-343.

12. Chiou, C.T.; Kile, D.E.; Rutherford, D.W.; Sheng, G.; Boyd, S. Sorption of selected compounds from water to a peat soil and its humic-acid and humin fractions: Potential sources of the sorption nonlinearity. *Environ. Sci. Technol*. 2000, 34, 1254-1258.

13. Cornelissen, G.; Rigterink, H.; Vrind, B.A.; ten Hulscherten, D. Th. E.M.; Ferdinandy, M.M.A.; van Noort, P.C.M. Two-stage desorption kinetics and in situ partitioning of hexachlorobenzene and dichlorobenzene in a contaminated sediment. *Chemosphere*, 1997, 35, 2405-2416.

14. Cornelissen, G.; Gustafsson, Ö.; Bucheli, T.D.; Jonker, M.T.O.; Koelmans, A.A.; van Noort, P.C.M. Extensive sorption of organic compounds to black carbon, coal, and kerogen in sediments and soils: mechanisms and consequences for distribtution, bioaccumulation, and biodegradation. *Environ. Sci. Technol*. 2005, 39, 6881-6895.

15. Culver, T.B.; Hallisey, S.P.; Sahoo, D.; Deitsch, J.J.; Smith, J.A. Modeling the desorption of organic contaminants from long-term contaminated soil using distributed mass transfer rates. *Environ. Sci. Technol.* 1997, 31, 1581-1588.

16. Crittenden, J.C.; Hutzler, N.J.; Geyer, D.G.; Oravitz, J.L.; Friedman, G. Transport of organic compounds with saturated flow: medel development and parameter sensitivity. *Water Resour. Res.* 1986, 22, 271-284.

17. Goldberg, E.D. *Black carbon in the environment.* John Wiley, New York, 1985.

18. Grathwohl, P. Influence of organic matter from soils and sediments from various origins on the sorption of some chlorinated aliphatic hydrocarbons: implications on K_{oc} correlations. *Environ. Sci. Technol*. 1990, 24, 1687.

19. Grathwohl, P. *Diffusion in natural porous media*. Kluwer Academic Publishers, Boston, 1998

20. Gustafsson, Ö.; Bucheli, T.D.; Kukulska, Z.; Andersson, M.; Largeau, C.; Rouzard, J.N.; Reddy, C.M.; Eglinton, T.I. Evaluation of a protocol for the quantification of black carbon in sediments. *Global Biogeochem. Cycles*. 2001, 15, 881

21. Hamaker, J.W.; Thompson, J.M. Adsorption. In C.A.I. Goring and J.W. Hamaker (eds.). *Organic chemicals in the soil environment*. Vol. 1. Marcel Dekker, Inc., New York, 1972, 49-143

22. Hassett, J.P.; Banwert, W.L. The sorption of nonpolar organics by soils and sediments. In B.L. Sawhney and K. Brown (eds). *Reactions and movement of organic chemicals in soils*. SSSA Special publication no.22. Sol Science Society of America and American Society of Agronomy, 1989, 31-44.

23. Hayduk, W; Laudie, H. Prediction of diffusion coefficients for nonelectronlytes in dilute aqueous solutions. *AIChEJ*. 1974, 20, 611-615.

24. Huang, W.; Young, T.T.; Schlautman, M.A.; Yu, H.; Weber, W.J., Jr. A distributed reactivity model for sorption by soils and sediments. 9. General isotherm nonlinearity and applicability of the dual reactive domain model. *Environ. Sci. Technol*. 1997, 31, 1703.

25. Huang, W.; Weber, W.J., Jr.; A distributed reactivity model for sorption by soils and sediments. 10. Relationships between desorption, hysteresis, and the chemical characteristics of organic domains. *Environ. Sci. Technol*. 1997, 31, 2562

26. Johnson, M.D.; Weber, W.J.Jr. Rapid prediction of long-term rates of contaminant desorption from soils and sediments. *Environ. Sci. Technol*. 2001, 35, 427-433

27. Karickhoff, S.W.; Brown, D.S.; Scott, T.A. Sorption of hydrophobic pollutants on natural sediments and soils. *Chemosphere*, 1981, 10, 833-846.

28. Klieneidam, S.; Rügner, H.; Ligouis, B.; Grathwohl, P. Organic matter facies and equilibrium sorption of phenanthrene. *Environ. Sci. Technol*. 1999, 33, 1637-1644.

29. Kleineidam, S.; Schüth, C.; Grathwohl, P. Solubility-normalized combined adsorption-partitioning sorption isotherms for organic pollutants. *Environ. Sci. Technol*. 2002, 36, 4689-4697.

30. LeBoeuf, E.J.; Weber, W.J., Jr. A distributed reactivity model for sorption by soils and sediments. 8. Sorbent organic domains: discovery of a humic acid glass transition and an argument for a polymer-based model. *Environ. Sci. Technol*. 1997, 31, 1697-1702.

31. Manes, M. Activated carbon adsorption fundamentals. In Encyclopedia of environmental analysis and remediation. R.A. Myers. Ed. Wiely, New York, 1998, 26-68.

32. McGinley P.M.; Katz, L.E.; Weber, W.J.,Jr. A distributed reactivity model for sorption by soils and sediments. 2. Multicomponent system and competitive effects. *Environ. Sci. Technol*. 1993, 27, 1524-1531.

33. Pignatello, J.J.; Ferrandino, F.J.; Huang, L.Q. Elution of aged and freshly added herbicides from a soil. *Environ. Sci. Technol*. 1993, 27, 1563-1571.

34. Pignatello, J.J.; Xing, B. Mechanisms of slow sorption of organic chemicals to natural particles. *Environ. Sci. Technol*. 1996, 30, 1-11.

35. Pignatello, J.J. The measurement and interpretation of sorption and desorption rates for organic compounds in soil media. *Advances in Agronomy*, 2000, 69, 1-73.

36. Rao, P.S.C.; Rolston, D.E.; Jseeup, R.E.; Davidson, J.M. Solute transport in aggregated porous media: theoretical and experimental evaluation. *Soil Sci. Soc. Am. J.*, 1980, 44, 1139-1146.

37. Rao, P.S.C.; Jessup, R.E.; Rolston, D.E.; Davidson, J.M.; Kilcrease, D.P. Experimental and mathematical description of nonadsorbed solute transfer by diffusion in spherical aggregates. Soil Sci. Soc. Am. J., 1980, 44, 684-688.

38. Rügner, H.; Kleineidam, S.; Grathwohl, P. Long term sorption kinetics of phenanthrene in aquifer materials. *Environ. Sci. Technol*. 1999, 33, 1645-1651.

39. Schmidt, M.W.I.; Noack, A.G. Black carbon in soils and sediments: Analysis distribution, implications, and current challenges. *Global Biogeochem. Cycles*. 2000, 14, 777.

40. Schwarzenbach, R.P.; Gschwend, P.M. Imboden, D.M. *Environmental organic chemistry*. 1993. John Wiley & Sons. New York.

41. Seth, R.; Mackay, D.; Muncke, J. Estimating the organic carbon partition coefficient and its variability for hydrophobic chemicals. *Environ. Sci. Technol*. 1999, 33, 2390-2394.

42. Sposito, G. *The Chemistry of soils*. Oxford University Press, New York. 1989

43. Spurlock, f.C.; Huang, K.; van Genuchten, M.T. Isotherm nonlinearity and nonequilibrium sorption effects on transport of fenuron and monuron in soil columns. *Eviron. Sci. Technol*. 1995, 29, 1000-1007.

44. Steinberg, S.M.; Pignatello, J.J.; Sawhney, B.L. Persistence of 1,2-Dibromoetnane in soil: Entrapment in intraparticle micropores. *Environ. Eng. Sci.* 1987, 21, 1201-1208.

45. Ten Hulscher,T.E.M.; Vrind, B.A.; van den Heuvel, H.; van der Velde, L.E.; van Noort, P.C.M.; Beurskens, J.E.M.; Govers, H.A.J. Triphasic desorption of highly resistant chlorobenzenes, polychlorinated biphenyls, and polycyclic aromatic hydrocarbons in field contaminated sediment. *Environ. Sci. Technol*. 1999, 33, 126-132.

46. van Genuchten, M.T.; Wierenga, P.J. Mass transfer studies in sorbing porous media. I. An analytical solutions. Soil Sci. Soc. Am, J. 1976, 40, 473-480.

47. van Genuchten, M.T.; Wierenga, P.J. Mass transfer studies in sorbing porous media. II. Experimental evaluation with tritium (^3H_2O). Soil Sci. Soc. Am, J. 1977, 41, 272-278.

48. van Genuchten, M.T.; Wierenga, P.J.; O'Connor, G.A. Mass transfer studies in sorbing porous media: III. Experimental evaluation with 2,4,5-T. *Soil Sci. Soc. Am, J.* 1977, 41, 278-285.

49. van Genuchten, M.T.; Wierenga, P.J. Two-site/two-region models for pesticide transport and degradation: Theoretical development and analytical solutions. *Soil Sci. Soc. Am, J.* 1989, 53, 1303-1310.

50. Verschueren, K. *Handbook of environmental data on organic chemicals*, 2nd Ed, van Nostrand Reinhold Company Inc., New York, 1983

51. Weber, W.J., Jr.; McGinley, P.M.; Katz, L.E. A distributed reactivity model for sorption by soils and sediments. 1. Conceptual basis and equilibrium assessments. *Environ. Sci. Technol*. 1992, 26, 1955-1962.

52. Wu, S.C.; Gschwend, P.M. Sorption kinetics of hydrophobic organic compounds to natural sediments and soils. *Environ. Sci. Technol*. 1986, 20, 717-725.

53. Xia, G.; Ball, W.P. Adsorption-partitioning uptake of nine low-polarity organic chemicals on a natural sorbents. *Environ. Sci. Technol*. 1999, 33, 262.

54. Xing, B.; Gigliotti, B.; Pignatello, J.J. Competitive sorption between atrazine and other organic compounds in soils and model sorbents. *Environ. Sci. Technol*. 1996, 30, 2432-2440.

55. Xing, B.; Pignatello, J.J. Dual-model sorption of low-polarity compounds in glassy poly(viny chloride) and soil organic matter. *Environ. Sci. Technol*. 1996, 31, 792-799.

56. Young, T.M.; Weber, W.J., Jr. A distributed reactivity model for sorption by soils and sediments. 3. Effects of diagenetic processes on sorption energetics. *Environ. Sci. Technol*. 1995, 29, 92.

Chapter 3

SAMPLE CHARACTERIZATION AND NATIVE PAH EXTRACTION

3.1 Sample Characterization

3.1.1 Sample Selection and Preparation

Sample selection. Natural and thermally-altered carbonaceous materials (coals, chars, coke) are nowadays found in many soils and sediments due to the anthropogenic impact (e.g. industrial activities, traffic) on the natural environment. In this study, carbonaceous samples from a range of natural organic materials following the rank of coalification (Pahokee peat, lignite and high-volatile bituminous coal (HC)) and two different soil samples (Anthrosol (AS5) and mineral soil chernozem (MS4)), which were known to contain carbonaceous particles, were selected for the hysteresis experiments. Anthrosol (AS5) was sampled in the western urban area of Krefeld (Germany), 1 km from a railway track. The area was a former agricultural site and had been transformed into grassland 7 years prior to collection. The mineral soil (MS4) was sampled in Hildesheim (Germany). This soil developed on loess and under agriculture. Organic petrographic analysis proved the existence of charred organic carbon (30 % of total OC) in this soil. The two soils were air-dried and the visible plant roots were removed manually. In addition to the above samples, more pure carbonaceous materials were characterized, including sub-bituminous coal, commercial charcoal, lignite coke and hard coal coke.

Pulverization. In order to shorten the sorption/desorption equlibrium time, the selected sorbents were pulverized using a zirconium oxide planet ball mill (Laborette, Fritsch) to a

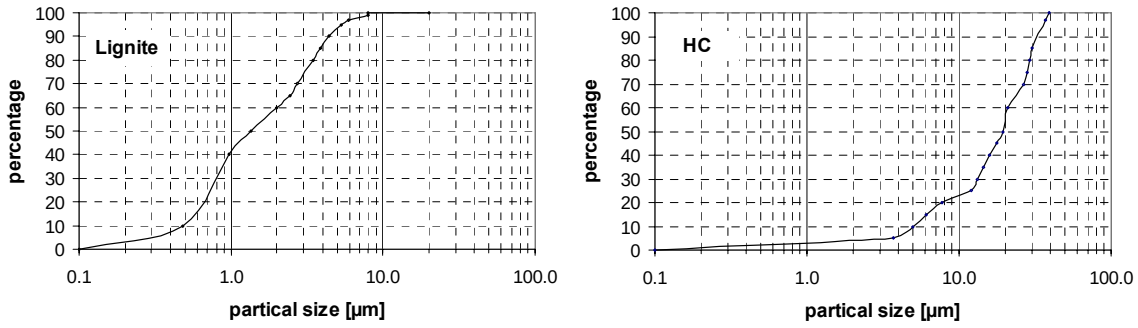

FIGURE 3.1 Two examples for the grain size distribution of geosorbents after pulverization

grain size of less than 0.01 - 0.03 mm (determined using a laser particle size analyzer GALAI CIS-50), except the AS5 sample in which the sieved size fraction of less than 0.063mm was used. Figure 3.1 shows two examples of the grain size distribution after pulverization.

3.1.2 Sample Physicochemical Characterization

All selected sorbents were characterized in terms of organic carbon content, hydrogen and nitrogen content, solid density, specific surface area and pore volume as well as microporosity. Organic petrographic analyses were also carried out to quantify the maceral distribution in the carbonaceous materials and to quantify the different organic carbon fractions in the soil samples.

Organic carbon content. The organic carbon content (OC), as well as the hydrogen (H) and nitrogen (N) contents of the samples were measured by elemental analysis (Vario EL, Elementar). The values determined are shown in Table 3.1 and in Table 4.1.

TABLE 3.1. Physico-chemical characterization of the investigated samples*

Geosorbents	OC [%]	H [%]	N [%]	SA[a] [m^2/ g]	IP[a] [cm^3/kg]	IP_M[a] [cm^3/kg]	Density[b] [g/cm^3]
Sub-bituminous coal	55.1	4.71	1.20	0.56	2.1	n.d.	1.43
Charcoal	81.7	3.01	0.27	210	112	64	1.41
Lignite coke	88.0	0.76	0.31	306	218	73	2.03

* Data from Kleineidam et al. (*3*)
Organic carbon (OC), hydrogen (H) and nitrogen (N) contents; n.d.: not determined
[a] Specific surface area (SA), pore volume (IP) and microporosity (IP_M) were determined by N_2-BET method (ASAP 2010 Micromeritics)
[b] Density was determined using a helium pycnometer Accu Pyc 1330 from Micromeretics.

Pore volume and specific surface area. Specific surface area (SA), intraparticle pore volumes (IP) and microporosity (IP_M) were measured using the N_2 BET-method (ASAP 2010 Micromeritics) with the pulverized samples. The N_2 adsorption isotherm (at a constant temperature of 77K) is determined by successively increasing the gas partial pressures, starting from low pressure until the saturation vapor pressure is reached. After this, desorption is started by decreasing the partial pressure stepwise. The sorption isotherm branch is used to calculate the internal surface area of the sample based on the

BET point B method. The desorption branch allows the calculation of pore size and distribution. Figure 3.2 shows the N_2 sorption/desorption isotherms of the samples investigated. The values measured are compiled in Table 3.1 and in Table 4.1 in chapter 4. It illustrates that, in general, the carbon content and total pore volume, as well as the micropore volume, increases with increasing rank of coals because of the thermal alteration of the organic matter during colification.

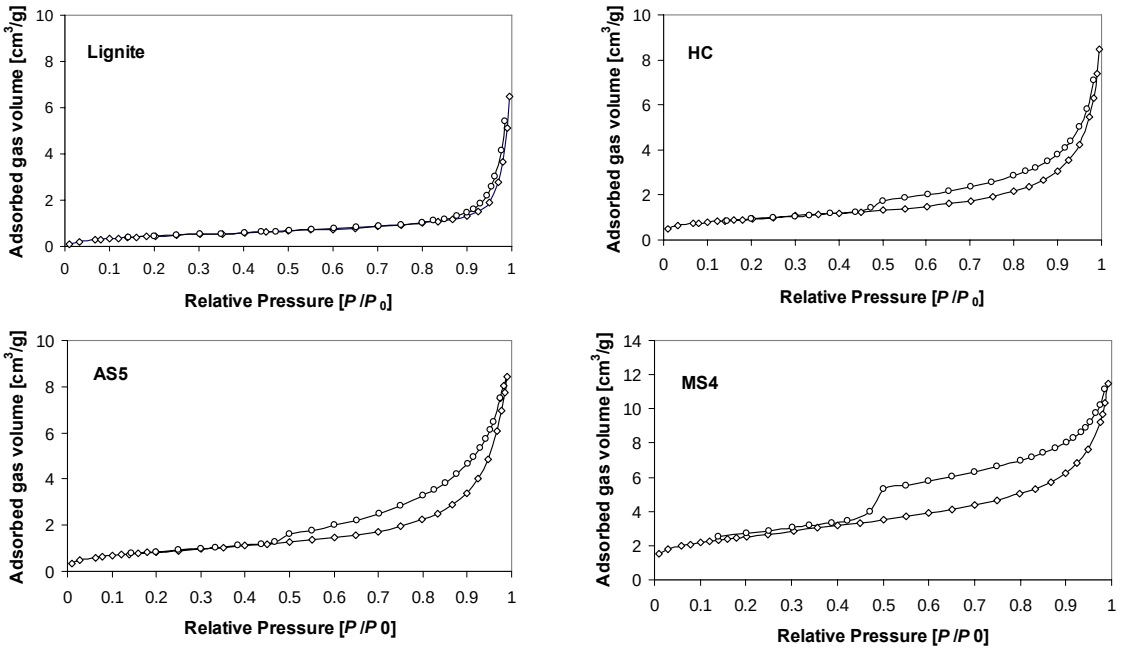

FIGURE 3.2 Sorption and desorption isotherms of pulverized samples using N_2-BET method

Organic petrographic analysis. The organic matter sources and maturation stages of the coals were determined using optical microscopy (transmitted and reflected light). While peat and lignite still show fluorescence, the higher rank coals and the different cokes show increasing reflectance under white light. The charcoals show the typical open cellular structure of wood tissue. The petrographic compositions of the two soil samples were also quantified (see Table 3.2).

Coal is an extremely complex heterogeneous material. Coal is a rock formed by geological processes and is composed of a number of distinct organic entities called macerals and smaller amounts of inorganic minerals. The term "maceral" describes

organic solids analogous to the minerals composing rocks. On the microscopic level, each maceral group has distinct physical and chemical properties and is defined according to their visual appearance. In coal petrography the macerals are grouped into three groups, each of which includes several maceral types. The groups are liptinite, vitrinite, and inertinite. Liptinites are composed of hydrogen-rich hydrocarbons derived from spores, pollens, cuticles, and resins in the original plant material. Vitrinites are composed of "gelified" wood, bark, and roots, derived from cell wall materials (woody tissue) of plants, which are chemically composed of cellulose and lignin. Inertinites are mainly oxidation products of other macerals and are consequently richer in carbon than liptinites or vitrinites. The inertinite group includes fusinite, most of which is fossil charcoal, derived from ancient peat fires. Table 3.2 shows the volume percentage of each maceral group in the investigated carbonaceous materials. In all samples, the huminite/vitrinite is the dominant maceral group, followed by liptinite.

TABLE 3.2. Percentage of different maceral groups in different coals*

Sample	Huminite[a]	Liptinite	Inertinite	Vitrinite	Natural char
Pahokee peat	73.6	16.8	9.6		n.d
Lignite	64	33	3		n.d
Sub-bituminous coal		10	16	73	1.8
High-volatile bituminous coal		19	4	76	2.4

* Data from Ligouis & Doubinger (*4*) and Ligouis et al. (*5*)

[a]The term huminite is defined only for lignites/soft brown coals. For other coals, the term vitrinite nomenclature is used. n.d: not detected

Organic petrography was also used to analyse the composition of the organic matter in Pahokee peat and the two soil samples. The quantification is shown in Table 3.3. Pahokee

TABLE 3.3. Composition of different organic matter in Pahokee peat and two soil samples*

Sample	Recent organic matter	Lignite-hc-charcoal	Coke forms	Residues of coal hydrogenation	Natural char
Pahokee peat	84.6	15.4	n.d	n.d	n.d
AS5[a]	54.6	8.3	23.3	4.6	7.8
MS4	69.8	22.5	6.5	n.d	1.1

* Data from Ligouis, B. (see Appendix); more sample characterization, see Abelmann et al. (*1*)

[a] The pulverized originate AS5 sample, not the portion of grain size < 0.0063 mm. n.d.: not detected

peat contains predominately recent organic matters (85%), whereas charred materials account for 30% of the organic matter in the MS4 sample. The organic petrograhic analysis was not possible for the size fraction < 0.0063 mm of the AS5 sample. Two examples of detailed information of the organic petrography are shown in Appendix I and II. Appendix III compiles the microscope images of the different coals.

3.2 Native PAH Loading

Polycyclic Aromatic Hydrocarbons (PAHs). PAHs include a class of toxic organic chemicals consisting of two or more benzene rings in linear, angular, or cluster arrangements. Out of the large number of PAHs and their isomers, the U.S. Environmental Protection Agency (EPA) selected 16 PAHs in the Consent Decree Priority Pollutant list due to their toxicity and frequent occurrence in the environment:

Naphthalene (Nap, $C_{10}H_8$)	Acenapthylene (Any, $C_{12}H_8$)
Acenaphthene (Ace, $C_{12}H_{10}$)	Fluorene (Fl, C13H10)
Phenanthrene (Phe, $C_{14}H_{10}$)	Anthracene (Ant)
Fluoranthene (Fth, $C_{16}H_{10}$)	Pyrene (Py, $C_{16}H_{10}$)
Benzo(a)anthracene (B(a)A, $C_{18}H_{12}$)	Chrysene (Chr, $C_{18}H_{12}$)
Bezo(b)fluoranthene (B(b)F, $C_{20}H_{12}$)	Benzo(k)fluoranthene (B(k)F, $C_{20}H_{12}$)
Benzo(a)pyrene (B(a)P, $C_{20}H_{12}$)	Dibenz(a,h)anthracene (D(ah)A), $C_{22}H_{14}$)
Benzo(ghi)perylene (BP, $C_{22}H_{12}$)	Indeno(1,2,3-cd)pyrene (IP, $C_{22}H_{12}$)

Accelerated solvent extraction (ASE). All samples in this study contain traces of native PAHs. Concentration loads of the native EPA PAHs (excluding Naphthalene due to its higher background) and their congenger distribution patterns were determined in the investigated samples by an accelerated solvent extraction (ASE) procedure. ASE is a method for extracting organic and inorganic compounds from a variety of solid sample and accelerates the traditional extraction process by using solvents at elevated temperatures and pressures. The ASE procedure was automated using an ASE 300. About 5 g pulverized samples were mixed with about 30 - 40g cleaned quartz sand in order to improve permeability. The mixture was packed into an extraction cell and contained by a double layer glass-fiber filter (1 μm diameter pore) at each end of the cell in order to prevent fine particles from eluting into the collection bottles. The samples were first

leached with Millipore water (see chapter 4). After the aqueous leaching, the sample is sequentially extracted with acetone and two times with toluene (100°C for acetone and 150°C for toluene; 100 bar) with an equilibration time of 10 minutes each. The second toluene extraction step is expected to recover less than 5% PAHs compared to the first toluene extraction, which implies a complete PAH extraction from the investigated samples. The collected extracts were analyzed for PAHs by GC/MS (Hewlett-Packard HP-6890 equipped with a 30 m DB-5 capillary column, coupled to the HP-5973 mass spectrometer; GC column temperature program: 65°C for 4 min, heated to 270°C at 10°C/min and held for 10 min, then to 310°C at 10°C/min and held for 6.5 min; carrier gas: helium at a constant flow rate of 1.0 mi/min; 1 µl sample injection size utilizing splitless mode). A stock solution of deuterated PAH surrogates (naphthalene-d8, acenaphthalene-d10, phenanthrene-d10, chrysene-d12 and perylene-d12) was added to the leachates as internal standard and a standard solution containing the 16 EPA PAHs and 5 deuterated surrogates was measured to determine the relative response factors. The extracted acetone was transferred into cyclohexane whereas the toluene extract was used directly for the GC/MS analysis. The total native PAH loading was calculated as the sum of PAHs detected in water, acetone, and toluene.

Ran et al. (*6*) compared the extraction efficiency of traditional Soxhlet extraction using dichloromethane (DCM) with the ASE method using a 1:1 acetone/hexane mixture, as well as a three step acetone and toluene extraction. Results showed that the acetone-toluene-ASE method recovered higher PAH concentrations than the 1:1 acetone/hexane-ASE or the Soxhlet extraction. In fact, the second and third toluene extraction steps still extracted considerable PAH amounts compared to the first acetone extraction step. The sum of the 16 EPA PAHs determined using acetone-toluene-ASE method were about 2 times the amount in the Soxhlet-extracted samples. The 1:1 acetone/hexane-ASE extracted about 1.5 times more than the Soxhlet, similar to the acetone extracted fraction in the acetone-toluene-ASE method. The above results demonstrate that ASE is a very effective, time saving extraction method for contaminated materials when the operating variables, such as sequence of solvents and temperature, are optimized.

Results. Figure 3.3 shows the total loading of the native 16 EPA PAHs for the investigated samples. The distribution pattern of the PAHs in each sample is illustrated in Figure 3.4. The high-volatile bituminous coal contains the highest PAHs concentration, up to 47 mg/kg, followed by Charcoal (16.1 mg/kg), AS5 (< 0.0063 mm fraction, 6.45 mg/kg), Pahokee peat (1.53 mg/kg), bituminous coal (1.1 mg/kg), and lignite (0.9 mg/kg). Less than 0.5 mg/kg PAHs were extracted from MS4 and the two coke samples. Despite the Naphthalene background (from the atmosphere), Figure 3.4 shows that in most cases phenathrene is a dominant compound in all the samples, up to 20-45%.

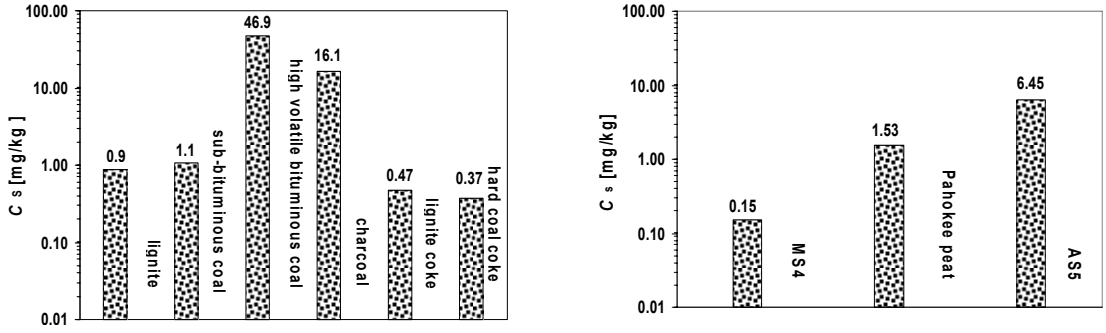

FIGURE 3.3 Concentration of the native 16 EPA PAHs in the investigated samples; three step acetone-toluene-toluene accelerated solvent extraction (ASE)

3.3 Leaching of Dissolved Organic Carbon (DOC)

For non-polar organic compounds, which have high affinity to natural organic matter, the solubility enhancement due to DOC present in the aqueous solution can be significant. The association of compounds with DOC leads to misinterpretation of the sorbate distribution in batch/column systems. To eliminate the DOC enhancement effect, the concentration of DOC (f_{doc} [mg L^{-1}]) in the aqueous phase has to be monitored and the impact on the aqueous concentration has to be taken into account. In this study, the DOC was measured in aqueous leachates of the samples (Elementar High TOC II device). Both batch and column leaching were considered.

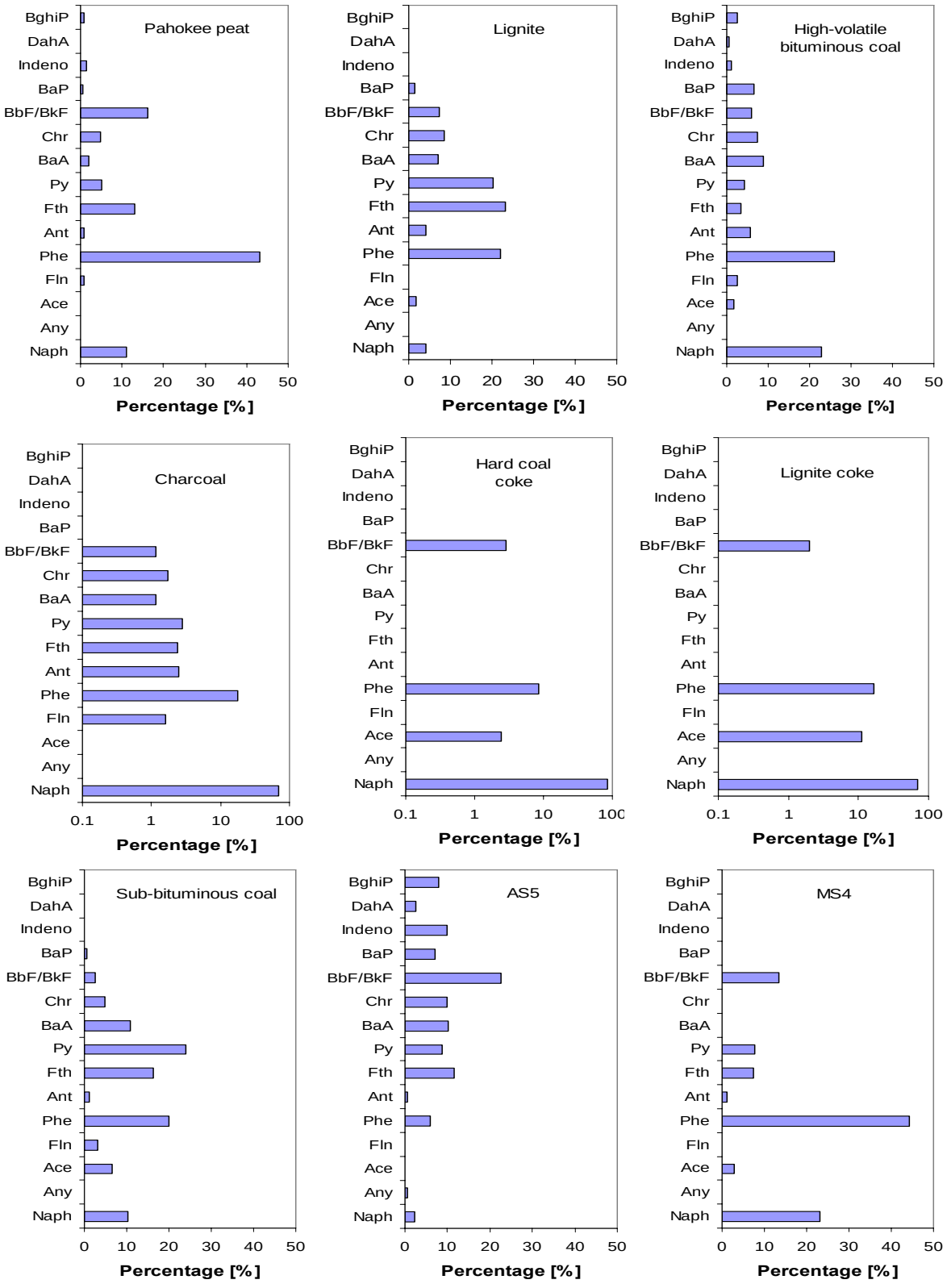

FIGURE 3.4 Native PAHs distribution patterns in the investigated materials

ASE DOC-leachates. The DOC contents determined in leachates collected using ASE at elevated temperatures are shown in Table 3.4. A wide range (about 10–1000 mg L^{-1} DOC) was observed. Much more DOC was released from Pahokee peat and lignite coal samples, which was also indicated by the yellow-brown color of the leachates. Comparison of DOC between different leaching steps illustrates two phenomena: (1) the first 3 or 4 steps under low temperatures shows higher DOC levels initially which decrease subsequently. This is because initially a large amount of readily available organic matter is released; (2) DOC release increases with temperature significantly (with the exception of MS4).

TABLE 3.4. DOC contents [mg L^{-1}] in the aqueous extracts using ASE from investigated samples under different temperatures

Temperature [°C]	Pahokee peat	Lignite	AS5	MS4
Weight of the extracted material in the ASE cell [g]	2.42	5	5.03	5.06
22/25	210.7	1035	57.8	101
22/25	233.9	781	(150)	95
22/25	149	341	57.5	51.6
40	178.7	374	69.3	24.9
47	175.9	340	-	14.8
53	145.4	260	62.2	9.4
53	156.8	274	69.4	11.1
61/64	175.2	340	72.8	10.4
73/75	223.6	420	114	14.3
86	276.7	552	155.8	17.5
100		722		

DOC in batch experiments. Two series of DOC experiments were carried out: (1) Triplicate samples were stored separately under the four experimental temperature conditions (4, 20, 46 and 77°C) for a week, with hand shaking two times per day; (2) the samples experienced the whole 7 temperature step processes (beginning at 77°C, stepping down to 4°C and then back to 77°C step again) and the DOC content in the batch vial (triplicates) at each step were measured. Figure 3.5a shows that the DOC increases with elevated temperature, but no decrease is observed when temperature were decreased again (see Figure 3.5b), which indicates an irreversible release of DOC at elevated temperature. The f_{doc} and the estimated $\log K_{ow}$ at different temperatures, as well as the relative enhancement factor ($1+ f_{doc}\, k_{doc}$), are listed in Table 3.5. It is obvious that DOC

enhanced release of PAHs (1+ f_{doc} k_{doc}) is significant for the AS5 sample, where DOC reached 106 mg L^{-1}.

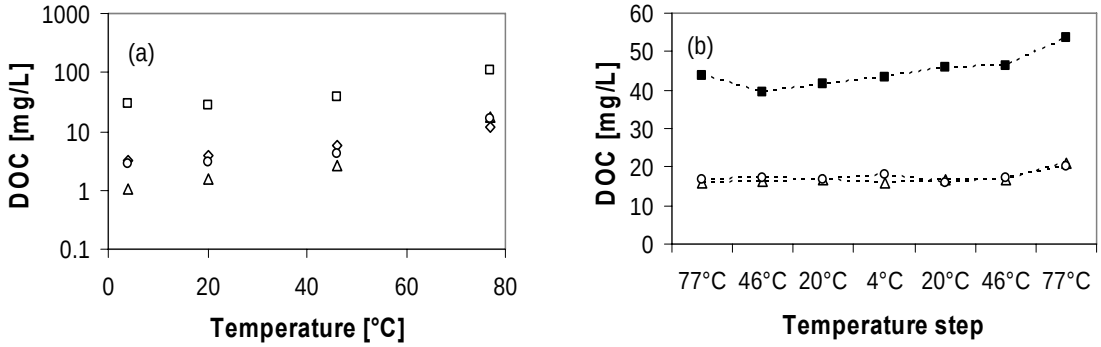

FIGURE 3.5 (a) Release of DOC with increasing temperatures from 4°C to 77°C. (b) DOC at decreasing and then increasing temperature are almost constant, indicating irreversible release of DOC at elevated temperatures. Triangles, diamonds, cycles and squares represent lignite, Pahokee peat, MS4 and AS5 (<0.0063 mm size fraction), respectively. The filled square represents the pulverized AS5 bulk sample.

TABLE 3.5. DOC [mg L^{-1}] at four different temperatures, logK_{ow} and the estimated logK_{oc} for phenanthrene as well as the solubility enhancement factor [-] at different temperatures

Temperature	**77°C**		**46°C**		**20°C**		**4°C**	
DOC/Enhancement	DOC	1+ f_{doc} k_{do}	DOC	1+ f_{doc} k_{do}	DOC	1+ f_{doc} k_{do}	DOC	1+ f_{doc} k_{do}
logK_{ow}, log$K$doc[a]	4.02, 3.30		4.40, 3.67		4.72, 3.96		4.84, 4.08	
Pahokee peat	11.5	-	5.90	1.03	3.88	1.05	3.11	1.07
Lignite	18.2	1.04	2.63	1.09	1.58	1.17	1.08	1.23
Anthrosol (AS5)	106.5	1.21	37.75	1.49	27.54	1.97	28.92	2.27
Mineral soil (MS4)	16.8	1.03	4.11	1.08	3.0	1.15	2.77	1.20

[a]LogK_{doc} was calculated using eq. 4.5 in Chapter 4, where logK_{ow} at different temperatures were estimated from the subcooled liquid aqueous solubility [mol L^{-1}] by using a empirical relationship of logK_{ow} = -*a* logS_{sub} + *b*. The regression parameters *a, b* are 0.87, 0.68 for polycyclic aromatic hydrocarbons (*8*).

Fluorescence due to DOC. Absorbance in the UV or visible spectrum has been used for monitoring the organic carbon content of fresh or wastewater at a certain wavelength (*2, 7*). In this study, fluorescence at a certain wavelength was used to monitor release of phenanthrene in column leaching tests. Therefore, fluorescence of native DOC had to be accounted for. Figure 3.6a shows the very good relationship between DOC content and fluorescence signal, despite the different sample origins (Pahokee peat, lignite, AS5 and

MS4) at the wavelengths of 249/345 nm (Exitation/Emmision). Figure 3.6b shows how the fluorescence signal increased with increased temperature.

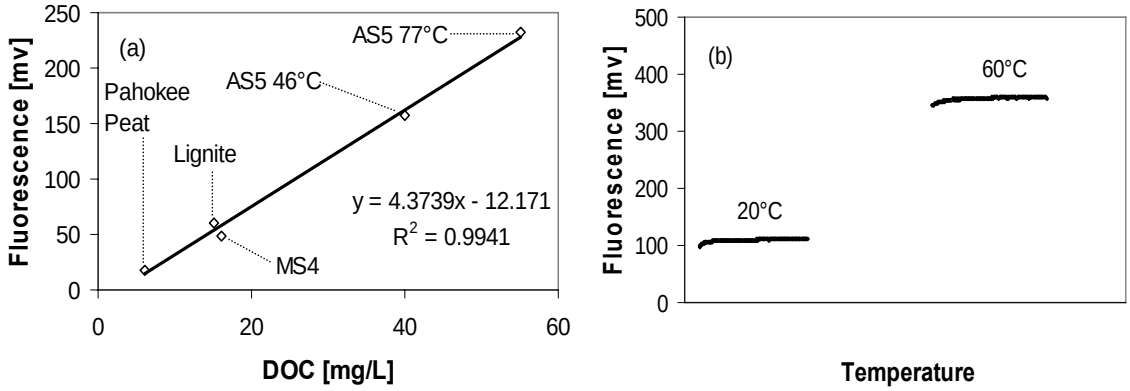

FIGURE 3.6 (a) Fluorescence signals *vs*. DOC for Pahokee peat, lignite, AS5 and MS4 (wavelengths: 249/345 nm); (b) increasing fluorescence and DOC contents with increasing temperature (Pahokee peat).

3.4 References

1. Abelmann, K.; Kleineidam, S.; Knicker, H., Grathwohl, P.; Kögel-Knabner, I. Sorption of HOC in soils with carbonaceous contamination: Influence of organic-matter composition. *J. Plant Nutr. Soil Sci*. 2005, 168, 293-306

2. Dobbs, R.A.; Wise, R.H.; Dean, R.B. The use of ultraviolet absorbance for monitoring the total organic carbon content of water and waste water. *Water Res.* 1972, 6, 1173-1180

3. Keineidam, S., Schüth, C., Grathwohl, P. Solubility-normalized combined adsorption-partitioning sorption isotherms for organic pollutants. *Environ. Sci. Technol.*, 2002, 36, 4689-4697

4. Ligouis, B; Doubinger, J. Bull. Soc. Geol. Fr. 1991, 162, 307-323.

5. Ligouis, B; Lu, J.; Pils, J. Bull. Soc. Geol. Fr. 1998, 169, 381-393

6. Ran, R.; Sun, K.; Ma, X.; Wang, G.; Grathwohl, P.; Zeng, E.Y. Effect of condensed organic matter on solvent extraction and aqueous leaching of polycyclic aromatic hydrocarbons in soils and sediments. *Environ. pollut.*, 2007, 148, 529-538

7. Tao, S.; Cui, J.; Zhang, S. Spectroscopic characteristics of aquatic substances ion UV-VIS region, *Acta Geographica Sinica*, 1990, 45, 484-489.

8. Schwarzenbach, R.P.; Gschwend, P.M.; Imboden, D.M. *Environmental Organic Chemistry*, John Wiely & Sons, Inc., New York, 1993

Chapter 4

SORPTION/DESORPTION REVERSIBILITY OF PHENANTHRENE IN SOILS AND CARBONACEOUS MATERIALS

Abstract: Sorption/desorption of phenanthrene in two soil samples and carbonaceous materials was found to yield co-incident equilibrium isotherms and no significant hysteresis was observed. Additionally, release of native phenanthrene was investigated. Equilibrium sorption and desorption isotherms were determined using pulverized samples of Pahokee peat, lignite and high-volatile bituminous coal, a mineral soil, and an anthropogenic soil. Instead of the conventional decant-and-refill batch method, sorption/desorption was driven by temperature changes using consistent samples. Sorption started at 77°C and was increased by reducing the temperature stepwise to 46, 20 and finally to 4°C. For desorption, the temperature was increased stepwise again until 77°C was reached. Besides the co-incident sorption and desorption isotherms at each temperature step, the solubility-normalized sorption/desorption isotherms of all different temperatures collapsed to unique overall isotherms. Leaching of native phenanthrene occurred at much lower concentrations but was well predicted by extrapolation of the spiked sorption isotherms indicating that the release of native phenanthrene involves the same sorption/desorption mechanisms as those for newly added phenanthrene.

4.1 Introduction

Quantification of sorption and desorption processes are an important prerequisite for the prediction of fate and transport of pollutants in the environment. Most transport models, for example, are based on the assumption of sorption reversibility. However, sorption/desorption hysteresis phenomena of organic compounds in soils or sediments are frequently reported (*1-10*). Many of these studies do not provide clear evidence for the physical or chemical mechanism leading to hysteresis.

Hysteresis has been attributed to either sorbent reconfiguration leading to physical entrapment of sorbates or experimental artifacts. Lu and Pignatello (*5*) suggested pore deformation as a cause of sorption/desorption hysteresis by demonstrating the "conditioning effect" under high concentrations. Similarly, Braida et al. (*7*) found sorption hysteresis of benzene in charcoal particles again at high concentrations and proposed a pore deformation mechanism as the cause for it. Often, the difference between sorption and desorption is minor, appears at relatively high concentrations, and sophisticated methods (e.g., isotope techniques) are required to verify irreversible sorption (*10*).

Other studies have shown that some of the reported hysteresis phenomena are due to experimental artifacts. Nonsingular sorption/desorption isotherms can be due to "pseudo-hysteresis", which is related to slow kinetics and non-attainment of equilibrium of the sorption before desorption was started (*11-20*). Recently, Sabbah et al. (*18*) modeled a hypothetical system in which sorption/desorption rates were controlled by retarded pore diffusion, and found that even 50 days is too short for equilibration of phenanthrene in 0.25-0.42 mm sized sand (Borden), and that sorption-desorption hysteresis vanishes after 1000 days pre-equilibration.

Furthermore, losses of solute to batch vial components, especially polymer liners and seals (PTFE-lined rubber septa), can lead to incomplete mass balances used to construct the sorption/desorption isotherms. Young and Weber (*21*) reported that phenanthrene loss

by sorption to new PTFE-lined septa of centrifuge bottles makes up to 5% of the total solute mass over a one-week reaction time at room temperature.

The third category leading to artifacts is the "colloid effect" in the conventional batch vial decant-and-refill methods. The removal of and replacement of supernatant water in subsequent desorption steps can change the dissolved organic carbon (DOC) concentration and the number of suspended particles in the aqueous solution (*22*).

Huang et al. (*3*) used three different batch experimental protocols to study sorption/desorption of phenanthrene on five EPA reference soils and sediments and found that different experimental setups introduced different types of artifacts and different degrees of apparent hysteresis. They concluded that the principal sources of artifacts are solute losses to reactor components, failure to achieve equilibrium sorption conditions and colloid effects.

The main objective of this work was to study sorption/desorption hysteresis by recovering the solute mass in the batch system, i.e., using a consistent sample. Three carbonaceous samples and two different soil samples, which were known to contain coal or black carbon particles, were selected for the batch experiments reported here. In order to establish sorption/desorption equilibrium in a relatively short time period, all samples were pulverized. A new experimental protocol was developed, where the sorption/desorption process is driven by temperature changes, rather than the usual decant-and-refill procedures, so as to avoid the potential artifacts. Additionally, the native loading of the samples with polycyclic aromatic hydrocarbons (PAHs) and the system loss were monitored and accounted for in the mass balances.

4.2 Materials and Methods

Sample selection and characteristics. Carbonaceous samples from a range of natural organic materials following the rank of coalification (Pahokee peat, lignite and high-volatile bituminous coal (HC)) and two different soil samples (anthropogenic soil (AS5)

and mineral soil (MS4)) were selected to cover a wide range of natural geosorbents. The carbonaceous samples were selected because of their relevance in sorption of hydrophobic organic compounds (HOCs) in soils and in sediments. All sorbents were pulverized to a grain size of less than 0.03 mm as determined by a laser particle size analyzer (GALAI CIS-50) using a zirconium oxide planet ball mill (Laborette, Fritsch). For the fine grained anthropogenic soil only the untreated size fraction <0.063 mm was used. The characteristics of the sorbents are listed in Table 4.1.

TABLE 4.1. Characteristics of the selected geosorbents[a]

Geosorbents	OC [%]	H [%]	N [%]	SA[e] [$m^2 g^{-1}$]	IP[e] (<nm) [$cm^3 kg^{-1}$]	IP_M[e] [$cm^3 kg^{-1}$]	Grain size [mm]
Pahokee peat[b]	48.0	5.18	3.71	n.d.	n.d.	n.d.	n.d.
Lignite[c]	38.9	4.11	0.39	1.78	7.9 (< 96 nm)	0	< 0.01
High volatile bituminous coal (HC)[c]	72.1	5.55	1.44	3.45	11.4 (< 108 nm)	0.022	< 0.03
Anthropogenic soil (AS5 < 0.063 mm)[d] (Anthrosol)	4.19	0.61	0.32	3.17	12.0 (< 63 nm)	0	< 0.063
Mineral soil (MS4)[d] (Chernozem)	1.74	0.38	0.17	9.09	16.0 (< 65 nm)	0.43	n.d.

[a] Organic carbon (OC), hydrogen (H) and nitrogen (N) contents; n.d.: not determined
[b] Data from Ran et al. 2002 (*8*)
[c] Detailed sample description is given in Kleineidam et al. 2002 (*23*)
[d] Sampling procedure and sample description is given in Abelmann et al. 2005 (*24*)
[e] Specific surface area (SA), pore volume (IP) and micropore volume (IP_M) were determined by N_2-BET method (ASAP 2010 Micromeritics)

Chemicals. Phenanthrene was used as the probe compound and was obtained as pure product (98%) from Aldrich Chemical Corp. Physicochemical properties and thermodynamic parameters are listed in Table 4.2.

Accelerated solvent extraction (ASE). The native loadings of the samples with PAHs and their release into water were determined using an automated accelerated solvent extraction device (ASE). The pulverized samples were subsequently leached under high pressure (100 bar) using first water, then extracted with acetone, and finally extracted two times with toluene at increasing temperatures (20, 40, 53, 61, 73 and 86°C for water; 100°C for acetone and 150°C for toluene). The extraction cell contained a stainless steel

frit and a glassfiber filter to prevent loss of particles. The extracts were analyzed with GC/MS; phenanthrene was the dominant native PAH in all samples (around 30% of the 16 EPA PAHs). Table 4.3 shows the loadings of native phenanthrene and the concentrations in spiked batch vials in both solid and aqueous phases. The results show that for the carbonaceous samples (Pahokee peat, lignite and HC) the native phenanthrene concentrations and its release into water can be neglected because of the very low overall contribution to the solute mass in the batch sorption tests (<1%) at the lowest concentration level used. For the two soil samples, the native phenanthrene loading was included in the mass balance calculations because it reached 4.5% (MS4) and 19% (AS5) at the lowest concentration levels of the spiked samples.

TABLE 4.2. Physicochemical and thermodynamic properties and estimated K_{doc} of phenanthrene[a]

Molecular weight (g moL^{-1})	178.24
Melting point (°C) (T_m)	99.5
Boiling point (°C)	340.2
Density (g cm^{-3})	1.02
Henry's law constant (25°C) (-)	0.001
Log K_{ow} (25°C)	4.57
Water solubility [mg L^{-1}] (S_{solid})	0.788[b] (20°C) 0.361[b] (4°C) 17.37[c] (77°C) 3.35[c] (46°C)
Subcooled liquid solubility [mg L^{-1}] (S_{sub})[d]	4.1 (20°C) 2.92 (4°C) 26.11 (77°C) 9.36 (46°C)
Log K_{doc} (25, 77, 46, 20, 4°C)[e]	3.82, 3.30, 3.67, 3.96, 4.08

[a] The molecular weight, melting point, boiling point, density, Henry's law constant and logK_{ow} values are from Verschueren (*25*)
[b] Experimental values from May et al. (*26*)
[c] Calculated values: $\ln S_{solid} = - \Delta H_{sol}/RT + A$, where ΔH_{sol} and constant A were taken from a series of measured values between 40.1 to 73.4°C (*27*); the enthalpy between 4 to 29.9°C (*34*) was determined based on experimental data from May et al. (*26*)
[d] Calculated values following Yalkowsky et al. (*28*): $\ln (S_{sub}/S_{solid}) = -\Delta H_{fus}/(T_m R) (1-T_m/T)$
[e] Estimated with eq. 4.5; temperature dependency of K_{ow} was corrected based on water solubility and log $K_{ow} = -0.84 \log S_{sub} + 0.87$ (*35*)

Sorption/desorption tests. Sorption and desorption isotherms were determined in batch experiments in 50 mL crimp-top reaction glass vials sealed with PTFE-lined butyl rubber septa (Alltech) at four temperatures: 77 (except the Pahokee peat sample), 46 (water bath), 20, and 4°C (temperature constant rooms). Sorption was started at high temperatures (low sorption), stepwise equilibrated at lower and lower temperatures

(increasing sorption) until 4°C was reached. After that, the process was reversed, which leads to desorption of phenanthrene with increasing temperature. A time period of 7 days was found to be sufficient to establish sorption/desorption equilibrium with pulverized samples for each temperature step (*29*), which was confirmed by experiments run for a longer time period of 14 days under 4ºC and which could be expected from calculations based on the spherical diffusion model that uses intraparticle porosities measured by application of the N_2-BET method. It should be noted that the grain size of the pulverized samples (<0.01–0.03 mm) is at least 10 times smaller than in the original samples and thus diffusion limited sorption kinetic is 100 times faster (*19*, *20*).

TABLE 4.3. Native phenanthrene loading and release into water in comparison to batch experiments with spiked phenanthrene

Sorbent	Pahokee peat	Lignite	HC	AS5	MS4
Native loading [mg kg^{-1}]	0.66	0.19	12.2	0.39	0.07
Mass of sorbent in vial [g]	0.005	0.005	0.005	0.4	0.4
Percentage of native phenanthrene at the lowest concentration level in the batch experiment	0.4%	0.1%	1.2%	19%	4.5%
Aqueous concentration from leaching of native phenanthrene at 20°C [µg L^{-1}] [a]	< 0.02	< 0.001	< 0.001	0.013	0.05
Equilibrium concentration C_w [µg L^{-1}] at the lowest concentration level in batch experiment at 20°C	2.38	1.40	1.60	1.63	1.79

[a] measured using ASE.

All experiments were conducted in triplicate. Concentrated methanol stock solutions were prepared with phenanthrene and added to the batch vials as needed. Methanol concentrations in the aqueous solutions were always less than 0.5%, a level at which methanol has no measurable effect on sorption (*30*). The batch vials contained 0.005 g (Pahokee peat, lignite and HC) or 0.4 g (AS5 and MS4) of the samples. The sorbents were first submerged in a small amount of deionized water (about 2 mL) and the vials were vacuum degassed to allow complete wetting of the sorbents. Then the batch vials were filled with deionized, degassed water to a volume of 50 mL, leaving a headspace of less than 5% of the total volume of the vial and spiked with the different initial phenanthrene concentrations. Sodium azide at a concentration of 200 mg L^{-1} was added to the aqueous solutions to inhibit bacterial growth. Reference vials containing no sorbent

were prepared and treated identically. The batch vials were shaken by hand two times per day during the equilibration period; before sampling particles were allowed to settle for at least 24 h until the supernatant water was clear. An aliquot of 100 µl of the supernatant water was sampled with a glass syringe equipped with a capillary needle and immediately analyzed for phenanthrene by a HPLC equipped with a fluorescence detector (separation column, Grom PAH, 125 mm x 3 mm, 5 µm C18 silica; mobile phase, 30-35% water, 65-70% acetonitrile; emission/extinction wavelengths for phenanthrene, 249/345). The PTFE-lined rubber septa were replaced after each sampling and analyzed for phenanthrene contents by solvent extraction (submerged in 10 mL toluene for one week and quantification of phenanthrene in the toluene by GC/MS).

It should be noted that high temperatures lead to a release of DOC from soils. In order to quantify a potential solubility enhancement effect, the DOC content was measured in triplicate at each temperature step in separate vials (containing the same mass of sorbents and water volume but no phenanthrene). Measurements were done using a TOC analyzer (Elementar High TOC II, Germany) in the DOC mode (the sample is acidified and filtered <0.45 µm before high-temperature combustion and CO_2 analysis). The DOC vials were treated the same way as the sample vials, i.e., experienced the all 7 temperature steps (beginning at 77°C, stepping down to 4°C and then back to 77°C again).

Data analysis. The sorbed concentration of phenanthrene was calculated based on the mass balance of solute between the aqueous and solid phase, including system loss (partitioning of the solute into the vial PTFE-lined rubber septa) at each temperature step:

$$C_s = \frac{(X_{input} + m_i) - C_w V_w - m_{loss}}{m_d} \tag{4.1}$$

where C_s [mg kg^{-1}] and C_w [mg L^{-1}] denote the concentrations in the solid and the aqueous phases. X_{input}, m_d, and V_w denote the injected phenanthrene mass [mg], the sorbent mass, and the volume of water in the batch vial [L], respectively. m_{loss} denotes the mass lost at each temperature step, which was confirmed by extraction of the PTFE-lined rubber septa with toluene as described above (except the HC sample). In the cases of the

soil samples, AS5 and MS4, the native phenanthrene loading m_i was additionally considered. For the carbonaceous samples m_i was relatively low and therefore neglected.

Additionally, the system losses were also quantified by carefully monitoring reference vials which contained only water and the solute but no sample:

$$m_{loss} = C_w V_{ref} \left(\frac{C_{ref,initial}}{C_{ref,t}} - 1 \right) \tag{4.2}$$

where $C_{ref,initial}$ and $C_{ref,t}$ denote the reference vial initial and measured aqueous concentrations [µg L^{-1}] at each temperature step, respectively. V_{ref} is the water volume in the reference vial. With this approach, the loss of solute is assumed to be proportional to the concentration in the aqueous phase. This approach was only used for the HC sample, which was the first sample investigated with this technique and which has the lowest loss in the system because of the relatively high sorption capacity. For all other samples the losses were based on the phenanthrene extracted from the PTFE-lined rubber septa. Figure 4.2 shows the relatively good agreement between both correction procedures and indicates that the loss of the solute is indeed due to diffusion into the septa. Headspace losses were not considered because of the small headspace volume and the low Henry's law constant of phenanthrene.

Equilibrium sorption and desorption data were fit by the traditional and solubility–normalized Freundlich model:

$$C_s = K_{Fr} C_w^{1/n} = K_{Fr}^* \left(\frac{C_w}{S_{sub}} \right)^{1/n} \tag{4.3}$$

where K_{Fr} [mg kg^{-1}: (mg L^{-1})$^{1/n}$] and $1/n$ [-] are the Freundlich coefficients. K_{Fr}^* denotes the solubility-normalized Freundlich coefficient [mg kg^{-1}] and S_{sub} [mg L^{-1}] is the subcooled liquid solubility at the temperature of interest.

For nonpolar organic compounds, especially PAHs, the solubility enhancement due to DOC present in the aqueous solution can be significant. In order to account for this, the

fraction of dissolved organic carbon (f_{doc} [kg L^{-1}]) was determined and the potential impact on the aqueous concentration was estimated with following relationship:

$$\frac{C_w^*}{C_w} = 1 + f_{doc} K_{doc} \tag{4.4}$$

where C_w^* is the measured apparent aqueous concentration [mg L^{-1}] and K_{doc} is the partitioning coefficient between water and DOC. K_{doc} values depend on the properties of the solute and the type of the dissolved organic matter. Here a relationship (eq 4.5) determined by Pyka (*31*) was used to estimate K_{doc}:

$$\log K_{doc} = 0.937 \log K_{ow} - 0.46 \tag{4.5}$$

Temperature dependency of K_{ow} and thus K_{doc} was accounted for as described in Table 4.2.

Recovery. The phenanthrene mass balance in the batch vial at the end of each experiment (after the final temperature step) was checked as follows: (1) by analyzing the aqueous solution (m_w), (2) by extracting of the sorbed mass from the sorbent (m_s) with ASE (including the native loading of the samples with PAHs (m_i) for AS5 and MS4), and (3) by determining the solute mass in all vial septa (m_l). The latter represents the system loss and was determined for each temperature step and each isotherm point, respectively. The total recovery in percentage therefore is:

$$\text{recovery} = \frac{m_s + m_w + m_l}{X_{input} + m_i} * 100 \tag{4.6}$$

The recoveries of the batch vials are listed in Table 4.4. The total average recovery at the end of all experiments was 101%.

4.3 Results and Discussion

Figure 4.1 shows the phenanthrene distribution among solid, water, and DOC phases as well as the system loss in the batch vials for two examples (Pahokee peat and AS5; 20°C sorption step). The mass potentially associated with DOC summarizes to 3.6–5.1% for AS5 and to 0.8–2.9% for Pahokee peat. For MS4 (20°C) and lignite (20°C) this amounts to 2.1–5.1% and 1.7-4.0%, respectively. This indicates that the DOC effect is

insignificant except for AS5, where a high release of DOC (up to 106 mg L^{-1} at 77°C) was observed. The system loss in the sample vials is in all cases lower than 8% which is illustrated more detailed in Figure 4.2, where system losses in reference vials are compared to losses in sample vials determined by toluene extraction and calculated based on eq 4.2. Losses in the reference vials are always higher than in the sample vials due to higher aqueous concentrations and thus the steeper concentration gradients for diffusion into the PTFE-lined rubber septa. System losses calculated (eq 4.2) and determined by septa extraction are very close and amount to several percent (of the total mass) within a time period of one week. Figure 4.2 shows that the system loss is high under higher temperatures probably due to faster diffusion of phenanthrene into the PTFE-lined rubber septa. This is consistent with the results from Lion et al. (*32*). They reported that losses of phenanthrene to PTFE-lined rubber septa are significantly greater than losses to glass components in a batch system.

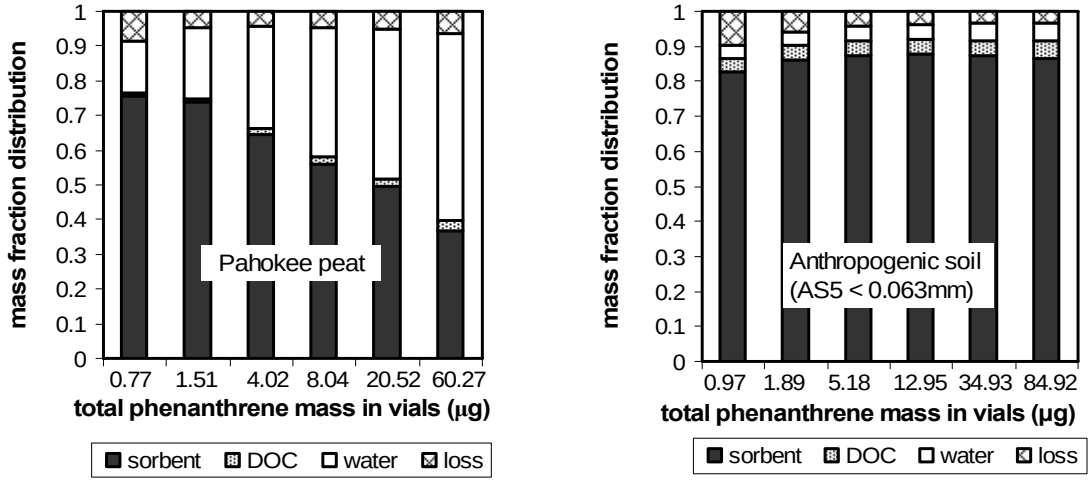

FIGURE 4.1. Examples for phenanthrene distribution among solid, water, DOC, and system loss (accumulated) in batch experiments for Pahokee peat and AS5 samples at the 20°C sorption step at increasing concentrations (numbers on the abscissa indicate the total phenanthrene mass in the vials; Table 4.4 lists the final mass balances of all experiments).

Figure 4.3 shows the equilibrium sorption/desorption isotherms of phenanthrene for the samples at the four different temperatures (77, 46, 20 and 4°C). Pahokee peat was not studied at 77°C because of the potentially high release of DOC. The sorption isotherms

were fit with the Freundlich model (see Table 4.5). This clearly demonstrates that within a single sorption/desorption cycle, the sorption and desorption isotherms at the same temperatures agree very well with each other. The hysteresis index (HI) calculated according to Huang et al. (*3*) shows only about ± 3% deviations in both directions between the sorption and desorption for Pahokee peat, lignite, and anthropogenic and mineral soils (see Table 4.5). Thus, significant differences in sorption/desorption isotherms were not observed except in the case of HC, where the desorption K_{Fr} values are on average 10% higher than the sorption K_{Fr}'s with a HI value of about 13%. HC shows strong nonlinear sorption and therefore very slow sorption/desorption kinetics is expected in the low concentration range where the hysteresis is observed. Despite pulverization, we can not exclude the possibility of some nonequilibrium in this concentration range, which could cause the observed hysteresis.

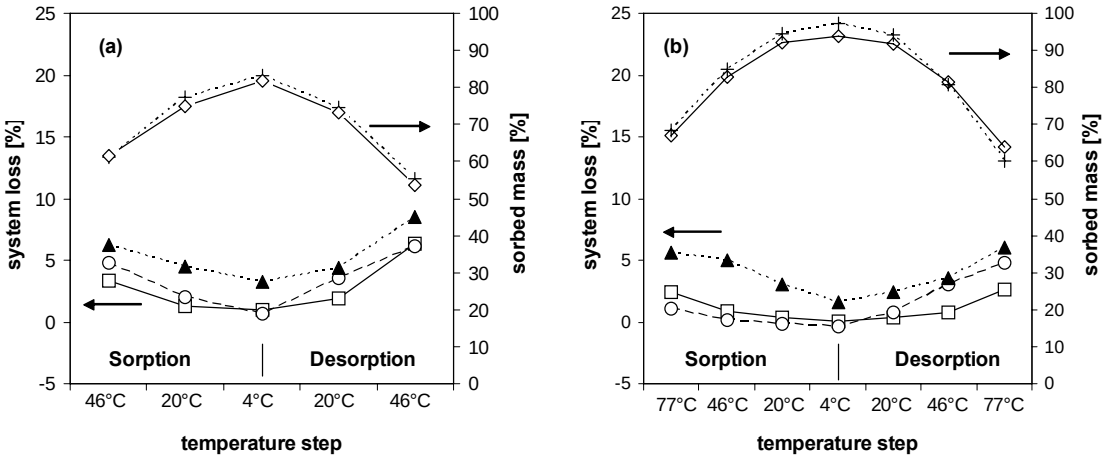

FIGURE 4.2. Percent of phenanthrene sorbed (open diamond and plus symbols) and solute lost during the experiments (open square and circle) compared to losses from the reference vials (solid triangles) using (a) Pahokee peat and (b) AS5 as examples. Open circles denote losses from samples calculated by eq. 4.2 based on the assumption that losses are due to diffusion of the solute into the septa, and the open squares indicate the percentage of solute found in the septa after extraction. Losses from reference vials are higher because of higher concentrations in aqueous phase and headspace which yield to higher diffusion rates into the septa. Plus symbols and open diamonds denote sorbed mass fraction development, where the system loss is calculated based on eq 4.2 or by septa extraction, respectively.

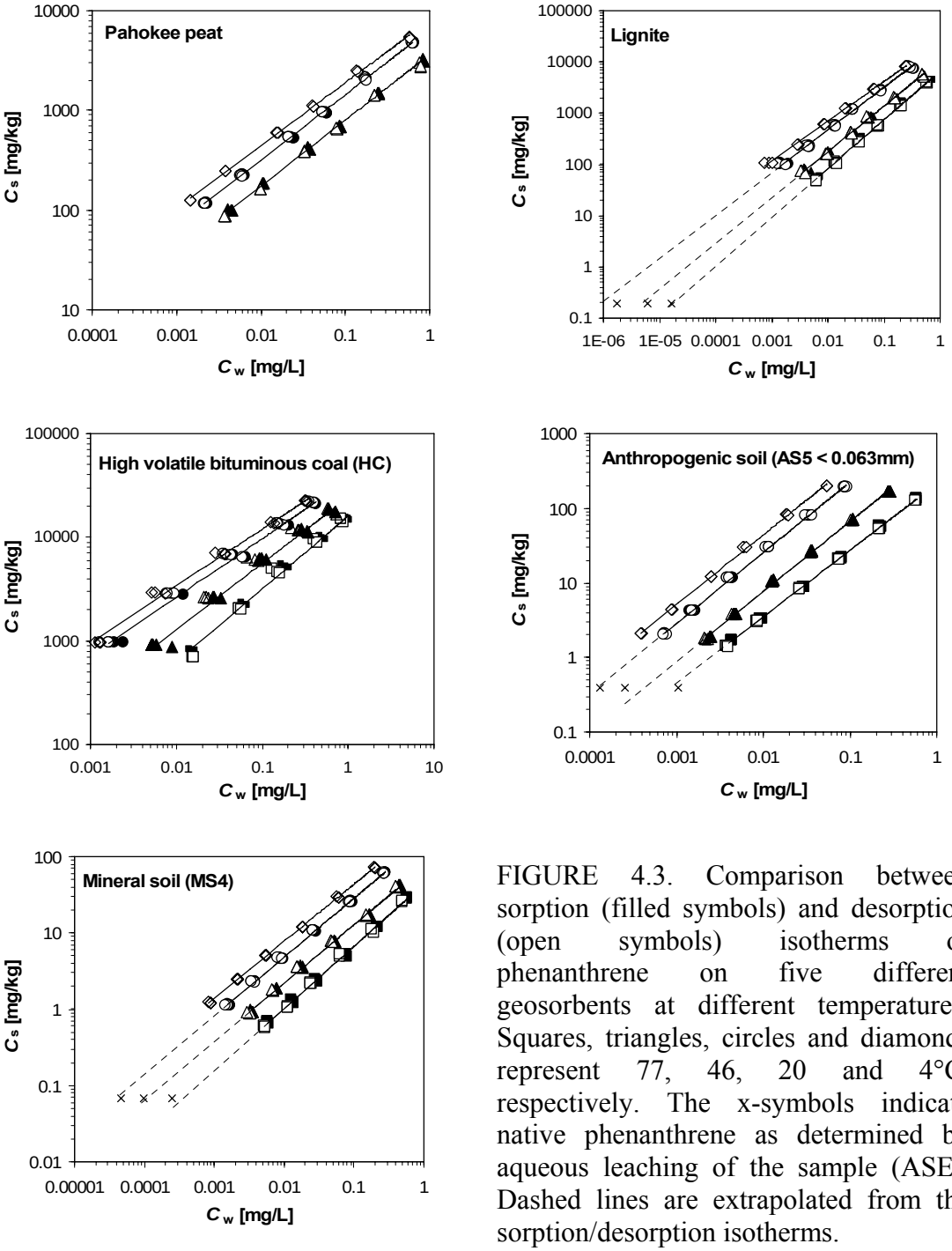

FIGURE 4.3. Comparison between sorption (filled symbols) and desorption (open symbols) isotherms of phenanthrene on five different geosorbents at different temperatures. Squares, triangles, circles and diamonds represent 77, 46, 20 and 4°C, respectively. The x-symbols indicate native phenanthrene as determined by aqueous leaching of the sample (ASE). Dashed lines are extrapolated from the sorption/desorption isotherms.

The sorption/desorption isotherm parameters are listed in Table 4.5. It illustrates that at the same temperature different sorbents show different sorption capacities and linearity

TABLE 4.5. Freundlich sorption/desorption isotherm parameters at different temperatures as well as the hysteresis index (HI) of phenanthrene on geosorbents (data in Figure 4.3 and Figure 4.4)[a]

Temperature		77°C		46°C		20°C		4°C
Geosorbent	Process	sorption	desorption	sorption	desorption	sorption	desorption	sorption
Pahokee Peat	Log K_{Fr}			3.56 ±0.01	3.55 ±0.01	3.80 ±0.01	3.81 ±0.01	3.91 ±0.01
	$1/n$			0.66 ±0.01	0.66 ±0.01	0.66 ±0.01	0.66 ±0.01	0.63 ±0.01
	R^2			1.0	1.0	1.0	1.0	1.0
	Log K_d at 0.1 S_{sub}			3.57 ±0.01	3.56 ±0.01	3.93 ±0.01	3.94 ±0.01	4.11 ±0.01
	HI			-0.03		0.03		
	S_{sub} – normalized parameters, all temperatures: Log K_{Fr}^* = 4.21 ± 0.01; $1/n$ = 0.65 ± 0.01							
Lignite	Log K_{Fr}	3.83 ±0.01	3.83 ±0.01	4.0 ±0.03	3.99 ±0.02	4.28 ±0.02	4.26 ±0.02	4.33 ±0.02
	$1/n$	0.95 ±0.01	0.97 ±0.03	0.89 ±0.02	0.88 ±0.01	0.83 ±0.01	0.82 ±0.01	0.78 ±0.01
	R^2	1.0	1.0	0.99	1.0	1.0	1.0	1.0
	Log K_d at 0.1 S_{sub}	3.81 ±0.01	3.82 ±0.01	4.0 ±0.03	3.99 ±0.02	4.35 ±0.02	4.33 ±0.02	4.45 ±0.02
	HI	-0.03		0.01		-0.01		
	S_{sub} – normalized parameters, all temperatures: Log K_{Fr}^* = 4.91± 0.02; $1/n$ = 0.86 ± 0.01							
High volatile bituminous coal (HC)	Log K_{Fr}	4.20 ±0.02	4.25 ±0.02	4.38 ±0.03	4.43 ±0.03	4.55 ±0.03	4.58 ±0.02	4.63 ±0.02
	$1/n$	0.70 ±0.02	0.76 ±0.02	0.64 ±0.02	0.62 ±0.02	0.57 ±0.02	0.56 ±0.01	0.55 ±0.01
	R^2	0.99	0.99	0.99	0.99	0.99	0.99	0.99
	Log K_d at 0.1 S_{sub}	4.07 ±0.02	4.15 ±0.02	4.39 ±0.03	4.44 ±0.03	4.72 ±0.03	4.75 ±0.02	4.87 ±0.02
	HI	- 0.11		0.15		0.11		
	S_{sub} – normalized parameters, all temperatures: Log K_{Fr}^* = 4.99± 0.02; $1/n$ = 0.61 ± 0.01							
Anthropo-genic soil (AS5<0.063 mm)	Log K_{Fr}	2.33 ±0.01	2.32 ±0.01	2.76 ±0.01	2.76 ±0.01	3.30 ±0.01	3.30 ±0.02	3.51 ±0.02
	$1/n$	0.89 ±0.00	0.89 ±0.00	0.94 ±0.01	0.93 ±0.01	0.95 ±0.01	0.94 ±0.01	0.93 ±0.01
	R^2	1.0	1.0	1.0	1.0	1.0	1.0	1.0
	Log K_d at 0.1 S_{sub}	2.28 ±0.01	2.27 ±0.01	2.76 ±0.01	2.76 ±0.01	3.32 ±0.01	3.32 ±0.02	3.55 ±0.02
	HI	-0.02		0.03		0.01		
	S_{sub} – normalized parameters, all temperatures: Log K_{Fr}^* = 3.71± 0.04; $1/n$ = 0.91 ± 0.01							
Mineral soil (MS4)	Log K_{Fr}	1.64 ±0.01	1.67 ±0.02	1.87 ±0.01	1.9 ±0.02	2.22 ±0.01	2.22 ±0.01	2.39 ±0.01
	$1/n$	0.82 ±0.01	0.83 ±0.01	0.76 ±0.01	0.76 ±0.01	0.77 ±0.01	0.76 ±0.01	0.75 ±0.00
	R^2	1.0	1.0	1.0	1.0	1.0	1.0	1.0
	Log K_d at 0.1 S_{sub}	1.56 ±0.01	1.60 ±0.02	1.88 ±0.01	1.91 ±0.02	2.31 ±0.01	2.31 ±0.01	2.52 ±0.01
	HI	0.03		0.07		0.02		
	S_{sub} – normalized parameters, all temperatures: Log K_{Fr}^* = 2.74 ± 0.02; $1/n$ = 0.80 ± 0.01							

[a] K_d at C_w = 0.1 S_{sub} was calculated from $K_d = K_{Fr}\ (0.1\ S_{sub})^{(1/n-1)}$;
HI = $(C_s^d - C_s^s)/C_s^s$ according to Huang et al. (*3*): (C_s^s and C_s^d are solid phase solute concentrations for the sorption/desorption cycle at same temperature steps). The HI values listed are averaged values from 4 different C_w levels at each temperature step.

reflecting the different sorption characteristics. The high nonlinearity indicates that adsorption mechanisms dominate sorption, especially for the coals. All isotherms in this study are significantly nonlinear except AS5 ($1/n$ = 0.95 at 20°C), where partitioning into soil organic matter is probably the main sorption mechanism. The strong nonlinearity of

the MS4 sample ($1/n$ = 0.77 at 20°C) is probably due to its charred organic carbon (*24*). HC shows the most nonlinear behavior ($1/n$ = 0.57 at 20°C) among the five sorbents, which correlates to its high specific surface area and existence of meso- as well as micropores (see Table 4.1). Table 4.5 also shows that with increasing temperature the sorption/desorption coefficients (K_{Fr} or K_d) decrease and a linear decrease of $\log K_{Fr}$ with T [°C] is observed. The sorption/desorption parameters obtained at 20°C agree reasonably well with data from Kleineidam et al. (*23*) who also used lignite and hard coal samples indicating that the elevated temperatures did not change the sorption properties of the samples significantly.

The distribution of the native phenanthrene between water and solids was determined using ASE in the same temperature range (20-86°C, 99 minutes equilibrium time, 100 bar pressure) as in the batch experiments. The results for lignite, AS5 and MS4 are plotted in Figure 4.3. The loading of native phenanthrene in lignite, AS5, and MS4 was calculated from the sum of the phenanthrene released into the water and extracted from the solids by acetone and toluene. For lignite, C_w at 20°C was below the detection limit and was obtained by extrapolation from higher temperatures (*34*), whereas the values for AS5 and MS4 were directly measured (Figure 4.3). For HC, C_w at all temperatures was below the detection limit. The approximate agreement of the native phenanthrene data with the determined sorption isotherms suggests that desorption of native phenanthrene is the same as for the spiked samples, provided that equilibrium is attained. This implies that the native phenanthrene behaves the same as the spiked phenanthrene, at least within the error of method used in this study.

Figure 4.4 shows the S_{sub}-normalized isotherms measured at all temperatures during the sorption/desorption cycles for each sorbent. For each sorbent, most of the data points collapse onto one nearly consistent line. The increased data scatter here can be due to uncertainties in the subcooled liquid solubilities additional to the analytical errors. The fitted "average" isotherm parameters based on all the temperature data points are shown in Figure 4.4 and Table 4.5. This is in agreement with Manes' work (*33*), where a characteristic curve on active carbon can be calculated from adsorption isotherms.

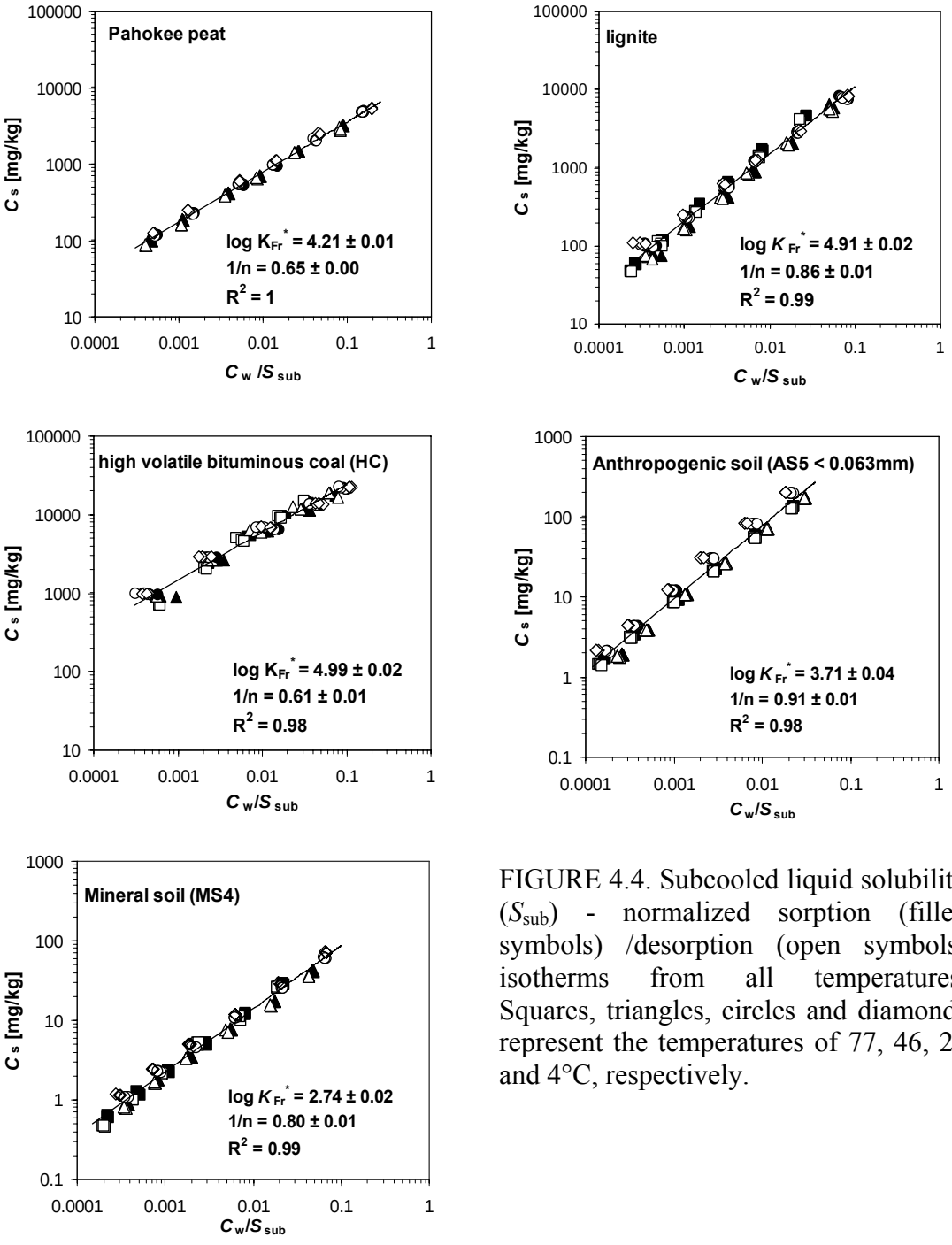

FIGURE 4.4. Subcooled liquid solubility (S_{sub}) - normalized sorption (filled symbols) /desorption (open symbols) isotherms from all temperatures. Squares, triangles, circles and diamonds represent the temperatures of 77, 46, 20 and 4°C, respectively.

Our results show that the sorption/desorption isotherms agree with each other very well at each temperature step, indicating that no significant hysteresis occurs for the samples investigated in this study. The slight hysteresis observed in the high-volatile bituminous

coal (HC) sample might be due to nonequilibrium at low concentrations, which has to be considered as an artifact. In contrast to our observations, in earlier work irreversible sorption was shown to occur predominantly at high concentrations (*10*). Additionally, the sorption/desorption data from all temperatures collapse into nearly one general isotherm for solubility-normalized aqueous concentrations. Finally, leaching of native phenanthrene fits results from the spiked experiments reasonably well, indicating that equilibrium was attained in the leaching and batch experiments. Our results also show that mass balance errors due to system losses are likely to occur, especially at high temperatures and during long experimental time, which, if not accounted for, leads to an artificial hysteresis.

4.4 References

1. Huang, W.; Weber, W. J., Jr. A Distributed Reactivity Model for Sorption by Soils and Sediments. 10. Relationships between Desorption, Hysteresis, and the Chemical Characteristics of Organic Domains. *Environ. Sci. Technol.* 1997, 31, 2562-2569

2. Mcgroddy, S. E.; Farrington, J. W.; Gschwend, P. M. Comparison of the in situ and desorption sediment-water partitioning of polycyclic aromatic hydrocarbons and polychlorinated biphenyls. *Environ. Sci. Technol.* 1996, 30, 172-177

3. Huang, W.; Yu, H.; Weber, W. J., Jr. Hysteresis in the sorption and desorption of hydrophobic organic contaminants by soils and sediments. 1. A comparative analysis of experimental protocols. *J. Contam.Hydrol.* 1998, 31, 129-148

4. LeBoeuf, E. J.; Weber, W. J., Jr. Macromolecular characteristics of natural organic matter. 2. Sorption and desorption behavior. *Environ. Sci. Technol.* 2000, 34, 3632-3640

5. Lu, Y.; Pignatello, J. J. Demonstration of the "conditioning effect" in soil organic matter in support of a pore deformation mechanism for sorption hysteresis. *Environ. Sci. Technol.* 2002, 36, 4553-4561

6. Weber, W. J., Jr.; Kim, S. H.; Johnson, M. D. Distributed reactivity model for sorption by soil and sediments. 15. High-concentration co-contaminant effects on phenanthrene sorption and desorption. *Environ. Sci. Technol.* 2002, 36, 3625-3634

7. Braida, W. J.; Pignatello, J. J.; Lu, Y.; Ravikovitch, P. I.; Neimark, A.V.; and Xing, B. Sorption hysteresis of benzene in charcoal particles. *Environ. Sci. Technol.* 2003, 37, 409-417

8. Ran, Y.; Huang, W.; Rao, P. S.C.; Liu, D.; Sheng, G.; Fu, J. The role of condensed organic matter in the nonlinear sorption of hydrophobic organic contaminants by a peat and sediments. *J. Environ. Qual*. 2002, 31, 1953-1962

9. Ran, Y.; Xiao, B.; Fu, J.; Sheng G. Sorption and desorption hysteresis of organic contaminants by kerogen in a sandy aquifer material. *Chemosphere.* 2003, 50, 1365-1376

10. Sander M.; Lu Y.F.; Pignatello J.J. A thermodynamically based method to quantify true sorption hysteresis. *J Environ Qual.* 2005, 34, 1063-1072

11. Ball, W.P.; Roberts, P.V. In *Organic substances in sediments and water*; Baker, R.A. Ed.; Lewis Publishers, Inc.: Chelsea, MI, Vol. 2, Chapter 13. 1991

12. Miller, C.T.; Pedit, J.A. Use of a reactive surface-diffusion model to describe apparent sorption-desorption hysteresis and abiotic degradation of lindane in a subsurface material. *Environ. Sci. Technol* 1992, 26, 1417-1427

13. Harmon, T.C.; Roberts, P.V. Comparison of intraparticle sorption and desorption rates for a halogenated alkene in a sandy aquifer material. *Environ. Sci. Technol.* 1994, 28, 1650-1660

14. Altfelder, S.; Streck, T.; Richter J. Nonsingular sorption of organic compounds in soil: the role of slow kinetics. *J. Environ. Qual.* 2000, 29, 917-25

15. Altfelder, S.; Streck, T.; Maraqa, M.A. Nonequilibrium sorption of dimethylphtalate - Compatibility of batch and column techniques. *Soil Sci. Soc. Am. J.* 2001, 65, 102-110

16. Allen-King, R.M.; Grathwohl, P.; Ball, W.P. New modeling paradigms for the sorption of hydrophobic organic chemicals to heterogeneous carbonaceous matter in soils, sediments, and rocks. *Advances in water resources*, 2002, 25, 985-1016

17. Kleineidam, S.; Rügner, H.; Grathwohl, P. Desorption kinetics of phenanthrene in aquifer material lacks hysteresis. *Environ. Sci. Technol.* 2004, 38, 4169-4175

18. Sabbah I.; Ball W.P.; Young D.F.; Bouwer E.J. Misinterpretations in the Modeling of contaminant desorption from environmental solids when equilibrium conditions are not fully understood. *Environ. Eng. Sci.* 2005, 22, 350-366

19. Ball, W.P.; Roberts, P.V. Long-term sorption of halogenated organic chemicals – part 2. Intraparticle diffusion. *Environ. Sci. Technol.* 1991b, 25, 1237-1249

20. Grathwohl, P.; Reinhard M. Desorption of trichloroethylene in aquifer material: rate limitation at the grain scale. *Environ. Sci. Technol.* 1993, 27, 2360-2366

21. Young, T.M.; Weber, W.J., Jr. A distributed reactivity model for sorption by soil and sediments. 3. Effects of diagenetic processes on sorption energetics. *Environ. Sci. Technol.* 1995, 29, 92-97

22. Gschwend, P.M.; Wu, S. On the constancy of sediment – water partition coefficient of hydrophobic organic pollutants. *Environ. Sci. Technol.* 1985, 19, 90-96

23. Kleineidam, S.; Schüth, C., Grathwohl, P. Solubility-normalized combined adsorption-partitioning sorption isotherms for organic pollutants. *Environ. Sci. Technol.* 2002, 36, 4689-4697

24. Abelmann, K.; Kleineidam, S.; Knicker, H., Grathwohl, P.; Kögel-Knabner, I. Sorption of HOC in soils with carbonaceous contamination: Influence of organic-matter composition. *J. Plant Nutr. Soil Sci*. 2005, 168, 293-306

25. Verschueren, K. *Handbook of environmental data on organic chemicals*, 2nd Ed, van Nostrand Reinhold Company Inc., New York, 1983

26. May W.E.; Waslk S. P.; Miller M.M.; Tewarl Y.B.; Brown-Thomas J.M.; Goldberg R.N. Solution thermodynamics of some slightly soluble hydrocarbons in water. *J. Chem. Eng. Data* 1983, 28, 197-200

27. Wauchope, R.D.; Getzen F.W. Temperature dependence of solubilities in water and heat of fusion of solid aromatic hydrocarbons. *J. Chem. Eng. Data* 1972, 17, 38-41

28. Yalkowsky S.H.; Valvani, S.C. Solubility and partitioning. 2. Relationships between aqueous solubilities, partition coefficients, and molecular surface areas of rigid aromatic hydrocarbons. *J. Chem. Eng. Data.* 1979, 24, 127-129

29. Kleineidam, S.; Rügner, H.; Ligouis, B.; Grathwohl, P. Organic matter facies and equilibrium sorption of phenanthrene. *Environ. Sci. Technol.* 1999, 33, 1637-1644

30. Nkedi-Kizza, P.; Rao, P.S.C.; Hornsby, A.G. Influence of organic cosolvents on leaching of hydrophobic organic chemicals through soils. *Environ. Sci. Technol.* 1987, 21, 1107-1111

31. Pyka, W. *Release of Coal Tar Constituents from Residual Coal Tar Contamination into Groundwater: Bench Scale Experiments on Dissolution Rate and Water Solubility Enhancement.* PhD thesis, Center for Applied Geology, University Tuebingen, 1994

32. Lion L.W.; Stauffer T.B.; MacINTYER W.G. Sorption of hydrophobic compounds on aquifer materials: analysis methods and the effect of organic carbon. *J. Contam. Hydrol.* 1990, 5, 215-234

33. Manes, M. Activated Carbon Adsorption Fundamentals, In *Encyclopedia of Environmental Analysis and Remediation*, R.A Myers, Ed., Wiley, New York, pp. 26-68, 1998

34. Wang, G.; Kleineidam, S.; Grathwohl, P. Thermodynamics of sorption/desorption of phenanthrene in soils and carbonaceous materials: Equilibrium batch studies. *Environ. Sci. Technol.* Submitted for publication.

35. Schwarzenbach, R. P.; Gschwend, P. M., Imboden, D. M. *Environmental Organic Chemistry*; Wiley-Interscience: New York, 1993.

Chapter 5

THERMODYNAMICS OF SORPTION/DESORPTION ON PHENANTHRENE IN SOILS AND CARBONACEOUS MATERIALS

Abstract: The equilibrium sorption/desorption thermodynamics of phenanthrene in carbonaceous materials and two soils has been investigated with regard to hysteresis phenomena. Equilibrium sorption and desorption isotherms were measured for phenanthrene on three carbonaceous materials (Pahokee peat, lignite and high-volatile bituminous coal) and two soil samples at four different temperatures (4, 20, 46 and 77°C). The Clausius-Clapeyron equation was used to calculate the isosteric heats of sorption and desorption (ΔH). In addition, the isosteric heat for desorption of the native phenanthrene was determined by aqueous leaching of the samples. The isosteric heats of sorption/desorption decrease with increasing solute concentration. The absolute values for ΔH are in the range of 19 - 35 kJ mol^{-1}, which is less than the heat of condensation of phenanthrene in water. No significant difference of the isosteric heats between sorption and desorption was observed, which is in accordance with the lack of significant hysteresis of the sorption/desorption isotherms in the samples used in this study (*1*). Furthermore values for ΔH of the native phenanthrene were not significantly higher than that during sorption experiments with spiked samples, indicating that release of native pollutants from soils and sediments is not different from laboratory spiked samples provided that the equilibration state of the spiked samples is appropriately considered.

5.1 Introduction

Sorption/desorption is a major process influencing the fate, transport and bioavailability of hydrophobic organic compounds in the environment. In the literature, hysteresis phenomena of organic compounds in natural soils or sediments are frequently reported, but reliable data on the thermodynamics of the sorption/desorption process are often lacking. Also most experimental artifacts lead to nonsingular sorption/desorption isotherms and these are often interpreted as hysteresis (*1*). Based on the thermodynamics, at equilibrium the contaminant distribution between solid and aqueous phases ultimately is governed by the isosteric heats (also called enthalpy ΔH) and entropies of sorption/desorption. The magnitude and sign of ΔH values gives valuable insight on the molecular interactions between sorbate and sorbent. Specifically, the ΔH values should differ significantly between sorption and desorption if hysteresis is significant.

Traditionally, sorption is classified into three categories according to the attractive forces governing the molecular interaction between solute and sorbent: physical, chemical and electrostatic forces. For hydrophobic molecules in aqueous systems, the so-called "hydrophobic bonding", a term describing the combination of the London dispersion forces between solute and sorbent and the repulsion forces from the solution, is the predominant driving force which leads to sorption. The magnitude of this physical sorption force can be determined from measurements of the isosteric heats (ΔH) transferred in the sorption/desorption processes.

The isosteric heats of sorption for various chemical compounds on different types of sorbents have been addressed already by previous investigators (*2-18*). Sorbate-sorbent interactions include sorption on mineral surfaces in vapor phase and aqueous systems. Chiou et al. (*2,3*) investigated partitioning and adsorption mechanisms and suggested that these two can be separated by comparing the isosteric heat of sorption with the heat of condensation as well as by monitoring the dependency of the isosteric heat on loading levels. Table 5.1 compiles literature values for ΔH for PAHs as well as other hydrophobic compounds to different sorbents. The values reported show a wide variety mostly in the

range of -20 - -40 kJ mol^{-1}. Different models for data interpretation also lead to different values of ΔH. For example, Huang and Weber (*14*) reported values of -22 to -24 kJ mol^{-1} for phenanthrene adsorption onto graphite surfaces based on the solute activities in aqueous phase, whereas a value of -47.1 kJ mol^{-1} was calculated by other based on concentrations (*19*).

TABLE 5.1 List of reported ΔH of PAHs as well as other hydrophobic compounds in different sorbents (Values after ± sign are the standard deviation)

Sorbents	Compounds	Sorption heats (ΔH) (kJ mol^{-1})	Temperature (°C)	Ref-erence
Mineral Oxides (α-Al_2O_3 / α -Fe_2O_3)	Naphthalene Phenanthrene Anthracene Fluoranthene Pyrene	-12.5 (±3.6) / -26 (±10) /-18.2 (±1.0) -16 (±2.8) / -17.2 (±1.9) -19.5 (±0.4) / -16.7 (±3.0) -20.8 (±0.4) / -20 (±0.9)	5 - 35	(*4*)
Silty loam soil	Phenanthrene Anthracene Fluoranthene Pyrene	-19 (±2.2) -22.7 (±0.6) -24.5 (±0.8) -37.7 (±10.7)	14 - 35	(*5*)
Soils and Ohio shale	Phenanthrene	-16.5 - +25.5	10 - 40	(*6*)
Aquifer sediment containing low organic carbon (batch / column)	Naphthalene Phenanthrene Pyrene	-11 / -1.1 -3.3 / -5.6 -14 / -14	4 - 26	(*7*)
Dissolved organic carbon (DOC)	Fluoranthrene Benzo[ghi]perylene	-18.3 -40.7	16 - 45	(*8*)
Natural sorbents	Hydrophobic pollutants	-13 - 3.8	0 - 55	(*9*)
Soils (Bayreuth, Germany)	PAHs and PCBs	0 - -20	20 - 80	(*10*)
Demolition waste and harbour sediments	PAHs	-32 - -58	25 - 100	(*11*)
Aquifer sediments and rock fragments	Phenanthrene	-23 - -36	20 - 40	(*12*)
Suspended particles	Phenanthrene	-4.5 - -3.2	2 - 20	(*13*)
Graphic surface α -Al_2O_3 Silica Gels (150/100/40)	Phenanthrene	-22 - -24 7.87 (±0.84) - 7.27 (±0.23) -0.11 (±5.32) - 10.18 (±0.6)	5 - 45	(*14*)
Granular activated carbon	VOCs	-40 - -80	20	(*15*)
Silica Gel Natural solids	TCE	-9.5 - -45 0- -34	15 - 60	(*16*)
Silica Gel Zeolite type NaX	TCE	-22.2 (±1.5) - -20.8 (±1.7) +20.3 (±12.1)	5 - 90	(*17*)
Silty clay soil	PCE	-12 (±0.3)	25 - 95	(*18*)

The variations in aqueous phase ΔH–values could originate from the different solids used, or potentially may be due to different experimental procedures leading to different experimental artifacts (*1*). Parameters used in the calculation of the sorption isosteric heat

in different studies often originate from different equilibration time periods, ranging from a few hours to days and weeks. Non-equilibrium during sorption/desorption, for instance, would lead to high ΔH-values because the activation energy of diffusion is then also included. Different geosorbents vary in physico-chemical properties depending on their origin, which again results in different values for ΔH. The heterogeneous composition of geosorbents in natural soils and sediments is a further complication for the interpretation of solute-sorbent interactions and the isosteric heat of sorption determined for such mixed materials.

In this study, relatively pure carbonaceous materials and soils containing carbonaceous materials were selected because of their relevance in sorption of hydrophobic organic compounds in soils and in sediments. A newly designed batch experimental protocol was employed, in which the laboratory artifacts are minimized, and the solute mass balance was carefully monitored. The objectives of this study were to measure the sorption/desorption isosteric heats for phenanthrene on pure carbonaceous materials and soils containing carbonaceous materials. The magnitudes of the measured isosteric heats relative to the solute heat of solution can help to elucidate the sorption/desorption mechanisms, and thus helps to understand sorption/desorption hysteresis. The sorption/desorption hysteresis was carefully checked by comparing the isosteric heats of sorption/desorption at different loading levels with phenanthrene. The isosteric heats of sorption/desorption are expected to be the same if no significant hysteresis occurs. As a very important and additional part of this study, ΔH for desorption native ("aged") PAHs were determined in leaching tests and compared with that from the laboratory spiked samples.

5.2 Experimental Section

Materials and characterization. Sample selection and sample characteristics were described in details earlier (*1*). Briefly, three carbonaceous samples (Pahokee peat, lignite and high-volatile bituminous coal (HC)) were selected, in which the organic carbon content and composition depends on the increasing rank of coalification. The samples

were characterized in terms of organic carbon content (OC) (38.9 - 72.1 wt %), specific surface area (SA) (1.78 - 3.45 m^2 g^{-1}) and pore volume (7.9 - 11.4 cm^3 kg^{-1}). In addition, two soil samples from Germany - an anthropogenic soil (AS5) and a mineral soil (MS4) - with OC contents of 4.91 and 1.74 wt % and SAs of 3.17 and 9.09 m^2 g^{-1} were selected for this study. AS5 was sampled in an urban environment close to a railway at Krefeld, where increased deposition of carbonaceous material originates from coal based industries; MS4 developed on loess near Harsum and has been under agriculture for many years. The existence of charred organic carbon in MS4 was proven by Schmidt et al. (*20*). All sorbents, except AS5, were pulverized to a grain size of less than 30 µm. For AS5, only the untreated fine grained size fraction < 0.063 mm was used in this study. Small grain sizes are important to allow rapid equilibration of the solute between the solids and water.

Phenanthrene from Aldrich Chemical Corp. was used as probe compound. Phenanthrene is representative of PAHs. Thermodynamic parameters of phenanthrene relevant for this study are listed in Table 5.2. Emphasis is on the heats of solution of phenanthrene in water (ΔH_{sol}) based on measured water solubilities (S_{solid}) between 4°C to 73.4°C (*23*, *24*, *25*). The difference of the heat of solution between the solid and subcooled liquid state of phenanthrene equals the heat of fusion (ΔH_{fus}).

TABLE 5.2. Physico-chemical properties of phenanthrene

Melting point (°C) (T_m)	99.5[a]
Boiling point (°C)	340.2[a]
Heat of fusion [kJ mol^{-1}] (ΔH_{fus})	18.6[b]
Heat of solution in water [kJ mol^{-1}] (ΔH_{sol}) (solid)[c]	36.7-39.1
Heat of solution in water [kJ mol^{-1}] (subcooled liquid)[d]	18.1-20.5

[a] melting point and boiling point are from Verschueren (*21*);
[b] data from Chiou (*22*, page 77);
[c] reported by May et al. (*23*) based on a series of water solubilities (S_{solid}) measured between 4-29.9°C (*23*); 25-73.4°C (*24*); 8-30°C (*25*)
[d] calculated as the difference between ΔH_{sol} and ΔH_{fus}

Desorption of native phenanthrene. All samples in this study contain traces of native phenanthrene as listed in Table 5.3. Isosteric heats for desorption of this native phenanthrene were determined using the same techniques as described above and the

results are compared with the spiked samples in Figure 5.2. Differences between ΔH at the same C_s level would indicate different sorbate – sorbent interaction forces for native and spiked phenanthrene. Instead of the classical batch system, high pressure aqueous leaching using an accelerated solvent extraction device (Dionex ASE 300) at different temperatures was used here to determine the desorption ΔH values. For the leaching tests about 5 g pulverized sample were mixed with about 30-40 grams of pre-cleaned quartz sand in order to improve the permeability of the packed bed during percolation with water. The mixture was packed into a stainless steel extraction cell (33 cm^3) contained by a double layer glass-fiber filter (1 µm nominal pore diameter) at each end of the cell in order to prevent fine particles leaching into the collection bottles. The samples were leached sequentially using Millipore water at elevated temperatures of 20, 40, 53, 61, 73 and 86°C under an elevated pressure of 100 bars. The equilibrium time for each step was 99 minutes, which was tested to be sufficient for equilibration of these pulverized samples at low water to solid ratios as confirmed by preliminary experiments. For example, aqueous leaching for 30 min and 99 min showed no significant concentration differences at a given temperature in several pretest experiments, indicating that 99 minutes were sufficient for equilibration. This is consistent with Lou et al. (*26*) and Wennrich et al. (*27*) works, where 20/30 minutes static time were used for optimal extraction with solvent/water using ASE.

After equilibration the aqueous leachate was purged out of the extraction cell by nitrogen for 100 seconds. The first leaching step at 20°C was repeated 3 times. Only the second and third leachate fractions were analyzed because the first flush still contained high particle concentrations despite the 1 µm filters. For each fraction leached, DOC was measured to account for a potential solubility enhancement by DOC especially released at elevated temperature. Each leaching step provided about 20 ml water which was weighted, then extracted with cyclohexane, and subsequently analyzed for PAHs by GC/MS (Hewlett-Packard HP-6890 equipped with a 30 m DB-5 capillary column, coupled to a HP-5973 mass spectrometer; temperature program: 65°C for 4 min, heated to 270°C at 10°C/min and held for 10 min, then to 310°C at 10°C/min and held for 6.5 min; carrier gas: helium at a constant flow rate of 1.0 ml/min; 1 µl of the extraction

solvent was injected with a splitless mode). A stock solution with deuterated PAH surrogates (naphthalene-d8, acenaphthalene-d10, phenanthrene-d10, chrysene-d12 and perylene-d12) was added to the leachates as internal standard, and a diluted standard solution containing the 16 EPA PAHs and 5 deuterated surrogates was measured to calculate the relative response factors.

Batch experiments. Details of the batch procedure were described earlier (*1*). In brief, equilibrium sorption/desorption isotherms were determined in batch vials sealed with PTFE-lined butyl rubber septa (Alltech) at four temperature levels (77, 46, 20 and 4°C). Instead of the conventional decant-and-refill batch method, sorption/desorption was driven by temperature changes using consistent samples. Sorption was started at high temperatures (low sorption), stepwise equilibrated at lower and lower temperatures (increasing sorption) until 4°C were reached. After that, the procedure was reversed, which leads to subsequent desorption of phenanthrene at the higher temperatures. A time period of 7 days was used for equilibration for each temperature. Each experimental step was carefully monitored in order to recognize and minimize experimental artifacts (see *1*). The aqueous phase concentration in the batch vials was measured using HPLC equipped with a fluorescence detector with the wavelengths of 249/345 nm. Additionally, DOC was measured in order to assess a potential solubility enhancement due to the presence of DOC (*1*).

Data evaluation. The molar isosteric heat of sorption (ΔH) is a general expression, which represents the enthalpy change involved in the transfer of a solute from the solution state to the sorbed state while holding the solid-phase loading (C_s) constant. It indicates the difference in binding energies between the sorbent and the sorbate and between the solvent (water) and the solute (sorbate). ΔH can be calculated using the Clausius-Clapeyron equation at a given C_s (*22*):

$$\Delta H_{a/d} = -2.303R\frac{d\log C_w}{d(1/T)} \qquad \text{with } C_w = \left(\frac{C_s}{K_{Fr}}\right)^n \tag{5.1}$$

where $\Delta H_{a/d}$ [kJ mol^{-1}] is the molar isosteric heat of sorption or desorption (ΔH_a and ΔH_d have opposite signs). R is the gas constant and T is the temperature in Kelvin. C_s [mg kg^{-}

^{1}] and C_w [mg L^{-1}] denote the concentrations in the solid and the aqueous phase, respectively. K_{Fr} [mg kg^{-1}: (mg L^{-1})$^{1/n}$] and $1/n$ [-] are the Freundlich coefficients. The change in C_w at a given C_s level was calculated based on the equilibrium isotherm parameters (K_{Fr} and $1/n$) determined at each temperature.

In addition to the batch experiments using spiked samples, ΔH_d of native phenanthrene from the samples using ASE was also determined with eq. 5.1, where the measured aqueous concentration after Doc-correction at each temperature were used instead of isotherm calculated C_w values. The change of C_s during the leaching experiments was carefully monitored over the temperature range and found to be insignificant and thus neglected.

5.3 Results and Discussion

Sorption isotherms. Equilibrium sorption/desorption isotherms of phenanthrene on Pahokee peat, lignite, HC, AS5 and MS4 were as mentioned already above determined at four different temperatures (4, 20, 46 and 77°C). The sorption/desorption isotherms were fit with the Freundlich model, and the isotherm parameters at each temperature were determined (see *1*). All the sorption/desorption isotherms in this study are significantly nonlinear, except AS5, which shows a relatively slight non-linearity. The high nonlinearity indicates that physical adsorption play an important role in the solute-sorbent interaction (especially pronounced in coals). In all samples K_{Fr} in sorption and desorption isotherms decreases with increasing temperature as expected for exothermic sorption and endothermic desorption processes.

Isosteric heats of sorption and desorption (ΔH). Figure 5.1 shows the regression of log C_w versus $1/RT$ for the determination of ΔH of sorption and desorption of phenanthrene on the five sorbents each with five different solid phase loading levels used in the study. The linear regressions (eq. 5.1) fit the data very well with a coefficient of determination (R^2) > 0.96 in all cases. The isosteric heats of sorption/desorption and their standard deviations determined for our samples are compiled in Table 5.3. They range from -19 kJ

mol^{-1} to -35 kJ mol^{-1}, which is higher than the subcooled heat of solution (about 19 kJ mol^{-1}), but much less than the heat of condensation of solid phenanthrene from water, which is about 38 kJ mol^{-1} in the temperature range of interest (see Table 5.2). The total

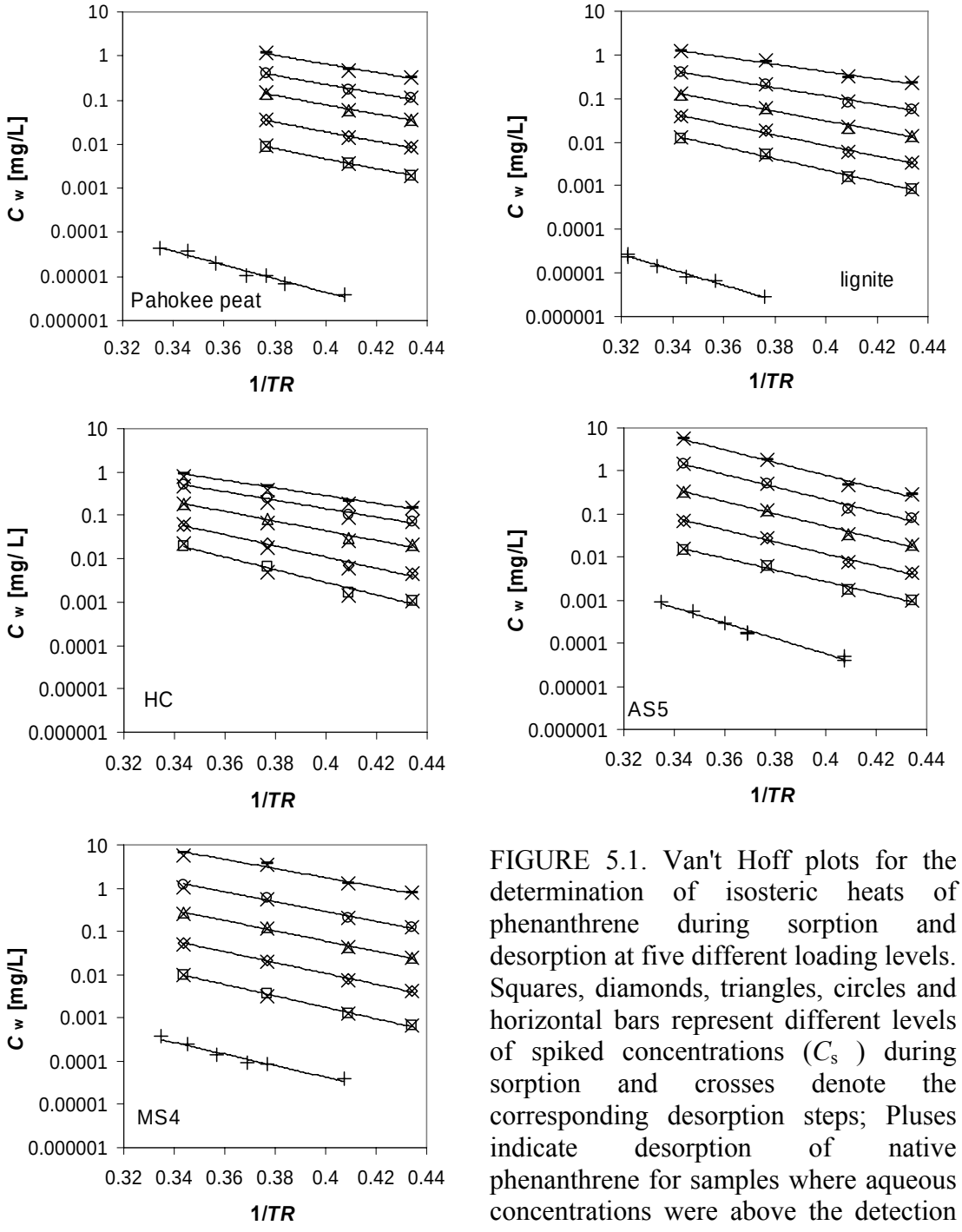

FIGURE 5.1. Van't Hoff plots for the determination of isosteric heats of phenanthrene during sorption and desorption at five different loading levels. Squares, diamonds, triangles, circles and horizontal bars represent different levels of spiked concentrations (C_s) during sorption and crosses denote the corresponding desorption steps; Pluses indicate desorption of native phenanthrene for samples where aqueous concentrations were above the detection limit.

TABLE 5.3. Isosteric heats of sorption and desorption (ΔH_a, ΔH_d) calculated from sorption/desorption isotherms at five concentration levels (C_s) and for the release of native phenanthrene for five geosorbents in a temperature range of 4°C to 86°C (values after ± sign are the standard deviation). $F_{adsorption}$ indicates the contribution of adsorption to the total sorption/desorption isosteric heat

Pahokee Peat	C_s level [mg kg^{-1}]	0.66*	160	400	1000	2000	4000
	ΔH_a [kJ mol^{-1}]		-26.0 ± 0.5	-25.0 ± 1.1	-23.9 ± 1.7	-23.1 ± 2.2	-22.3 ± 2.6
	R^2 [-]		1.0	1.0	0.99	0.99	0.99
	ΔH_d [kJ mol^{-1}]	35.6 ± 2.4	27.1 ± 1.9	25.9 ± 2.5	24.6 ± 3.0	23.6 ± 3.4	22.7 ± 3.8
	R^2 [-]	0.98	0.99	0.99	0.99	0.98	0.97
	$F_{adsorption}$	59%	25%	21%	18%	14%	11%
Lignite	C_s level [mg kg^{-1}]	0.19*	100	300	900	2700	8000
	ΔH_a [kJ mol^{-1}]		-30.6 ± 1.9	-27.8 ± 1.9	-24.9 ± 1.9	-22.1 ± 2.0	-19.3 ± 2.1
	R^2 [-]		0.99	0.99	0.99	0.98	0.98
	ΔH_d [kJ mol^{-1}]	40.5 ± 2.1	31.2 ± 1.6	28.2 ± 1.6	25.1 ± 1.6	22.0 ± 1.7	19.0 ± 1.7
	R^2 [-]	0.99	0.99	0.99	0.99	0.99	0.98
	$F_{adsorption}$	77%	43%	32%	21%	11%	1%
HC	C_s level [mg kg^{-1}]	12.2*	1000	2200	5000	10000	15000
	ΔH_a [kJ mol^{-1}]		-33.5 ±3.2	-29.7 ±2.6	-25.7 ±2.0	-22.4 ±1.5	-20.4 ±1.2
	R^2 [-]		0.98	0.99	0.99	0.99	0.99
	ΔH_d [kJ mol^{-1}]		34.8 ± 4.9	30.2 ± 4.0	25.4 ± 2.1	21.3 ± 2.4	19.0 ± 2.0
	R^2 [-]		0.96	0.97	0.97	0.98	0.98
	$F_{adsorption}$		53%	39%	25%	11%	4%
AS5	C_s level [mg kg^{-1}]	0.39*	5	20	80	300	1000
	ΔH_a [kJ mol^{-1}]		-31.2 ± 2.1	-31.9 ± 2.0	-32.7 ± 2.1	-33.4 ± 2.3	-34.1 ± 2.5
	R^2 [-]		0.99	0.99	0.99	0.99	0.99
	ΔH_d [kJ mol^{-1}]	41.0 ± 2.3	31.3 ± 1.8	32.1 ± 1.9	32.9 ± 2.1	33.7 ± 2.3	34.4 ± 2.5
	R^2 [-]	0.98	0.99	0.99	0.99	0.99	0.99
	$F_{adsorption}$	78%	44%	46%	49%	52%	54%
MS4	C_s level [mg kg^{-1}]	0.07*	1	4	15	50	200
	ΔH_a [kJ mol^{-1}]		-30.3 ± 0.6	-28.8 ± 0.9	-27.3 ± 1.3	-26.0 ± 1.8	-24.4 ± 2.3
	R^2 [-]		1.0	1.0	1.0	0.99	0.98
	ΔH_d [kJ mol^{-1}]	31.0 ± 3.4	30.1 ± 1.1	28.2 ± 0.8	26.5 ± 1.0	24.9 ± 1.5	23.0 ± 2.0
	R^2 [-]	0.97	1.0	1.0	1.0	0.99	0.98
	$F_{adsorption}$	43%	39%	36%	28%	25%	18%

* Native phenanthrene loadings

molar isosteric heat of adsorption for a partially miscible solute is the sum of the condensation heat and molecular attractive heat (*22*). Therefore, for comparison, the total molar isosteric heat of adsorption for solid phenanthrene should be larger than 38 kJ mol^{-1}. For pure partitioning of phenanthrene between octanol and water a value of -19 kJ mol^{-1} is reported (*28*). Thus the observed isosteric heats for sorption and desorption indicate that adsorption as well as partitioning into organic matter are involved in sorption/desorption of phenanthrene in the samples studied. The determined ΔH values are a superposition of partitioning and adsorption processes with different weights. If we

use -47.1 kJ mol^{-1} (adsorption heat of phenanthrene onto graphite surface, see *19*) as the value for the standard adsorption isosteric heat, and -19 kJ mol^{-1} as the value for the standard partitioning isosteric heat, then the adsorption contribution ($F_{adsorption}$) from the total sorption/desorption isosteric heat could be calculated and the results are compiled in Table 5.3. The $F_{adsorption}$ data in Table 5.3 show that large values of ΔH are commonly attributed to adsorption, especially for the desorption of native phenanthrene. The partitioning contribution increases with increased loading, i.e. with increasing aqueous concentrations C_w. For example, the adsorption contribution almost vanishes at a loading of 8000 mg kg^{-1} in lignite, which corresponds to C_w of 38% of the phenanthrene solubility at 20°C. The significance of adsorption contribution in the total sorption process could be reduced in real field environments, where multicomponent contaminants are coexistent.

Potential slow ad-/desorption of phenanthrene is indicated by the dependency of the ΔH on the solid phase loadings, which is summarized in Figure 5.2. For the three carbonaceous materials (Pahokee peat, lignite and HC), the isosteric heat becomes less exothermic/endothermic with increasing solid loading during sorption and desorption, respectively. This effect is consistent with a nonlinear surface adsorption process, where ΔH_a has the largest negative value (i.e., the molar exothermic heat) at the lowest loading (*22*). From the five sorbents used in this study, the high-volatile bituminous coal (HC) shows the strongest dependency of $\Delta H_{a/d}$ on concentration in coincidence with the strongest nonlinearity of sorption for this sorbent. Here, a maximum value of $\Delta H_{a/d}$ of -55 kJ mol^{-1} is reached if C_s decreases below 10 mg kg^{-1} (i.e., the natural loading of phenanthrene on this sample). These findings apply in general to the other carbonaceous samples as well as for the char containing soil sample MS4. The AS5 sample, however, shows an opposite trend of slightly increasing isosteric heat with increasing concentration levels. It is hard to interpret this phenomenon at this moment, and more sample characterization work for the < 0.063 mm fine grain material is needed.

Regressions for the release of native phenanthrene in cases where the concentrations of C_w were above the detection limit are shown in Figure 5.1. The desorption isosteric heats

from desorption of native phenanthrene (ΔH_d) for the soils, Pahokee peat, and lignite samples range between 31 kJ mol^{-1} and 41 kJ mol^{-1} and are thus in good agreement with the $\Delta H_{a/d}$ values obtained from the spiked experiments (see Table 5.3) if lower loadings are considered. ΔH for the native phenanthrene in AS5 is 41 kJ mol^{-1}. In the case of high-volatile bituminous coal, C_w was below the detection limit at almost all temperatures.

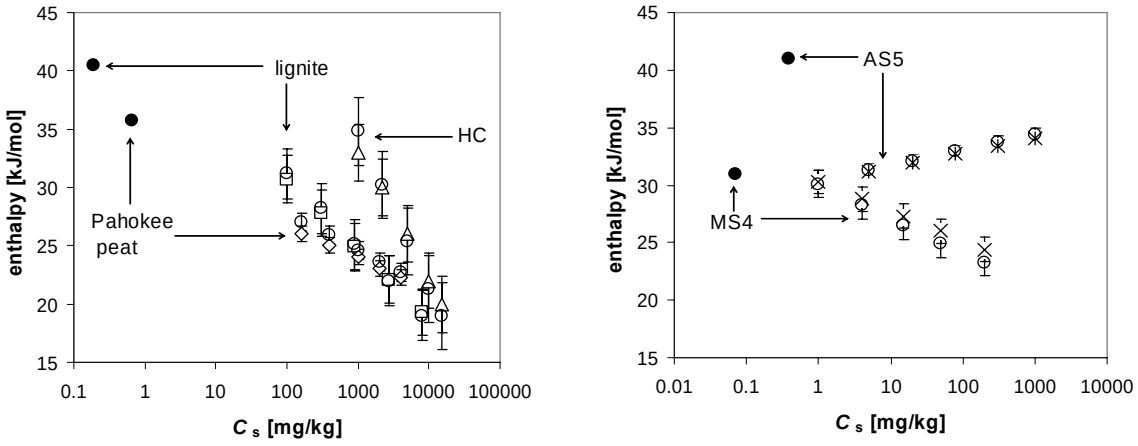

FIGURE 5.2. Isosteric heats of sorption and desorption (with standard error bars) as a function of the sorbed phenanthrene concentrations. Squares, triangles, diamonds, stars and crosses represent the phenanthrene sorption onto lignite, high-volatile bituminous coal, Pahokee peat, AS5 and MS4, respectively, whereas the corresponding open circles indicate desorption isosteric heats; filled circles represent the desorption isosteric heats for leaching of native phenanthrene from the different sorbents.

The comparison of the isosteric heats (ΔH_a, ΔH_d) for sorption and desorption of phenanthrene (Figure 5.2) shows that with slight deviations, no significant hysteresis exists. This indicates that no significant changes occurred concerning the interaction mechanism between sorbate and sorbent during the sorption/desorption cycle. This also implies that no significant irreversible configurational changes of the organic geopolymer occurred either by uptake of the sorbate, or by the elevated temperatures in the samples investigated. The isosteric heats of desorption of the native phenanthrene are also in reasonable agreement with the $\Delta H_{a,d}$ values obtained from the spiked experiments (see Figure 5.2 and Table 5.3). This findings are further confirmed by exhaustive desorption of phenanthrene from the samples during column leaching experiments with stepwise temperature increase in the tailing part which are reported in a subsequent paper (Wang

and Grathwohl, 2008). Overall we find no significant sorption/desorption hysteresis of phenanthrene within the group of samples investigated in this study.

5.4 References

1. Wang, G.; Kleineidam, S.; Grathwohl, P. Sorption/desorption reversibility of phenanthrene in soils and carbonaceous materials. *Environ. Sci. Technol.* 2007, 41, 1186-1193

2. Chiou, C. T. ; Peters, L. J. ; Freed, V. H. A physical concept of soil-water equilibria for nonionic organic compounds. *Science* (Washington, DC), 1979, 206, 831-832

3. Chiou, C. T.; Shoup, T. D.; Porter, P. E. Mechanistic roles of soil humus and minerals in the sorption of nonionic organic compounds from aqueous and organic solutions. *Org. Geochem*, 1985, 8, 9-14

4. Mader, B. T.; Uwe-Goss, K.; Eisenreich, S. J. Sorption of non-ionic, hydrophobic organic chemicals to mineral surfaces. *Environ. Sci. Technol.* 1997, 31, 1079-1086

5. Woodburn, K. B; Lee, L. S.; Rao, P. S. C.; Delfino, J. J. Comparison of sorption energetics for hydrophobic organic chemicals by synthetic and natural sorbents from methanol/water solvent mixtures. *Environ. Sci. Technol.* 1989, 23, 407-413

6. Young, T. M.; Weber, W. J., Jr. A distributed reactivity model for sorption by soils and sediments. 3. Effects of diagenetic processes on sorption energetics. *Environ. Sci. Technol.* 1995, 29, 92-97

7. Pitta, J. J.; Bachus, D. A.; Capel, P. D.; Eisenreich, S. J. Temperature-dependent sorption of naphthalene, phenanthrene, and pyrene to low organic carbon aquifer sediments. *Environ. Sci. Technol.* 1996, 30, 751-760

8. Lüres, F.; Ten Hulscher, Th. E. M. Temperature effect on the partitioning of polycyclic aromatic hydrocarbons between natural organic carbon and water. *Chemosphere*, 1996, 33, 643-657

9. Ten Hulscher, Th. E. M.; Cornelissen, G. Effect of temperature on sorption equilibrium and sorption kinetics of organic micropollutants- a review. *Chemosphere*, 1996, 32, 609-626

10. Krauss, M.; Wilcke, W. Prediction soil-water partitioning of polycyclic aromatic hydrocarbons and polychlorinated biphenyls by desorption with methanol-water mixtures at different temperatures. *Environ. Sci. Technol.* 2001, 35, 2319-2325

11. Madlener, I.; Henzler, R.; Grathwohl, P. Material investigations to determine the leaching behaviour of PAH at elevated temperatures. In *Proceedings of the 2nd International Workshop on Groundwater Risk Assessment at Contaminated Sites (GRACOS) and Integrated Soil and Water Protection (SOWA)*. Halm, D.; Grathwohl, P. Eds. Center for

Applied Geoscience, Tübingen, Germany. 2003, pp 193-198 (http://w210.ub.uni-tuebingen.de/portal/tga_c)

12. Kleineidam, S.; Rügner, H.; Grathwohl, P. Desorption kinetics of phenanthrene in aquifer material lacks hysteresis. *Environ. Sci. Technol.* 2004, 38, 4169-4175

13. Tremblay, L.; Kohl, S. D.; Rice, J. A.; Gagne, J. P. Effects of temperature, salinity, and dissolved humic substances on the sorption of polycyclic aromatic hydrocarbons to estuarine particles. *Marine Chemistry* 96. 2005, 21-34

14. Huang, W.; Weber, W. J., Jr. Thermodynamic considerations in the sorption of organic contaminants by soils and sediments. 1. The isosteric heat approach and its application to model inorganic sorbents. *Environ. Sci. Technol.* 1997, 31, 3238-3243

15. Pre, P.; Delage, F.; Faur-Brasquet, C.; Cloirec, P. L. Quantitative structure-activity relationships for the prediction of VOCs adsorption and desorption energies onto activated carbon. *Fuel Processing Technology* 77-78, 2002, 345-351

16. Werth, C. J.; Reinhard, M. Effects of temperature on trichloroethylene desorption from silica gel and natural sediments. 1. Isotherms *Environ. Sci. Technol.* 1997, 31, 689-696

17. Farrell, J., Hauck, B., Jones, M. Thermodynamic investigation of trichloroethylene adsorption in water-saturated microporous adsorbents. Environ. Toxicol. Chem. 1999, 18, 1637-1642 new1

18. Costanza, J., Pennell K. D. Distribution and abiotic degradation of chlorinated solvents in heated field samples. *Environ. Sci. Technol.* 2007, 41, 1729-1734

19. Su, YH., Zhu, Y. G., Sheng, G., Chiou, C. T. Linear adsorption of nonionic organic compounds from water onto hydrophilic minerals: Silica and Alumina. *Environ. Sci. Technol.* 2006, 40, 6949-6954

20. Schmidt, M. W. I., Skjemstad, J. O., Gehrt, E., Kogel-Knabner, I. Charred organic carbon in German chernozemic soils. *Eur. J. Soil Sci*. 1999, 50, 351-365

21. Verschueren, K. *Handbook of environmental data on organic chemicals*, 2nd Ed, van Nostrand Reinhold Company Inc., New York, 1983

22. Chiou, C. T. *Partition and Adsorption of Organic Contaminants in Environmental Systems*, John Wiley & Sons, Inc., New Jersey, 2002

23. May W. E.; Waslk S. P.; Miller M. M.; Tewarl Y. B.; Brown-Thomas J. M.; Goldberg R. N. Solution thermodynamics of some slightly soluble hydrocarbons in water. *J. Chem. Eng. Data* 28. 1983, 197-200

24. Wauchope, R. D.; Getzen F. W. Temperature dependence of solubilities in water and heats of fusion of solid aromatic hydrocarbons. *J. Chem. Eng. Data* 17, 1972, 38-41

25. Schwarz, F. P. Determination of temperature dependence of solubilities of polycyclic aromatic hydrocarbons in aqueous solutions by a fluorescence method. *J. Chem. Eng. Data*, 1977, 22, 273-277

26. Lou, X., Janssen, H. G., Cramers, C. A. parameters affecting the accelerated solvent extraction of polymeric samples. *Anal. Chem*., 1997, 69, 1598-1603

27. Wennrich, L., Popp, P., Moder, M. Determination of chlorophenols in soils using accelerated solvent extraction combined with solid-phase microextraction. Anal. Chem., 2000, 72, 546-551

28. Lei, Y. D.; Wania, F.; Shiu, W. Y.; Boocock, D. G. B. HPLC-based method for estimating the temperature dependence of *n*-octanol-water partition coefficients. *J. Chem. Eng. Data*, 2000, 45, 738-742

29. Wang, G.; Grathwohl, P. Activation energies of phenanthrene desorption from carbonaceous materials: Column studies. *Environ. Sci. Technol.* (in preparation), 2008

Chapter 6

ACTIVATION ENERGIES OF PHENANTHRENE DESORPTION FROM CARBONACEOUS MATERIALS: COLUMN STUDIES

Abstracts. Sorption/desorption kinetics of phenanthrene from two carbonaceous samples (lignite and high-volatile bituminous coal (HC)) at different temperatures was monitored using an on-line column method. Pulverized samples were equilibrated in the column for 2 months before desorption began. The desorption effluent concentrations declined initially fast, followed by an extended tailing part, which could be described reasonably well by a spherical diffusion model. Desorption was carried out at stepwise increased temperatures (20°C to 90°C), and desorption activation energies were calculated based on the Arrhenius relationship at each concentration step. The determined activation energies were in an order of 58–66 kJ mol^{-1} or 70–71 kJ mol^{-1} for lignite and HC, respectively. Activation energies were always constant and did not increase significantly during leaching. The experiment desorption was almost completed, when only 0.2% (lignite) and 6% (HC) of the initially sorbed mass was present at the last temperature step. Comparison between activation energies and sorption/desorption enthalpies obtained for the same samples from equilibrium isotherms implies that the diffusion also occurred in organic matter and micropores, where higher activation energies were determined.

6.1 Introduction

Dependency of sorption/desorption rates on temperature is determined by the activation energy, which essentially describes how chemical rate constants vary with temperatures. It is popularly accepted that two mechanisms limit the mass-transfer in sorption/desorption of hydrophobic organic compounds (HOCs) in natural organic matter: (1) molecular diffusion in an organic matrix (*1-3*) and (2) aqueous diffusion in intraparticle pores (*4-6*). Since diffusion is positively temperature-dependent, both mechanisms are considered to be activated processes. Diffusion in an organic matrix is postulated to be analogous to diffusion in polymers, where diffusion occurs through holes that are distributed discontinuously throughout the material (*7*). Pore diffusion depends on diffusion coefficients and sorption sites distributed along the pore walls, which retards the solute transport. Diffusion through micropores is considered as molecule jumps from one low-energy site to the next (*8*). ten Hulscher & Cornelissen (*7*) reviewed the diffusion of organic compounds in polymers and report average activation energies of 60 kJ mol^{-1}. Values higher than 100 kJ mol^{-1} can be expected for glassy or highly cross-linked polymeric matrixes (*9*). A number of studies have been carried out to investigate the desorption kinetics and related activation energies using different organic compounds in different sorbents (model substances, soils and sediments). Cornelissen et al. (*10*) studied the slow desorption of PAHs and PCBs from laboratory-spiked and field-contaminated sediment samples and determined activation energies in the range of 60-70 kJ mol^{-1}. Werth et al. (*11*) determined activation energies in column experiments on desorption of trichloroethene from model substances and natural geosorbents (silica gel, soil, sediment) of 47-94 kJ mol^{-1}, which is consistent with the values found for diffusion in micropores. Chihara et al. (*12*) found activation energies between 10 and 50 kJ mol^{-1} for diffusion of hydrocarbons in zeolites and molecular sieves. Johnson and Weber (*9*) investigated desorption of phenanthrene using heated and superheated water at different temperatures (75°C to 150°C) and report activation energies of 40-80 kJ mol^{-1}. Ghosh et al. (*13*) measured the activation energies of PAHs from a coal containing subfraction and clay/silt subfraction of a harbor sediment, and found that the activation energies for the coal containing subfraction is 3 times higher than that for the clay/silt subfraction.

Recently, Kleineidam et al. (*14*) carried out column desorption experiments using aquifer materials which experienced more than a 1000 days long-term sorptive uptake of phenanthrene. The desorption rates were very well fit by the retarded pore diffusion model simply by forward modeling using the parameters from the long-term sorptive uptake batch experiment. No hysteresis was observed and desorption activation energies in the range from 45 to 59 kJ mol^{-1} were determined.

Generally, the calculation of the activation energy is based on the Arrhenius relationship by plotting the log values of desorption rate constants *vs.* the inverse of temperature. Desorption rate constants are obtained by fitting models to data from desorption experiments (such as concentration, flux, remaining mass). Intraparticle diffusion or two/multi-site first-order models are widely combined with the advection-dispersion equation to represent desorption kinetics in column studies (*5-6, 15-20,* (pore diffusion model); *10, 21-23* (multi-site model)). In addition, mobile/immobile two-region models are also used (*24-26*). The multi-site models need more than two rate constants as fitting parameters whereas for the diffusion models (e.g. the spherical diffusion model) usually only one rate constant to simulate desorption kinetics is sufficient for a homogeneous sample (for heterogeneous samples again multi-rate models are needed).

In this study, sorption and desorption kinetics of phenanthrene from two carbonaceous materials was investigated in flow through column experiments with stepwise increases of the temperature. The main objectives of this study were (1) to determine desorption activation energies from stepwise temperature increases using a high resolution on-line column technique; (2) to find out if the activation energy changes with increasing desorption in order to elucidate potentially hysteresis phenomenon which should lead to increased activation energies along with the increased degree of desorption; (3) and to compare them with existing thermodynamic data on diffusion in polymers, micropores and water in order to elucidate potential desorption mechanisms; and (4) to carefully check the phenanthrene in the samples after the completed desorption experiments for significant residuals using an exhaustive accelerated solvent extraction (ASE) device.

6.2 Theory

Activation energy (E_a). If in the tailing part of a desorption experiment, the temperature is stepwise increased a corresponding increase of the desorption rates and thus an increase of the effluent concentrations is expected. Then desorption activation energy (E_a [kJ mol^{-1}]) for each individual temperature step (from T to T') can be calculated according to the Arrhenius relationship:

$$E_a = -R\left(\frac{T\,T'}{T-T'}\right)\ln\left(\frac{C'}{C}\right) \qquad (6.1)$$

where C or C' is the transient effluent aqueous concentrations [in µg L^{-1} or fluorescence signal (mV)] before and after the temperature step. R is the gas constant. This equation requires that the solid loading (C_s) stays constant at each step.

6.3 Materials and Methods

Pulverized lignite and high-volatile bituminous coal (HC) were selected for the column experiments in this study. Two soil samples (anthropogenic soil (AS5) and mineral soil (MS4)) from the previous study could not be used because of plugging problems due to mobilization of fine particles (probably swelling clay minerals). Phenanthrene was used as the probe compound and was obtained as pure product (98%) from Aldrich Chemical Corp. Physicochemical properties, thermodynamic parameters (on sorption/desorption) and sample characteristics are listed in (*27*) and (*28*).

Column package and pretreatment. Stainless steel HPLC columns with 8 cm length and 1 cm inner diameter were used. About 0.2 g pulverized sample was scattered evenly on a clean glass wool mat, which was then rolled and packed into the column. Two metal frits were placed at both ends of the column to prevent leaching of fine particles. Then the column was filled with Millipore water from the bottom using a HPLC pump at a flow rate of 0.5 ml min^{-1}. The total filling time was recorded and the pore volume was

calculated from mass of water in the column. The dead volume of all the stainless steel capillary connection tubes was considered as well, but was less than 0.25% of the total pore volume.

On – line column experiments. The sorption and subsequently desorption column experiments were monitored on line. The column setup is shown in Figure 6.1. The packed column was connected to a HPLC system instead of the usual separation column. A fluorescence detector with emission/extinction wavelengths of 249/345 nm was used to measure phenanthrene concentrations and the signals were recorded using chromatography software every 5 seconds. This high resolution of the measurement was needed in order to monitor the effluent concentrations in sufficient detail at each temperature step. Temperature control was assured by placing the column in a water bath. Calibration of the fluorescence signal was carried out before and after each experiment in order to account for any baseline shift in the signal. For each calibration 4 to 6 standard solutions (2-150 μg L^{-1}) were used and electrical signals [mV] were converted to concentrations [μg/L]. Phenanthrene solutions were prepared using degassed Millipore water and stock solutions in methanol, then were kept in the dark and poisoned with sodium azide at a concentration level of 200 mg L^{-1} in order to inhibit bacterial growth and thus to limit biodegradation of the phenanthrene. For the breakthrough percolation experiments, the inflow phenanthrene solution was renewed every 24 hours. The inflow solution was directly connected to the HPLC pump using stainless steel capillary tubing to avoid any potential memory effects (see Figure 6.1). The phenanthrene solution was pumped through the sample column with a constant flow rate of 1.42 or 1.45 ml/min under a controlled temperature (25°C for lignite and 20°C for HC). The concentrations of the inflow phenanthrene solutions were around 10-12% of the solid phenanthrene aqueous solubility at 25°C (121 μg/L for lignite and 150 μg/L for HC, respectively). After the sorption uptake step, the sample column was detached from the HPLC system, closed tightly with stainless steel fittings and kept at 20°C for about two months. Sorption equilibrium was established for the fine particles in the column after this two-month period (*27*). Thereafter, desorption experiments were carried out. The equilibrated column was reinstalled in the HPLC system again, where another HPLC pump (no

phenanthrene history to avoid memory effects) was used to purge the column with clean water at a pumping rate of 2.96 ml/min. The water used for purging was again deionized, degassed and spiked with sodium azide (200 mg L^{-1}) and tested for potential phenanthrene background. After the concentrations in the effluent decreased significantly at 20°C (about 120–250 hours), the temperature was stepwise increased first to 46°C, then to 77°C and finally to 90°C in the case of the HC sample (see Figure 6.3). After the desorption experiments, the samples together with the glass wool mat were moved from the column to an extraction cell quickly and extracted with acetone and toluene solvent in an ASE device in order to determine the residual phenanthrene in the column after the desorption procedure. In order to check the reproducibility of the procedure, the experiment with the lignite sample was repeated under slightly different temperature steps of 30, 40, 50 and 77°C.

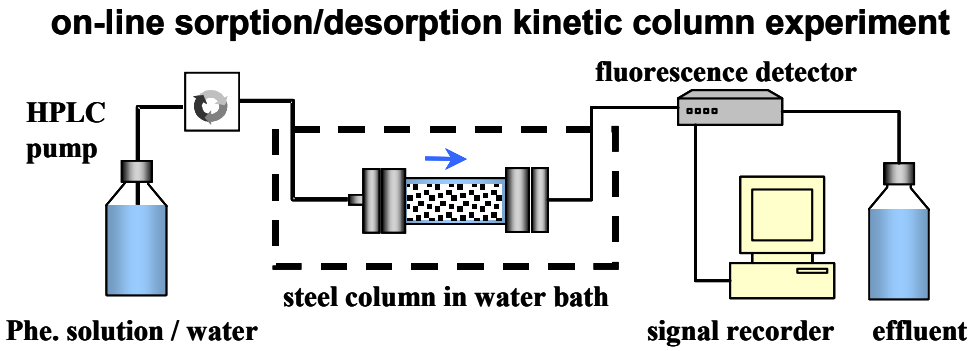

FIGURE 6.1 On-line sorption/desorption kinetic column experimental setup

6.4 Results and Discussion

Phenanthrene sorption. Breakthrough curves of phenanthrene in the columns are shown in Figure 6.2. Pumping lasted 121/92 hours for lignite/HC columns, and the sorbed mass as compared to the expected uptake at equilibrium (M/M_{eq}) was 0.79 and 0.16 for lignite and HC, respectively. The sorbed mass M at time t was calculated by integration of the breakthrough curve. The equilibrium sorptive uptake (M_{eq}) expected at the inflow concentration was calculated based on results from previous batch equilibrium sorption

experiments (see *27*). The total mass present in the column after sorptive uptake was 480 µg and 330 µg for lignite and HC, respectively.

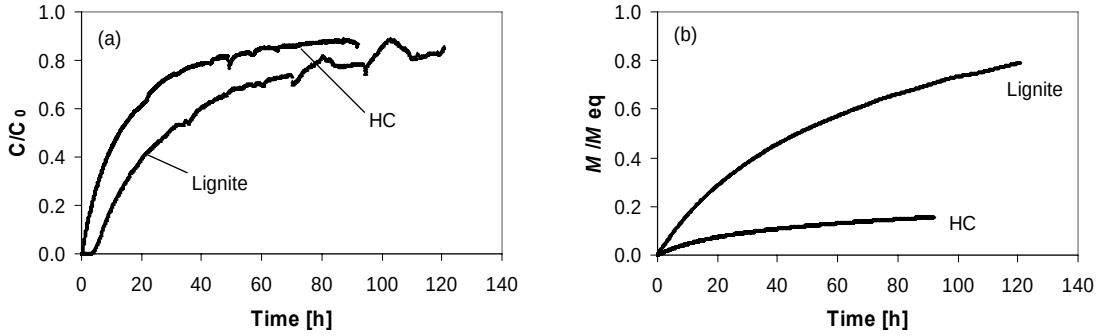

FIGURE 6.2 (a) Phenanthrene breakthrough curves in lignite and HC columns; (b) relative accumulated mass in the sorbents.

Desorption breakthrough curve. Figure 6.3 shows the desorption concentrations in the leachate of the lignite and HC columns. Desorption was initially fast and followed by an extended tailing part, which is interpreted in other studies as fast and slow two-site desorption (*10*). The temperature was increased in the extended tailing part of each desorption study where the release of phenanthrene is believed to be purely diffusion limited (non dispersion effects). The stepwise increase of temperature caused immediate concentration increases, which reflects that desorption is thermodynamically a heat favorable process.

In the case of the lignite, the phenanthrene desorption concentrations can be predicted very well with the intraparticle pore diffusion model (see Figure 6.3). The fitted apparent diffusion coefficient at 20°C was $4.83e^{-16}$ cm^2 s^{-1}. The predicted concentrations are slightly lower than the experimental data in the beginning of desorption probably due to background fluorescence because of DOC leaching. The initial high DOC leaching (indicated by yellow colored effluent) is probably due to production of DOC during the two-month equilibration of the lignite column. Yellow colored aqueous effluent was again observed at the 77°C step immediately after the temperature increase. The DOC release from soil and sediment is reported as a rate-limited process (*29-30*). Thurman (*31*) reported that the DOC content of uncolored fresh water could be still up to 2-8 mg L^{-1}.

Therefore, a certain DOC related fluorescence can not be excluded for the lignite sample even if the column effluent was non-colored.

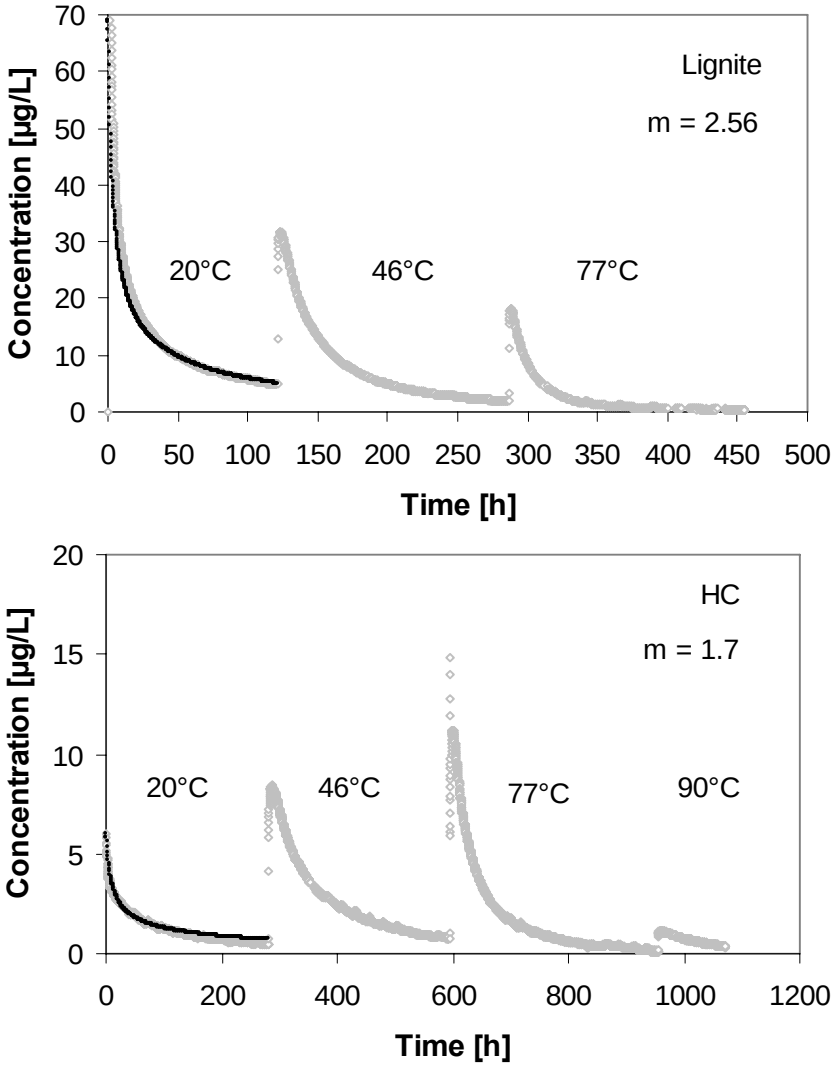

FIGURE 6.3 Phenanthrene concentrations (open diamonds) during column desorption with stepwise increased temperatures from spiked lignite and HC samples starting at sorption equilibrium. The solid line denotes the intraparticle pore diffusion model simulation, where "m" is a fitted empirical exponent accourting for pore geometry (tortuosity).

For the HC sample, the desorption concentrations again are well fit in the tailing part using a single diffusion rate parameter (apparent diffusion coefficient: $6.27e^{-15}$ cm^2 s^{-1}) but overestimated initially. This might be due to fast desorbing domains in the coal followed by slow diffusion from micropores (*19-20*). Ahn et al. (*32*) investigated the

intraparticle diffusion of phenanthrene and pyrene in polymers, coke, and activated carbon, and found that the sorption kinetics in the polymer and coke samples can be described well by the intraparticle diffusion model, whereas a branched pore model combining the macro- and micropore domains has to be used to simulate the sorptive uptake in activated carbon, which is characterized by a high micropore volume.

Mass balance. Table 6.1 shows the mass balance of phenanthrene sorbed and desorbed in the column experiments based on integration of the breakthrough curves. The "residual" indicates mass recovered by the ASE extraction after the desorption experiment was finished. In the case of the lignite, the desorption seems to recover more mass than sorbed during the loading of the column, which likely is due to the background fluorescence from DOC. As the most important result from Table 6.1, the residual mass in the column after desorption is only 0.8 μg, which accounts for only 0.17% of the initially sorbed phenanthrene. In the case of the HC column, 5.9% of sorbed phenanthrene still remained in the sorbent after more than 1000 hours of leaching even at elevated temperatures.

TABLE 6.1. Phenanthrene mass (μg) of uploaded and desorbed in the column experiments

Samples	Sorption	Residual	Desorption
	On-line curve integration	GC/MS	On-line curve integration
Lignite	480	0.8	524.3 [a]
HC	330	19.4	340 [b]

[a] Based on the stable effluent concentrations after 12 pore volumes (first 15 minutes); the earlier signal was affected by background fluorescence attributed to DOC.
[b] The fluorescence signal was baseline corrected (3 mV) by the signal measured before desorption was started.

Temperature-dependent desorption and activation energies. Figure 6.4 shows the Arrhenius plots based on concentration increases at each temperature step. The activation energies determined are compiled in Table 6.2. For both samples the Arrhenius plots are parallel for the different temperature steps except the 77°C to 90°C step for HC. In addition, similar activation energies were determined for the second lignite sample, which was examined at slightly different temperature steps, indicating that the experimental technique provides robust results. As an important result, no trend of

increasing E_a with progressing desorption is observed. Activation energies determined are 70–71 kJ mol^{-1} and 58–66 kJ mol^{-1} within the temperature range of 20–77°C for HC and lignite, respectively. Only in the case of 0.21g-lignite experiment was a difference in the activation energy observed, where the determined activation energy at the 46-77°C step (66 kJ mol^{-1}) is 8 kJ mol^{-1} larger than that at the 20-46°C step (58 kJ mol^{-1}). This, again, might be due to DOC leaching which was obvious at 77°C from a yellowish colored effluent. The HC sample seems to show an elevated E_a at the 77-90°C step which, however, is uncertain because of the very low recorded signals (4.6 mV and 9.3 mV after the step) close to the baseline signal (3 mV) measured before the desorption.

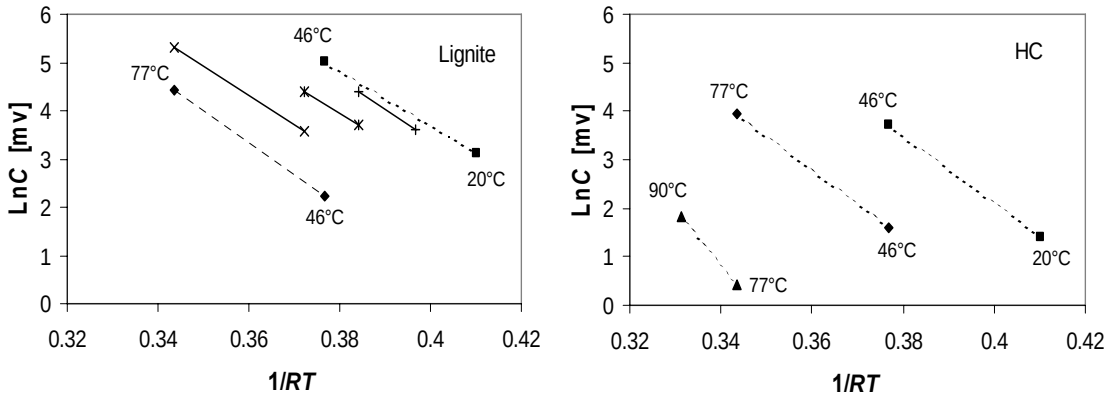

FIGURE 6.4 Arrhenius plot for the determination of desorption activation energies (E_a) from concentration increases at each temperature step.

Table 6.2 also illustrates certain reported activation energies from literature. In general, high E_a values have been associated with diffusion of HOCs in condensed organic matter, coals, and shale materials. In contrast, diffusion in amorphous organic matrices which occurs in soils show lower values for E_a. The activation energies determined in this study compare well with the literature values. The equilibrium desorption enthalpies determined at the same loading level (*28*) can be compared to the E_a values compiled in Table 6.2 and can give some hints on the diffusion process. This comparison is illustrated in Figure 6.5. If diffusion in the pore water controls the sorption/desorption kinetics, then differences between the activation energy of desorption and equilibrium enthalpy of sorption/desorption should correspond to the activation energy of aqueous diffusion of

TABLE 6.2. Activation energies (kJ mol^{-1}) at the individual temperature steps, desorption enthalpies determined in equilibrium batch experiment for two carbonaceous samples, as well as certain activation energies from literature

Samples	Temperature step	20-46°C	46-77°C	77-90°C
HC 0.17g	E_a	70	71	(114)
	ΔH [a]	32	36	47
Lignite 0.21g	E_a	58	66	
	ΔH [a]	24	28	
Lignite 0.20g (repeated)	Temperature step	30-40°C	40-50°C	50-77°C
	E_a	60	58	61
	ΔH [a]	24	25	27

Literature reported activation energies				
Sample	Compound	E_a	Temperature	
Sediments	PCBs and PAHs	60-70	20-60°C	Cornelissen et al., 1997 (*10*)
Silica gel / solids	TCE	47-94	30–60°C	Castilla et al., 2000 (*33*)
Soil	Phenanthrene	41-69	75–150°C	Johnson & Weber, 2001 (*9*)
Shale	Phenanthrene	83-86	75–150°C	Johnson & Weber, 2001 (*9*)
Soil	EDB	66	40–97°C	Steinberg et al. 1987 (*34*)
Coal particles	PAHs	115-139	30–400°C	Ghosh et al., 2001 (*13*)
Silt/clay	PAHs	37-41	30–400°C	Ghosh et al.,2001 (*13*)
Aquifer materials	Phenanthrene	45-59	20–70°C	Kleineidam et al., 2004 (*14*)
Polymers	Organic compounds	60	Ten Hulscher & Cornelissen, 1996 (*7*)	

[a] ΔH : Desorption enthalpies determined from equilibrium batch experiments (see *ref. 28*) for the respective solid loading (C_s) at each temprature step; if diffusion occurs in water then additionally 16.9 kJ mol^{-1} are expected corresponding to the activation energy of phenanthrene diffusion in water (see *ref. 14*).

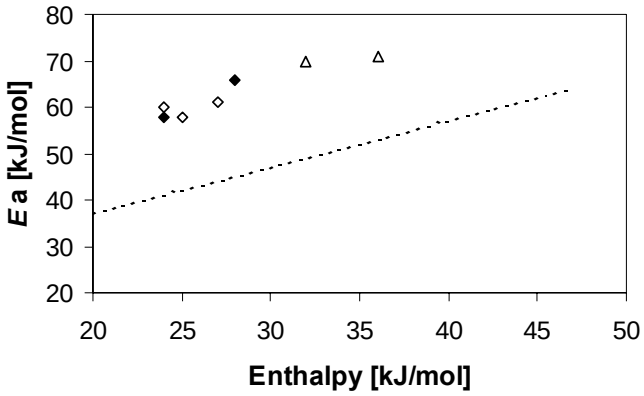

FIGURE 6.5 Comparison of equilibrium enthalpies and activation energies for phenanthrene in the lignite (diamonds) and HC (triangles) samples. Filled and open diamonds represent duplicate lignite samples. Dished line represents the sum of equilibrium enthalpies and the activation energy of aqueous diffusion of phenanthrene in bulk water (16.9 kJ mol^{-1}).

phenanthrene in bulk water (16.9 kJ mol^{-1}, see *ref. 14*). The comparison shows that all plotted data are above the dashed line (i.e., equilibrium enthalpies plus 16.9 kJ mol^{-1}), which means much slower diffusion rates than expected from phenanthrene diffusion in the pore water. In the case of lignite, diffusion in the organic matter matrix could explain this difference. For instance, a diffusion coefficient of 1 x 10^{-10} cm^2 s^{-1} is reported for phenanthrene diffusion at 25°C in fine polyoxymethylene particles (*32*). This value is about 4 orders of magnitude lower than phenanthrene diffusion in water (6.7 x 10^{-6} cm^2 s^{-1}). For HC samples, higher activation energies can be expected because of diffusion in micropores. Activation energies for diffusion are larger in micropores than in mesopores, macropores, liquids and gases (*18*).

This study shows that the activation energies of phenanthrene desorption from two carbonaceous samples (lignite and high-volatile bituminous coal) do not increase more than expected from the increase of the sorption enthalpy at lower and lowers loadings (C_s) along proceeding desorption, which indicates that there is no significant slower desorption mechanism appearing which limits desorption in the long term. Furthermore, the residual mass recoveries indicate that more than 94% of the uploaded phenanthrene mass was released during the desorption experiments. These results indicate that no significant hysteresis occurred in these investigated samples. In addition, the pore intraparticle diffusion model well describes the desorption concentration from the lignite sample. The comparison between the determined activation energies and the enthalpies from equilibrium sorption/desorption isotherms combined with activation energy expected for the diffusion in water implies that diffusion in the coals occurs in the organic matter matrix (lignite) and in micropores (HC).

6.5 References

1. Brusseau, M. L.; Rao, P. S. C. The influence of sorbent-organic matter interactions on sorptive nonequilibrium. *Chemosphere*, 1989, 18, 1691-1706

2. Brusseau, M. L.; Rao, P. S. C. Influence of sorbate structure on nonequilibrium sorption of organic compounds. *Environ. Sci. Technol*. 1991, 25, 1501-1506.

3. Brusseau, M. L.; Jessup, R. E.; Rao, P. S. C. Nonequilibrium sorption of organic chemicals: Elucidation of rate-limiting processes. *Environ. Sci. Technol*. 1991, 25, 134-142.

4. Rao, P. S. C.; Jessup, R. E.; Rolston, D. E.; Davidson, J. M.; Kilcrease, D. P. Experimental and mathematical description of nonadsorbed solute transfer by diffusion in spherical aggregates. Soil Sci. Soc. Am. J., 1980, 44, 684-688.

5. Wu, S. C.; Gschwend, P. M. Sorption kinetics of hydrophobic organic compounds to natural sediments and soils. *Environ. Sci. Technol*. 1986, 20, 717-725

6. Ball, W. P.; Roberts, P. V. Long-term sorption of halogenated organic chemicals – part 2. Intraparticle diffusion. *Eviron. Sci. Technol*. 1991b, 25, 1237-1249.

7. Ten Hulscher, T. E. M; Cornelissen, G. Effect of temperature on sorption equilibrium and sorption kinetics of organic micropollutants –a review. *Chemosphere*, 1996, 32, 609-626.

8. Karger, J.; Ruthven, D. M. *Diffusion in zeolites and other microporous solid*, John Wiely & Sons: New York, 1992.

9. Johnson, M. D.; Weber, W. J. Jr. Rapid prediction of long-term rates of contaminant desorption from soils and sediments. *Environ. Sci. Technol*. 2001, 35, 427-433

10. Cornelissen G.; van Noort, P. M; Parsons, J. R.; Govers, H. A. J. Temperature dependence of slow adsorption and desorption kinetics on organic compounds in sediments. *Environ. Sci. Technol*. 1997, 31, 454-460.

11. Werth, C. J.; MicMillan, S. A.; Castilla, H. J. Structural evaluation of slow desorbing sites in model and natural solids using temperature stepped desorption profiles. 2. Column results. *Environ. Sci. Technol*. 2000, 34, 2966-2972.

12. Chihara, K.; Suzuki, M.; Kawazoe, K. *AIChEJ*. 1978, 24, 237-246.

13. Ghosh, U.; Talley, J. W.; Luthy, R. G. Particle-scale investigation of PAH desorption kinetics and thermodynamics from sediment. *Environ. Sci. Technol*. 2001, 35, 3468-3475.

14. Kleineidam, S.; Rügner, H.; Grathwohl, P. Desorption kinetics of phenanthrene in aquifer material lacks hysteresis. *Environ. Sci. Technol*. 2004, 38, 4169-4175.

15. Pignatell, J. J.; Ferrandino, F. J.; Huang, L. Q. Elution of aged and freshly added herbicides from soil. *Environ. Sci. Technol*. 1993, 27, 1563-1571.

16. Grathwohl, P. Reinhard, M. Desorption of trichloroethylene in aquifer material: Rate limitation at the grain scale. *Environ. Sci. Technol.* 1993, 27, 2360-2366.

17. Pedit J. A.; Miller, C. T. Use of a reactive surface-diffusion model to describe apparent sorption-desorption hysteresis and allotic degradation of lindane in a subsurface material. *Environ. Sci. Technol.* 1992, 26, 1417-1427.

18. Werth, C. J.; Reinhard, M. Effect of temperature on trichloroethylene desorption from silica gel and natural sediments. 2. Kinetics. *Environ. Sci. Technol*. 1997, 31, 697-703.

19. Li, J.; Werth, C. J. Slow desorption mechanism of volatile organic chemical mixtures in soil and sediment micropores. *Environ. Sci. Technol.* 2004, 38, 440-448

20. Cheng, H.; Reinhard, M. Measuring hydrophobic micropore volumes in geosorbents from trichloroethylene desorption data. *Environ. Sci. Technol.* 2006, 40, 3595 –3602.

21. Cornelissen G.; van Noort, P. M; Parsons, J. R.; Govers, H. A. J. Mechanism of slow desorption of organic compounds from sediments: a study using model sorbents. *Environ. Sci. Technol*. 1998, 32, 3124-3131.

22. Cornelissen G.; van Zuilen, H.; van Noort, P. C. M. Particle size dependence of slow desorption of *in situ* PAHs from sediments. *Chemosphere*. 1999, 38, 2369-2380.

23. Ten Hulscher, T. E. M.; Vrind, B. A.; van den Heuvel, H.; van de Velde, L. E.; van Noort, P. C. M.; Beurkens, J. E. M. Govers, H. A. J. Triphasic Desorption of Highly Resistant Chlorobenzenes, Polychlorinated Biphenyls, and Polycyclic Aromatic Hydrocarbons in Field Contaminated Sediment. *Environ. Sci. Technol*. 1999, 33, 126-132.

24. Spurlock, f. C.; Huang, K.; van Genuchten, M. T. Isotherm nonlinearity and nonequilibrium sorption effects on transport of fenuron and monuron in soil columns. *Environ. Sci. Technol*. 1995, 29, 1000-1007.

25. Van Genuchten, M. T.; Wierenga, P. J. Mass transfer studies in sorbing porous media. I. An analytical solutions. *Soil Sci. Soc. Am, J*. 1976, 40, 473-480.

26. Van Genuchten, M. T.; Wierenga, P. J. Mass transfer studies in sorbing porous media. II. Experimental evaluation with tritium (^3H_2O). *Soil Sci. Soc. Am, J*. 1977, 41, 272-278.

27. Wang, G.; Kleineidam, S.; Grathwohl, P. Sorption/desorption reversibility of phenanthrene in soils and carbonaceous materials. *Environ. Sci. Technol.* 2007, 41, 1186-1193

28. Wang, G.; Kleineidam, S.; Grathwohl, P. Thermodynamics of sorption/desorption of phenanthrene in soils and carbonaceous materials: Equilibrium batch studies. *Environ. Sci. Technol.* 2008a (submitted)

29. Weher, M.; Totsche, K. U. Determination of effective release rates of polycyclic aromatic hydrocarbons and dissolved organic carbon by column outflow experiments. *European Journal of Soil Science*. 2005, 56, 803-813.

30. Cao, J.; Tao, Li, B. G. Leaching kinetics of water soluble organic carbon (WSOC) from upland soil. *Chemosphere*, 1999, 39, 1771-1780

31. Thurman, E. M. *Organic chemistry of natural waters*. Martonus Nijhoff/Dr W. Junk Publ, Dordrecht, 1985

32. Ahn, S. ; Werner, D. ; Karapanagioti, H. K. ; Mcglothlin, D. R. ; Zare, R. N. ; Luthy, R. G. Phenanthrene and pyrene sorption and intraparticle diffusion in polyoxymethylene, coke, and activated carbon. *Environ. Sci. Technol.* 2005, 39, 6516-6526.

33. Castilia, H. J. ; Werth, C. J. ; Mcmillan, S. A. Structural evaluation of slow desorbing sites in model and natural solids using temperature stepped desorption profiles. 2. Column results. *Environ. Sci. Technol.* 2000, 34, 2966-2972.

34. Steinberg, S. M.; Pignatello, J. J.; Sawhney, B. L. Persistence of 1,2-Dibromoetnane in soil: Entrapment in intraparticle micropores. *Environ. Eng. Sci.* 1987, 21, 1201-1208.

SUMMARY

Sorption/desorption reversibility has been investigated in many studies, but it is still controversially discussed in the scientific community. Except for one hypothesis - sorbent structural reconfiguration, clear experimental evidence for the physical or chemical mechanisms proposed to lead to hysteresis are still lacking. A common problem in sorption hysteresis studies is laboratory artifacts, which may result from non-equilibrium conditions before desorption, or solute losses in the system resulting in poor mass recoveries.

In this study such artifacts were eliminated with a newly designed batch experimental setup. The temperature-driven sorption/desorption cycles avoid "colloid effect" artifacts occurring in the conventional decant-and-refill batch method. Sorbent pulverization enables sorption/desorption equilibrium to be established in a relatively short time period. The solute loss in the batch system was accounted for by mass balance monitoring, thus making the data analysis more accurate in the isotherm measurement. The average recovery rate from all experiments was 101%. The desorption of native ("aged") phenanthrene was compared with freshly spiked samples. In addition, desorption activation energies along exhaustive desorption process were monitored using on-line column experiments under elevated temperatures.

All isotherms determined in this study are significantly non-linear except for one sample (AS5). For all individual temperature steps sorption and desorption isotherms coincide. Furthermore, the solubility-normalized sorption/desorption isotherms at different temperatures collapse to one unique overall isotherm. Leaching of native phenanthrene occurred at much lower concentration but was well predicted by extrapolation of the spiked sorption isotherms.

The isosteric heats of sorption/desorption decrease with increasing solute concentrations, which indicates existence of an adsorption process, especially for the coals. The absolute

values are in a range of 19-35 kJ mol^{-1}, which is higher than the heat of solution of subcooled phenanthrene (about 19 kJ mol^{-1}) but much less than the heat of condensation of solid phenanthrene from water (about 38 kJ mol^{-1}). No significant difference of the isosteric heats between sorption and desorption was observed. Furthermore, the desorption enthalpy of the native phenanthrene was not significantly higher than expected from the sorption experiments with spiked samples if lower loadings are considered.

The results from the on-line column experiments support the findings from the batch experiments. The determined activation energies during long-term desorption range from 58–71 kJ mol^{-1}. No significant trend of increasing desorption activation energies along with the increased degree of desorption was observed although desorption was almost completed, i.e., only 0.2% (lignite) and 6% (HC) of the initially sorbed mass were present after the last temperature step. The comparison between the determined activation energies and the enthalpies based on equilibrium sorption/desorption isotherms combined with activation energy expected for the diffusion in water implies that diffusion in the coals occurs in the organic matter matrix (lignite) and in micropores (HC).

The results imply that no significant hysteresis occurs in sorption/desorption of phenanthrene with the samples investigated in this study. In many models for predicting fate and transport of organic pollutants in the environment the local equilibrium assumption (which is based on reversibility) is a crucial element. The results from this study support this assumption and indicate that many reports about sorption/desorption hysteresis actually arise from artifacts.

APPENDIX I

Composition of the organic matter by organic petrography analysis (% vol.) for Chernozem soil (MS4) (Ligouis, B., 2004)

Recent organic matter	Non-gelified woody phytoclast (tissues & structureless humic detritus)	22.5	69.8
	Gelified woody phytoclast (tissues & structureless humic detritus)	42.0	
	Gelified matrix with humic detritus		
	Homogeneous humic gels		
	Seed coatings		
	Suberinized tissues (bark, root)		
	Pollen and spores	1.5	
	Resinous substances		
	Cuticles (epidermal tissues)		
	Liptodetrinite (fine liptinite fragments)		
	Fungal phytoclast	3.8	
Raw brown coal	Matrix coal	0.8	0.8
	Xylite		
Hard coal	Sub-bituminous coal	a	6.9
	High volatile bituminous coal	0.8	
	Medium volatile bituminous coal		
	Low volatile bituminous coal		
	Anthracite		
	Vitrite	6.1	
Charcoal: recent & fossil	Low reflecting (grey)	13.0	14.5
	High reflecting (white)	1.5	
Brown-coal coke			0.4
Coke carbon forms (coal carbonization)	Matrix particles	6.5	6.5
	Matrix with fused & unfused inclusions	a	
	Oxidized maceral & coal with oxidation rims (heated altered)	a	
Char	<25% unfused material, 40-90% porosity	1.1	1.1
Petrographic composition	huminite	73.6	100
	Liptinite	16.8	
	Inertnite	9.6	

APPENDIX II

Composition of the organic matter by organic petrography analysis (% vol.) for Pahokee Peat (Ligouis, B., 2005)

Maceral Group	Maceral Subgroup	Maceral	Submaceral		Sample PAHOKEE PEAT
			Textinite A Textinite B		
		Textinite			2.2
			Texto-Ulminite A Texto-Ulminite B		
			Texto-Ulminite total		2.2
			Eu-Ulminite A Eu-Ulminite B		
			Eu-Ulminite total		
		Ulminite			2.2
	Humotelinite				4.4
		Attrinite			63.8
		Densinite			2.8
	Humodetrinite				66.6
			Levi-gelinite	Detrogelinite	
				Telogelinite	0.2
				Eugelinite	1.4
			Porigelinite		0.2
		Gelinite			1.8
		Corpohuminite			0.8
		Phlobaphinite			x
	Humocollinite				2.6
Huminite					**73.6**
		Sporinite			x
		Cutinite			1.8
		Resinite			4.8
		Fluorinite			x
		Suberinite			1.6
		Alginite			
		Bituminite			5.8
		Liptodetrinite			2.8
		Bitumen			
Liptinite					**16.8**
		Fusinite			0.4
		Semifusinite			x
		Funginite			x
		Secretinite			x
		Macrinite			x
		Micrinite			x
		Inertodetrinite			8.4
		High reflecting groundmass ("Steinkohlenartige Teilchen")*			0.8
Inertinite					**9.6**
Natural char**					x

* inertinite component similar to the maceral macrinite (Teichmüller, 1950)

** organic component with pyrolysis char morphology (Kwiecinska & Petersen, 2004)

x present, but not expressed as percentage due to scarcity

APPENDIX III

Microscopic images of recent organic matter, peat, coals, charcoal, char and coke

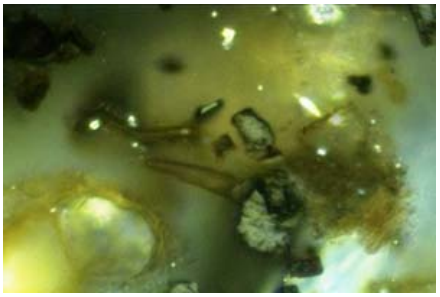

Recent organic matter

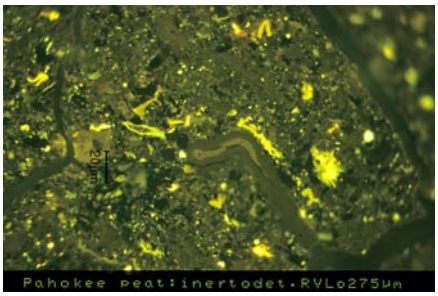

Pahokee peat

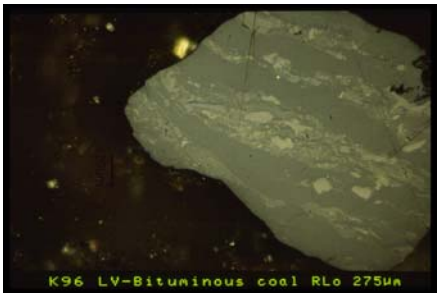

High-volatile bituminous coal

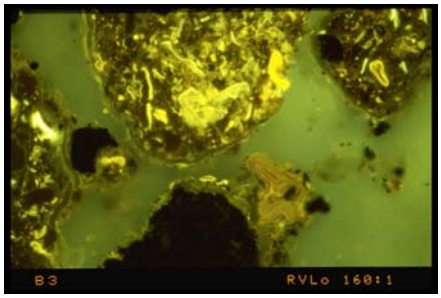

Lignite

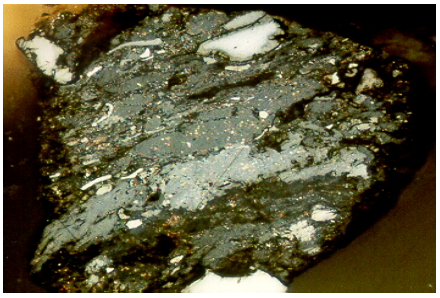

Sub-bituminous coal

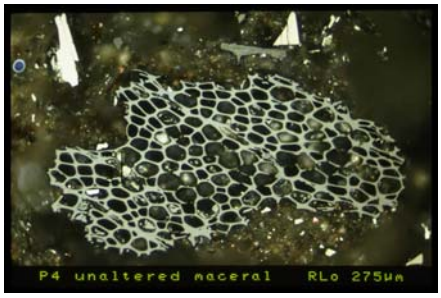

Charcoal

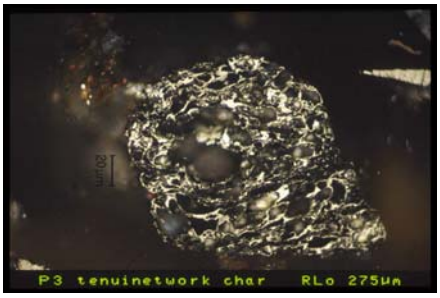

Char

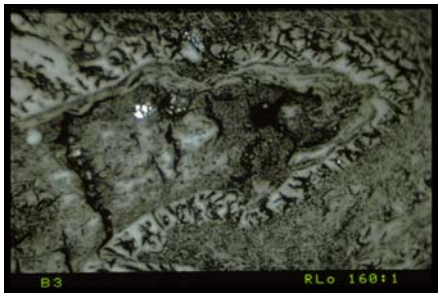

Lignite coke

In der Reihe C Hydro-, Ingenieur- und Umweltgeologie
der Tübinger Geowissenschaftlichen Arbeiten (TGA) sind bisher erschienen:

Nr. 1: Grathwohl, Peter (1989): Verteilung unpolarer organischer Verbindungen in der wasserun-gesättigten Bodenzone am Beispiel der leichtflüchtigen aliphatischen Chlorkohlenwasser-stoffe. 102 S.

Nr. 2: Eisele, Gerhard (1989): Labor- und Felduntersuchungen zur Ausbreitung und Verteilung leichtflüchtiger chlorierter Kohlenwasserstoffe (LCKW) im Übergangsbereich wasserunge-sättigte/wassergesättigte Zone. 84 S.

Nr. 3: Ehmann, Michael (1989): Auswirkungen atmogener Stoffeinträge auf Boden- und Grund-wässer sowie Stoffbilanzierungen in drei bewaldeten Einzugsgebieten im Oberen Buntsand-stein (Nordschwarzwald). 134 S.

Nr. 4: Irouschek, Thomas (1990): Hydrogeologie und Stoffumsatz im Buntsandstein des Nord-schwarzwaldes. 144 S.

Nr. 5: Sanns, Matthias (1990): Experimentelle Untersuchungen zum Ausbreitungsverhalten von leichtflüchtigen Chlorkohlenwasserstoffen (LCKW) in der wassergesättigten Zone. 122 S. **(Vergriffen!)**

Nr. 6: Seeger, Thomas (1990): Abfluß- und Stofffrachtseparation im Buntsandstein des Nord-schwarzwaldes. 154 S.

Nr. 7: Einsele, Gerhard & Pfeffer, Karl-Heinz (Hrsg.) (1990): Untersuchungen über die Auswir-kungen des Reaktorunfalls von Tschernobyl auf Böden, Klärschlamm und Sickerwasser im Raum von Oberschwaben und Tübingen. 151 S.

Nr. 8: Douveas, Nikon G. (1990): Verwitterungstiefe und Untergrundabdichtung beim Talsper-renbau in dem verkarsteten Nord-Pindos-Flysch (Projekt Pigai-Aoos, NW-Griechenland).
165 S.

Nr. 9: Schlöser, Heike (1991): Quantifizierung der Silikatverwitterung in karbonatfreien Deck-schichten des Mittleren Buntsandsteins im Nordschwarzwald. 93 S.

Nr. 10: Köhler, Wulf-Rainer (1992): Beschaffenheit ausgewählter, nicht direkt anthropogen beein-flußter oberflächennaher und tiefer Grundwasservorkommen in Baden-Württemberg. 144 S.

Nr. 11: Bundschuh, Jochen (1991): Der Aquifer als thermodynamisch offenes System. – Untersu-chungen zum Wärmetransport in oberflächennahen Grundwasserleitern

unter besonderer Berücksichtigung von Quellwassertemperaturen (Modellversuche und Geländebeispiele). 100 S. **(Vergriffen!)**

Nr. 12: Herbert, Mike (1992): Sorptions- und Desorptionsverhalten von ausgewählten polyzyklischen aromatischen Kohlenwasserstoffen (PAK) im Grundwasserbereich. 111 S.

Nr. 13: Sauter, Martin (1993): Quantification and forecasting of regional groundwater flow and transport in a karst aquifer (Gallusquelle, Malm, SW-Germany. 150 S.

Nr. 14: Bauer, Michael (1993): Wasserhaushalt, aktueller und holozäner Lösungsabtrag im Wutachgebiet (Südschwarzwald). 130 S.

Nr. 15: Einsele, Gerhard & Ricken, Werner (Hrsg.) (1993): Eintiefungsgeschichte und Stoffaustrag im Wutachgebiet (SW-Deutschland). 215 S.

Nr. 16: Jordan, Ulrich (1993): Die holozänen Massenverlagerungen des Wutachgebietes (Süd-schwarzwald). 132 S. **(Vergriffen!)**

Nr. 17: Krejci, Dieter (1994): Grundwasserchemismus im Umfeld der Sonderabfalldeponie Billigheim und Strategie zur Erkennung eines Deponiesickerwassereinflusses. 121 S.

Nr. 18: Hekel, Uwe (1994): Hydrogeologische Erkundung toniger Festgesteine am Beispiel des Opalinustons (Unteres Aalenium). 170 S. **(Vergriffen!)**

Nr. 19: Schüth, Christoph (1994): Sorptionskinetik und Transportverhalten von polyzyklischen aromatischen Kohlenwasserstoffen (PAK) im Grundwasser - Laborversuche. 80 S.

Nr. 20: Schlöser, Helmut (1994): Lösungsgleichgewichte im Mineralwasser des überdeckten Muschelkalks in Mittel-Württemberg. 76 S.

Nr. 21: Pyka, Wilhelm (1994): Freisetzung von Teerinhaltsstoffen aus residualer Teerphase in das Grundwasser: Laboruntersuchungen zur Lösungsrate und Lösungsvermittlung. 76 S.

Nr. 22: Biehler, Daniel (1995): Kluftgrundwässer im kristallinen Grundgebirge des Schwarzwaldes – Ergebnisse von Untersuchungen in Stollen. 103 S.

Nr. 23: Schmid, Thomas (1995): Wasserhaushalt und Stoffumsatz in Grünlandgebieten im württem-bergischen Allgäu. 145+ 92 S.

Nr. 24: Kretzschmar, Thomas (1995): Hydrochemische, petrographische und thermodynamische Untersuchungen zur Genese tiefer Buntsandsteinwässer in Baden-Württemberg. 142 S. **(Vergriffen!)**

Nr. 25: Hebestreit, Christoph (1995): Zur jungpleistozänen und holozänen Entwicklung der Wutach (SW-Deutschland). 88 S.

Nr. 26: Hinderer, Matthias (1995): Simulation langfristiger Trends der Boden- und Grundwasser-versauerung im Buntsandstein-Schwarzwald auf der Grundlage langjähriger Stoffbilanzen. 175 S.

Nr. 27: Körner, Johannes (1996): Abflußbildung, Interflow und Stoffbilanz im Schönbuch Waldgebiet. 206 S.

Nr. 28: Gewald, Thomas (1996): Der Einfluß der Desorptionskinetik bei der Freisetzung von Tri-chlorethen (TCE) aus verschiedenen Aquifersanden. 67 S.

Nr. 29: Schanz, Ulrich (1996): Geophysikalische Untersuchungen im Nahbereich eines Karst-systems (westliche Schwäbische Alb). 114 S.

Nr. 30: Renner, Sven (1996): Wärmetransport in Einzelklüften und Kluftaquiferen – Untersuchungen und Modellrechnungen am Beispiel eines Karstaquifers. 89 S.

Nr. 31: Mohrlok, Ulf (1996): Parameter-Identifikation in Doppel-Kontinuum-Modellen am Beispiel von Karstaquiferen. 125 S.

Nr. 32: Merkel, Peter (1996): Desorption and Release of Polycyclic Aromatic Hydrocarbons (PAHs) from Contaminated Aquifer Materials. 76 S.

Nr. 33: Schiedek, Thomas (1996): Auftreten und Verhalten von ausgewählten Phthalaten in Wasser und Boden. 112 S.

Nr. 34: Herbert, Mike & Teutsch, Georg (Hrsg.) (1997): Aquifersysteme Südwestdeutschlands - Eine Vorlesungsreihe an der Eberhard-Karls-Universität Tübingen. 162 S.

Nr. 35: Schad, Hermann (1997): Variability of Hydraulic Parameters in Non-Uniform Porous Media: Experiments and Stochastic Modelling at Different Scales. 233 S.

Nr. 36: Herbert, Mike & Kovar, Karel (Eds.) (1998): GROUNDWATER QUALITY 1998: Remediation and Protection - Posters -.- Proceedings of the GQ'98 conference, Tübingen, Sept. 21-25, 1998, Poster Papers. 146 S.

Nr. 37: Klein, Rainer (1998): Mechanische Bodenbearbeitungsverfahren zur Verbesserung der Sanierungseffizienz bei In-situ-Maßnahmen. 106 S.

Nr. 38: Schollenberger, Uli (1998): Beschaffenheit und Dynamik des Kiesgrundwassers im Neckartal bei Tübingen. 74 S.

Nr. 39: Rügner, Hermann (1998): Einfluß der Aquiferlithologie des Neckartals auf die Sorption und Sorptionskinetik organischer Schadstoffe. 78 S.

Nr. 40: Fechner, Thomas (1998): Seismische Tomographie zur Beschreibung heterogener Grund-wasserleiter. 113 S.

Nr. 41: Kleineidam, Sybille (1998): Der Einfluß von Sedimentologie und Sedimentpetrographie auf den Transport gelöster organischer Schadstoffe im Grundwasser. 82 S.

Nr. 42: Hückinghaus, Dirk (1998): Simulation der Aquifergenese und des Wärmetransports in Karstaquiferen. 124 S.

Nr. 43: Klingbeil, Ralf (1998): Outcrop Analogue Studies – Implications for Groundwater Flow and Contaminant Transport in Heterogeneous Glaciofluvial Quaternary Deposits. 111 S.

Nr. 44: Loyek, Diana (1998): Die Löslichkeit und Lösungskinetik von polyzyklischen aromatischen Kohlenwasserstoffen (PAK) aus der Teerphase. 81 S.

Nr. 45: Weiß, Hansjörg (1998): Säulenversuche zur Gefahrenbeurteilung für das Grundwasser an PAK-kontaminierten Standorten. 111 S.

Nr. 46: Jianping Yan (1998): Numerical Modeling of Topographically-closed Lakes: Impact of Climate on Lake Level, Hydrochemistry and Chemical Sedimentation. 144 S.

Nr. 47: Finkel, Michael (1999): Quantitative Beschreibung des Transports von polyzyklischen aro-matischen Kohlenwasserstoffen (PAK) und Tensiden in porösen Medien. 98 S.

Nr. 48: Jaritz, Renate (1999): Quantifizierung der Heterogenität einer Sandsteinmatrix (Mittlerer Keuper, Württemberg). 106 S.

Nr. 49: Danzer, Jörg (1999): Surfactant Transport and Coupled Transport of Polycyclic Aromatic Hydrocarbons (PAHs) and Surfactants in Natural Aquifer Material - Laboratory Experi-ments. 75 S.

Nr. 50: Dietrich, Peter (1999): Konzeption und Auswertung gleichstromgeoelektrischer Tracer-versuche unter Verwendung von Sensitivitätskoeffizienten. 130 S.

Nr. 51: Baraka-Lokmane, Salima (1999): Determination of Hydraulic Conductivities from Discrete Geometrical Characterisation of Fractured Sandstone Cores. 119 S.

Nr. 52: M^{c}Dermott, Christopher I. (1999): New Experimental and Modelling Techniques to Investigate the Fractured System. 170 S.

Nr. 53: Zamfirescu, Daniela (2000): Release and Fate of Specific Organic Contaminants at a Former Gasworks Site. 96 S.

Nr. 54: Herfort, Martin (2000): Reactive Transport of Organic Compounds Within a Heterogeneous Porous Aquifer. 76 S.

Nr. 55: Klenk, Ingo (2000): Transport of Volatile Organic Compounds (VOC's) From Soilgas to Groundwater. 70 S.

Nr. 56: Martin, Holger (2000): Entwicklung von Passivsammlern zum zeitlich integrierenden Depositions- und Grundwassermonitoring: Adsorberkartuschen und Keramikdosimeter. 84 S.

Nr. 57: Diallo, Mamadou Sanou (2000): Acoustic Waves Attenuation and Velocity Dispersion in Fluid-Filled Porous Media: Theoretical and Experimental Investigations. 101 S.

Nr. 58: Lörcher, Gerhard (2000): Verarbeitung und Auswertung hyperspektraler Fernerkundungsdaten für die Charakterisierung hydrothermaler Systeme (Goldfield/Cuprite, Yellowstone National Park). 158 S.

Nr. 59: Heinz, Jürgen (2001): Sedimentary Geology of Glacial and Periglacial Gravel Bodies (SW-Germany): Dynamic Stratigraphy and Aquifer Sedimentology. 102 S.

Nr. 60: Birk, Steffen (2002): Characterisation of Karst Systems by Simulating Aquifer Genesis and Spring Responses: Model Development and Application to Gypsum Karst. 122 S**.**

Nr. 61: Halm, Dietrich & Grathwohl, Peter (Eds.) (2002): Proceedings of the 1st International Workshop on Groundwater Risk Assessment at Contaminated Sites (GRACOS). 280 S.

Nr. 62: Bauer, Sebastian (2002): Simulation of the genesis of karst aquifers in carbonate rocks.
143 S.

Nr. 63: Rahman, Mokhlesur (2002): Sorption and Transport Behaviour of Hydrophobic Organic Compounds in Soils and Sediments of Bangladesh and their Impact on Groundwater Pollution – Laboratory Investigations and Model Simulations. 73 S.

Nr. 64: Peter, Anita (2002): Assessing natural attenuation at field scale by stochastic reactive transport modelling. 101 S.

Nr. 65: Leven-Pfister, Carsten (2002): Effects of Heterogeneous Parameter Distributions on Hydrau-lic Tests - Analysis and Assessment. 94 S.

Nr. 66: Schwarz, Rainer (2002): Grundwasser-Gefährdungsabschätzungen durch Emissions- und Immissionsmessungen an Deponien und Altlasten. 100 S.

Nr. 67: Abel, Thekla (2003): Untersuchungen zur Genese des Malmkarsts der Mittleren Schwäbi-schen Alb im Quartär und jüngeren Tertiär. 187 S.

Nr. 68: Prokop, Gundula & Bittens, Martin & Cofalka, Piotr & Roehl, Karl Ernst & Schamann, Martin & Younger, Paul (Eds.) (2003): Summary Report on the 1st IMAGE-TRAIN Advanced Study Course "Innovative Groundwater Management Technologies". 119 S.

Nr. 69: Halm, Dietrich & Grathwohl, Peter (Eds.) (2003): Proceedings of the 2nd International Workshop on Groundwater Risk Assessment at Contaminated Sites (GRACOS) and Integrated Soil and Water Protection (SOWA). 260 S.

Nr. 70: Bayer, Peter (2004): Modelling, economic assessment and optimisation of in-situ groundwater remediation systems. 78 S.

Nr. 71: Kraft, Siegfried (2004): Untersuchungen zum Langzeiteinsatz der in-situ Aktivkohlefiltration zur Entfernung von organischen Schadstoffen aus Grundwasser. 64 S.

Nr. 72: Bold, Steffen (2004): Process-based prediction of the long-term risk of groundwater pollution by organic non-volatile contaminants. 76 S.

Nr. 73: Maier, Ulrich (2004): Modelling of Natural Attenuation in Soil and Groundwater. 81 S.

Nr. 74: Susset, Bernd (2004): Materialuntersuchungen und Modellierungen zur Unterscheidung Gleichgewicht / Ungleichgewicht in Säulenversuchen für die Sickerwasserprognose organischer Schadstoffe. 100 S.

Nr. 75: Madlener, Iris (2004): Quantifizierung und Modellierung des PAK-Desorptionsverhaltens aus feinkörnigem Material mittels Säulenversuchen (DIN V 19736) und Hochdruck-Temperatur-Elution (ASE). 86 S.

Nr. 76: Henzler, Rainer (2004): Quantifizierung und Modellierung der PAK-Elution aus verfestigten und unverfestigten Abfallmaterialien. 98 S.

Nr. 77: Valley, Stephan (2004): Natural Attenuation of Volatile Organic Compounds (VOC) in Groundwater: A Method for the Determination of Compound-Specific Stable Carbon Isotope Ratios at Low Concentration Levels. 67 S.

Nr. 78: Röttgen, Klaus Peter (2004): Kritische Analyse des Aufwandes zur Erkundung von Kontami-nationen in niedersächsischen Grundwassergeringleitern. 84 S.

Nr. 79: Gocht, Tilman (2005): Die vier Griechischen Elemente: Massenbilanzierung von polyzyk-lischen aromatischen Kohlenwasserstoffen (PAK) in Kleineinzugsgebieten des ländlichen Raumes. VI, 140, 42.

Nr. 80: Halm, Dietrich & Grathwohl, Peter (Eds.) (2004): Proceedings of the 2nd International Work-shop on Integrated Soil and Water Protection (SOWA). 161 S.

Nr. 81: Prokop, Gundula, Bittens, Martin, Moraczewska-Maikut, Katarzyna, Roehl, Karl Ernst, Schamann, Martin & Younger, Paul (Eds.) (2004): Summary Report on the 3rd IMAGE-TRAIN Advanced Study Course "Quantitative Risk Assessment". 66 S.

Nr. 82: Hoffmann, Ruth (2004): Optimierungsansätze zur Datenerfassung und Interpretation von Multielektrodenmessungen. 91 S.

Nr. 83: Kostic, Boris (2004): 3D sedimentary architecture of Quaternary gravel bodies (SW-Germany): implications for hydrogeology and raw materials geology. 103 S.

Nr. 84: Bayer-Raich, Marti (2004): Integral pumping tests for the characterization of groundwater contamination. 112 S.

Nr. 85: Piepenbrink, Matthias (2006): **– Im Druck.**

Nr. 86: Becht, Andreas (2004): Geophysical methods for the characterization of gravel aquifers: case studies and evaluation experiments. 75 S.

Nr. 87: Brauchler, Ralf (2005): Characterization of Fractured Porous Media Using Multivariate Statistics and Hydraulic Travel Time Tomography. 74 S.

Nr. 88: Stefan Gödeke (2004): Evaluierung und Modellierung des Natural Attenuation Potentials am Industriestandort Zeitz. 139 S.

Nr. 89: Nicolai-Alexeji Kummer (2005): Entwicklung eines kommerziell einsetzbaren Katalysators zur Grundwassersanierung: Katalytische Hydrodehalogenierung und Hydrierung umwelt-relevanter (Chlor-) Kohlenwasserstoffverbindungen an trägergestützten Edelmetallkatalysa-toren. 122 S.

Nr. 90: Beinhorn, Martin (2005): Contributions to computational hydrology: Non-linear flow processes in subsurface and surface hydrosystems. 87 S.

Nr. 91: Olsson, Asa (2005): Investigation and Modelling of Dispersion-Reaction Processes in Natural Attenuation Groundwater. 68 S.

Nr. 92: Safinowski, Michael (2005): Anaerobic biodegradation of polycyclic aromatic hydrocarbons. 65 S.

Nr.93: Bürger, Claudius (2005): Technical-economic optimization of in-situ reactive barrier systems under uncertainty. 94 S.

Nr. 94: Jahn, Michael (2006): Microbial dissimilatory iron(III) reduction: Studies on the mechanism and on processes of environmental relevance. 63 S.

Nr. 95: Bi, Erping (2006): Sorption and transport of heterocyclic aromatic compounds in soils. 63 S.

Nr. 96: Kübert, Markus (2006): Modelling and Technical-Economic Evaluation of Point Scale and Integral Approaches for Investigating Contaminant Plumes in Groundwater. 124 S.

Nr. 97: Chen, Cui (2006): Integrating GIS Methods for the Analysis of Geosystems. 157 S.

Nr. 98: Regierungspräsidium Freiburg, Abt. Landesamt für Geologie, Rohstoffe und Bergbau (Hrsg.) (2006): Untersuchungen zur Aquiferdynamik im Einzugsgebiet des Blautopfs (Oberjura, Süddeutschland). 77 S.

Nr. 99: Jochmann, Maik (2006): Solventless Extraction and Enrichment for Compound Specific Isotope Analysis. … S. **– Im Druck.**

Nr. 100: Kouznetsova, Irina (2006): Development and application of a phenomenological modelling concept for simulating the long-term performance of zero-valent iron. 99 S.

Nr. 101: Gronewold, Jan (2006): Entwicklung eines Internet Informationssystems zur Modellierung natürlicher Rückhalte- und Abbauprozesse im Grundwasser. 72 S.

Nr. 102: Rein, Arno (2006): Remediation of PCB-contaminated soils – Risk analysis of biological in situ processes. 181 S.

Nr. 103: Dietze, Michael (2007): Evaluierung von Feldmethoden zur Quantifizierung von Schad-stoffminderungen im Fahnenbereich am Beispiel eines BTEX-Schadens. 156 S.

Nr. 104: Kunapuli, Umakanth (2007): Anaerobic degradation of monoaromatic hydrocarbons by dissimilatory iron(III)-reducing pure and enrichment cultures. 73 S.

Nr. 105: Miles, Benedict (2007): Practical Approaches to Modelling Natural Attenuation Processes at LNAPL Contaminated Sites. 127 S.

Nr. 106: Walsh, Robert (2007): Numerical Modeling of THM Coupled Processes in Fractured Porous Media. 98 S.

Nr. 107: Wang, Guohui (2008): Sorption / Desorption Reversibility of Polycyclic Aromatic Hydrocarbons (PAHs) in Soils and Carbonaceous Materials. 100 S.